

# **Novel approaches for quantitative analysis of small biomolecules in MALDI-MS and SALDI-MS**

Dissertation  
zur Erlangung des Grades  
des Doktors der Naturwissenschaften  
der Naturwissenschaftlich-Technischen Fakult ä  
Universit ä des Saarlandes

von  
**M.Sc. Zhen Liu**

Saarbr ücken  
2020

**Tag des Kolloquiums:** 24.09.2020

**Dekan:** Prof. Dr. Guido Kickelbick

**Berichterstatter:** Prof. Dr. Dietrich A. Volmer  
Prof. Dr. Christoph Wittmann

**Vorsitzender:** Prof. Dr. Gregor Jung

**Akad. Mitarbeiter:** Dr. Agnes-Valencia Weiß

*To my families, Peng and Alexander, with love*

“Few things are impossible in themselves; and it is often for want of will, rather than of means, that man fails to succeed.”

*-La Rocheforcauld, French writer*

## Acknowledgements

It is my pleasure to acknowledge a number of people who supported and helped me during the whole period of my PhD study at Saarland University. First of all, I would like to express my deep gratitude to Prof. Dietrich A. Volmer for giving me the opportunity to conduct my PhD research in his laboratory, for his advice and support of my research ideas, for his stimulating discussions we had over these years, and particularly for his support in publishing the results of my research.

Furthermore, I would like to thank the group members from the Institute of Bioanalytical Chemistry at Saarland University, Dr. Yulin Qi, Ms. Elizabeth Crawford, Dr. Ignacy Rzagalinski, Dr. Tobias Karl-Fridolin Dier, Dr. Klaus Hollemeyer, Dr. Miriam Müller and Mr. Pascal Schorr for creating a free working environment, as well as scientific and stimulating discussions we had throughout the last three years. I would like to thank Ms. Elizabeth Crawford for her kind help to solve technical problems of the mass spectrometer, Dr. Ignacy Rzagalinski for providing pig brain extraction samples for my MS experiments.

This thesis would not be possible without the great support from Prof. Tobias Kraus in Leibniz Institute of New Materials and Prof. Geroge Jung from Saarland University. Prof. Tobias Kraus is acknowledged for the stimulating discussions about AuNPs as well as his group members Mr. Thomas Kister and Ms. Andrea Pyttlik for providing the excellent AuNPs. Prof. Geroge Jung is an excellent secondary supervisor who helps me a lot during my PhD study. I would like to thank Prof. Lars Kaestner from Saarland University for help to prepare the plasma sample. In addition, I would like to thank my friends and colleagues, Mr. Jun Feng (Leibniz Institute for New Materials), Ms. Xinhon Xiong (Leibniz Institute for New Materials) for their assistance in structural characterization, Ms. Caroline Hoffmann (Saarland University) and Mr. Nils Steinbruck (Saarland University) for the UV/Vis measurements.

My special thanks would go to my families for their consistent support. I would like to thank my parents for their encouragement and endless love. In particular, my deepest gratitude goes to my husband, Prof. Peng Zhang, for his guidance, patience, company and understanding and above all, for his unconditional believe, support and being my light in tough and dark times. Simple words cannot express my feelings, nor my thanks for all their help. I would like to thank my little prince, Alexander, who brings laugh and sunshine for my life. I would like to thank my friend, Meijuan Zhou (Saarland University) for her concern and company during my PhD study.

Last but not least, I would like to acknowledge China Scholarship Council (CSC) for the financial support for my PhD study.

## Table of Contents

<b>Acknowledgements</b> .....	<b>iv</b>
<b>Table of Contents</b> .....	<b>vi</b>
<b>I Abstract</b> .....	<b>1</b>
<b>II Zusammenfassung</b> .....	<b>2</b>
<b>III Abbreviations</b> .....	<b>3</b>
<b>IV Introduction</b> .....	<b>5</b>
4.1 MALDI-MS .....	5
4.2 SALDI-MS.....	10
4.3 Quantitative analysis in MALDI-MS and SALDI-MS .....	20
4.4 Objective .....	26
<b>V List of publications</b> .....	<b>28</b>
Publication 1 .....	29
Publication 2 .....	37
Publication 3 .....	63
<b>VI Conclusion and outlook</b> .....	<b>80</b>
<b>VII Reference</b> .....	<b>83</b>
<b>VIII Curriculum vitae</b> .....	<b>96</b>
<b>IX Scientific contribution</b> .....	<b>97</b>

## I Abstract

The aim of this work is to develop novel approaches to improve signal reproducibility and sensitivity in matrix-assisted laser desorption/ionization (MALDI) and surface-assisted laser desorption/ionization (SALDI) mass spectrometry (MS), for quantitative analysis of small biomolecules including endogenous metabolites and small lipids. Firstly, regular channels were designed in the target plate to inhibit the inhomogeneous deposition of the samples during solvent evaporation, to improve the signal reproducibility in MALDI-MS. Secondly, a series of ultra-thin and homogeneous AuNP substrates ( $[\text{AuNP}]_n$ ) were prepared at the air/water interface by using a Langmuir-Blodgett inspired approach. The optimized  $[\text{AuNP}]_n$  substrates exhibited not only high SALDI-MS signal intensity but also excellent signal reproducibility, both of which benefits the quantitative analyses in SALDI-MS. Thirdly, influences of gold core size and surface ligands on the MS signal were systematically studied to further improve the function of AuNP substrates in SALDI-MS. The results indicated that the AuNPs with bigger core size and hydrophobic surface ligands showed higher signal intensity. Moreover, removing the organic ligand of the as-deposited AuNP substrates could further increase the signal intensity.

## II Zusammenfassung

Ziel dieser Arbeit war es, neue Methoden zur Verbesserung der Signalreproduzierbarkeit und -empfindlichkeit bei der matrix-unterstützten Laser Desorption/Ionisation (MALDI)- und der oberflächen-unterstützten Laser Desorption/Ionisation (SALDI)-Massenspektrometrie (MS) zur quantitativen Analyse kleiner Biomoleküle einschließlich endogener Metaboliten und kleine Lipide zu entwickeln. Im ersten Teil haben wir regelmäßige Kanäle in der Probenplatte eingebracht, um die inhomogene Ablagerung der Probe während der Lösungsmittelverdampfung zu verhindern und die Signalreproduzierbarkeit bei MALDI-MS zu verbessern. In Anbetracht der Tatsache, eine Reihe ultradünner und homogener AuNP-Substrate ( $[\text{AuNP}]_n$ ) wurde unter Verwendung eines einfachen Luft/Wasser-Grenzflächenansatzes für SALDI-MS-Substrate hergestellt. Die optimierten  $[\text{AuNP}]_n$ -Substrate zeigten nicht nur eine hohe SALDI-MS-Signalintensität, sondern auch eine hervorragende Reproduzierbarkeit der Analytsignale, was eine quantitative Analyse von Fettsäuren ermöglichte. Um die Qualität des AuNP-Substrats für die quantitative Analyse bei SALDI-MS weiter zu verbessern, führten wir eine systematische Untersuchung des Einflusses der Goldkorngröße und der Oberflächenliganden auf das MS-Signal durch.

### III Abbreviations

<b>MALDI</b>	matrix-assisted laser desorption/ionization
<b>SALDI</b>	surface-assisted laser desorption/ionization
<b>SELDI</b>	surface-selected laser desorption/ionization
<b>NALDI</b>	nano-assisted laser desorption/ionization
<b>MS</b>	mass spectrometry
<b>MSI</b>	mass spectrometry imaging
<b>MS/MS</b>	tandem mass spectrometry
<b>ESI</b>	electrospray ionization
<b>TOF</b>	time of flight
<b>FTICR</b>	fourier-transform ion cyclotron resonance
<b>qqq</b>	triple-quadrupole
<b>AP</b>	atmospheric pressure
<b>GC</b>	gas chromatography
<b>LC</b>	liquid chromatography
<b>m/z</b>	mass to charge ratio
<b>DIE</b>	desorption/ionization efficiency
<b>IS</b>	internal standard
<b>RSD</b>	relative standard deviation
<b>CV</b>	coefficient of variation
<b>LOD</b>	limit of detection
<b>LOQ</b>	limit of quantification
<b>CHCA</b>	$\alpha$ -cyano-4-hydroxycinnamic acid

<b>DHB</b>	2,5-dihydroxybenzoic acid
<b>SA</b>	sinapic acid
<b>DIOS</b>	desorption/ionization on silicon
<b>NAPA</b>	nanopost arrays
<b>NIMS</b>	nanostructure-initiator mass spectrometry
<b>ESD</b>	electrospray deposition
<b>LBL</b>	layer by layer
<b>NPs</b>	nanoparticles

## IV Introduction

Mass Spectrometry (MS) is considered as a powerful technique to analyze complex bio-mixtures, which can provide details about molecular weight as well as chemical structures of analytes. This technique is not used to detect molecular weight directly, but to detect mass-to-charge ( $m/z$ ) ratio of a molecule, where  $m$  is the molecular weight in Daltons (Da), and  $z$  is the charge of the molecule. In the bioanalysis with MS, the generation of molecule ions is obligatory. For electron ionization (EI) and chemical ionization (CI), they always require the analytes to be transferred into the gas phase and generate fragments, which are only suitable for volatile and stable small molecules. Therefore, they fail to ionize the biomolecules which are non-volatile and with large molecular weight, such as proteins. The invention of „soft ionization“ methods, particularly matrix assisted laser desorption/ionization (MALDI) and electrospray ionization (ESI), are milestones in the development of bioanalysis. MALDI enables the generation of intact molecular ions without fragments for larger molecules, which revolutionizes the application of MS in bioanalysis [1]. In the following part, more details about MALDI-MS will be described.

### 4.1 MALDI-MS

The laser desorption/ionization mass spectrometry was introduced in 1960s. However, the potential of this technique was not discovered until the event that Hillenkamp *et al.* applied it to analyze peptides and proteins with organic matrix in 1980s [2–4], with the term of MALDI-MS. As demonstrated in the previous reports, the MALDI-MS has the following advantages: sensitive and rapid detection, small amount of sample consumption, in-situ and soft ionization and suitable for non-volatile samples. MALDI is known as a soft ionization method which usually generates singly charged molecular ions as  $1^+$  or  $1^-$  without fragments, which is good with analyzing complex mixtures. Therefore, MALDI-MS was considered as a powerful tool to analyze many kinds of biomolecules, including proteins, peptides, lipids, as well as small metabolites [2, 3, 5–9].

The MALDI process usually includes three steps: firstly, a mixture of a highly concentrated matrix solution and a dilute analyte solution is dropped on target plate. The solvent vaporizes, leaving the matrix recrystallized with the analytes embedded into it. This process is also

called co-crystallization. Secondly, a pulsed laser is fired on the sample, subsequently causing ablation and desorption of matrix. Finally, the analytes are ionized by ablated species in hot plume as protonated or deprotonated ions and then they are transferred to the analyzer of a mass spectrometer [10].

#### 4.1.3 Ion formation in MALDI-MS

When the laser irradiates on the surface of samples, the matrix absorbs the laser energy and is primarily desorbed and ionized, generating the hot plume (Figure 4.1). In the hot plume, there are a lot of species including matrix clusters and nanodroplets, neutral and ionized matrix molecules, protonated and deprotonated matrix molecules. The ablated species may participate in the ionization process of analytes, though the desorption/ionization process is still not clearly [10, 30]. Then analytes are desorbed and ionized via a complex energy transfer from matrix. The ions generated from this process consist the neutral molecules (M) with ions added or removed, which is called molecular ions, e.g.  $[M+H]^+$  and  $[M+Na]^+$  in the case of adding a proton or sodium. In a MALDI mass spectra, there are many ion signals, including matrix and analyte ions, major monocharged molecular ions and little multicharged ions and fragment ions.

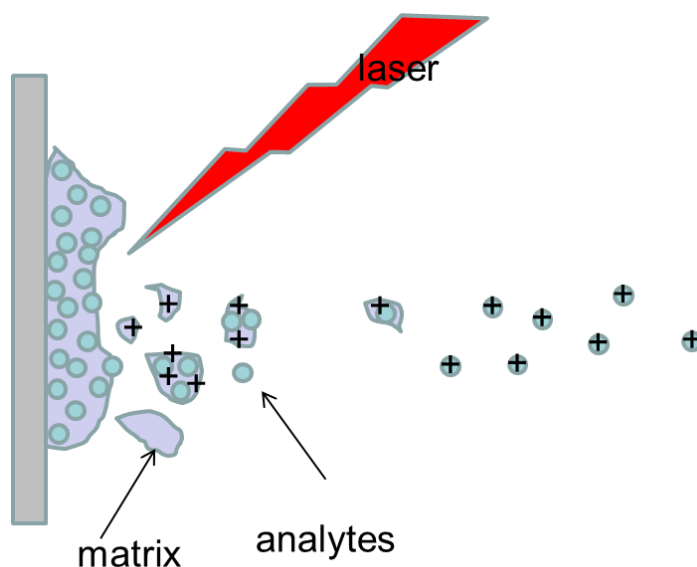


**Figure 4.1** Schematic illustration of desorption/ionization process in MALDI.

The ion formation process is very complex in MALDI, and several different theoretical modes have been proposed to explain the ion-generation process, including gas phase proton transfer model, lucky survivor model, thermal model and so on [10, 11, 31]. Although many scientific work have been done, the mechanism is still on debate. One of the major reasons is that no single mechanism could explain all ions observed in MALDI-MS.

#### 4.1.1 Matrix used in MALDI-MS

MALDI matrix are small organic crystalline solids, which have low vapor pressure in order not to be vaporized during sample preparation or standing in a mass spectrometer. The function of the matrix is to isolate analyte molecules and absorb energy from the pulsed laser [11]. Therefore, they usually have a chemical structure with conjugated double bonds, which enable them to have strong optical absorption in either UV or IR range. Over the last several decades, a large number of matrices have been developed in MALDI-MS [12, 13]. However, only a few of them are widely used (Figure 4.2), including  $\alpha$ -cyano-4-hydroxycinnamic acid (CHCA), 5-dihydroxybenzoic acid (DHB), sinapic acid (SA), 9-aminoacridine (9-AA), diiodotyrosine (DIT) and 2,4,6-trihydroxyacetophenone (THAP). During experiment, the matrix solution is usually made in a mixture of water and organic solvent, such as methanol and acetonitrile. Meanwhile, a counter ion source is usually added to help the ion formation process. For example, trifluoroacetic acid is always added for positive mode measurements.

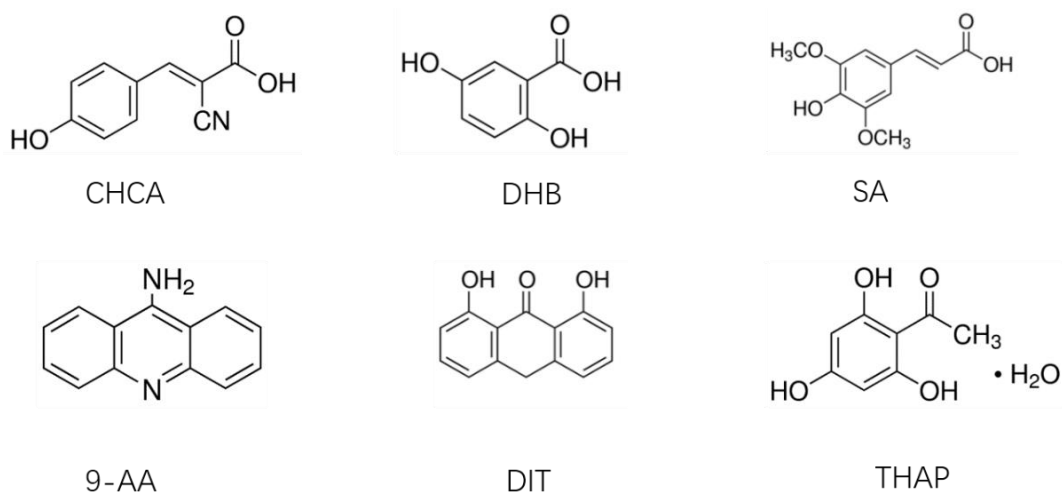


**Figure 4.2** Molecular structures of the popular matrices in MALDI-MS.

According to previous report, the desorption/ionization efficiency (DIE) in MALDI-MS was affected by several aspects of matrix, such as choice of matrix and the co-crystallization process of matrix and analytes [14–16]. Then many scientific researches were focused on these aspects to increase signal intensity and detection sensitivity in MALDI-MS. Choosing a right matrix is very important for MALDI-MS and sometimes may show magic effect. As a thumb rule, polar matrices are used to ionize polar analytes, and nonpolar matrices are applied for nonpolar analytes. Besides, the acidity of matrix is also a judgement to predict the protonating or deprotonating effect of analytes [17, 18]. Moreover, according to the previous experimental results: DHB is usually applied to analyze low molecular weight compounds such as carbohydrates and lipids; CHCA is often used for detection of middle molecular weight compounds such as peptides and lipids; SA is a common matrix for high molecular weight compounds such as proteins with molecular weight larger than 5000 Da. In addition, binary mixture of the standard matrices could achieve significant improvements in signal identification and detection limit [19, 20]. For example, DHB and CHCA were mixed as an optimized matrix for the detection of phospholipids distribution in tissues, which provided unprecedented detail in imaging mass spectrometry (IMS) [19]. By adding trifluoroacetic acid and piperidine, more than 100 peaks of phospholipids were detected in both positive and negative ion modes. Furthermore, the co-crystallization process of matrix and analyte is also very important for achieving a higher DIE in MALDI-MS. Many methods have been developed to tune and improve the co-crystallization process of matrix and analytes [8, 21–24]. The results showed that small and homogeneous crystal formation would be favorable to get stable signals and higher DIE values. Recently, novel matrices, such as ion liquid, have demonstrated the capabilities to serve as a powerful toolkit in MALDI-MS [25, 26]. For example, the ion liquid matrix of 1,1,3,3-tetramethylguanidium (TMG) salt of *p*-coumaric acid (G<sub>3</sub>CA) was reported as a magic matrix for the detection of sulfated/sialylated/neutral oligosaccharides and glycopeptides without fragmentation in both positive and negative ion extraction modes [25]. The dissociation of sulfate head groups was effectively suppressed due to soft ionization character of G<sub>3</sub>CA and the detection sensitivity of sulfated/sialylated/neutral oligosaccharides was improved to be as high as 1 fmol.

#### **4.1.2 Laser used in MALDI-MS**

Only pulsed laser works for MALDI-MS. Because the required energy for desorption/ionization must be transferred to sample in the time that is shorter than the thermal

diffusion time [27]. A MALDI source usually employs an ultraviolet (UV) laser or an infrared (IR) lasers (Figure 4.3). For UV laser, there are nitrogen laser with a wavelength of 337 nm and frequency-tripled and quadrupled Nd:YAG laser with wavelength of 355 nm and 266 nm, respectively. For IR laser, Er:YAG laser with a wavelength of 2.94  $\mu\text{m}$ , optical parametric oscillator (OPO) lasers with wavelength range from 1.7 to 2.5  $\mu\text{m}$  and carbon dioxide laser with a wavelength of 10.6  $\mu\text{m}$  are usually used. Although there are both UV and IR lasers available in the market, the majority of commercial MALDI instruments are equipped with UV laser, because most matrices have the absorption in the UV range. Laser irradiation conditions including laser wavelength, laser beam size and laser pulse duration have been investigated to clarify desorption/ionization process of MALDI-MS [28, 29]. It was found that sufficient energy absorption by matrix at irradiated laser wavelength was most important for a high DIE.

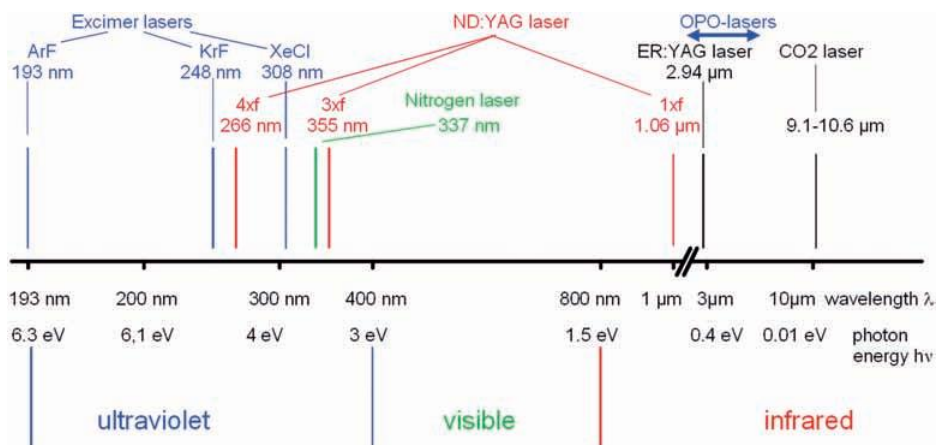


**Figure 4.3** Wavelength and photon energy of frequently used laser. Reproduced with permission from reference [27].

#### 4.1.4 Application in MALDI-MS

During the development of MALDI-MS, it has been applied in many areas including chemistry, biology, medicine, pharmacy and forensic [1, 13, 32–34]. Nowadays, scientists have more interest in applying it in the clinical laboratory for fingerprinting analytes in quite complex samples [35]. As reported by Brulina *et al.*, it is convenient to use MALDI-TOF-MS to study the cell-penetrating peptides (CPP) in eukaryote cells [36]. MALDI-MS enables direct peptide detection, which improves the distinction between membrane-bound and internalized species, leading to accurate measurements. In addition, MALDI-MS have been used to directly evaluate and identify bacteria successfully from urine and blood samples,

allowing real-time diagnosis [37–39]. 1325 anaerobes were analyzed by Scola *et al.* with MALDI-MS and 92.5 % of them were correctly identified at species' level, demonstrating routine identification methods for anaerobes could rely on MALDI-MS [40].

It should be noted that MALDI-MS is usually coupled with a TOF analyzer which has merits in large molecule detection in the present commercial applications. Until now, large compounds up to 1.5 million Da could be detected by MALDI-TOF-MS [41]. However, MALDI-MS is not suitable for small molecules (smaller than 500  $m/z$ ) analysis due to the matrix signals in low mass range and the resulting signal suppression. To overcome this obstacle, many protocols have been reported. For example, Cohen *et al.* [7] have summarized the methods to analyze small molecules ( $\leq 1500$   $m/z$ ) by minimizing interference through sample preparation and matrix selection using MALDI-MS technology. However, these methods were not universally applicable. Meanwhile, some reports have demonstrated the capabilities of detecting small molecules by replacing the organic matrix in MALDI-MS with inorganic materials. This updated technique is called surface assisted laser desorption/ionization (SALDI) MS [42], which will be introduced in the following section.

## 4.2 SALDI-MS

Almost at the same time of MALDI-MS, Tanaka *et al.* published cobalt nanoparticles (NPs) (around 30 nm diameter) with glycerol to successfully analyze large proteins (with molecular weight of 35 kDa) [43]. This was considered as the first report in SALDI-MS. After the pioneerwork, SALDI-MS was introduced as promising method with great potential application in bioanalysis. In 2002, Tanaka and his co-workers were awarded Noble Prize in Chemistry for developing a soft desorption/ionization method for mass spectrometric analyses of biological macromolecules.

As mentioned above, SALDI-MS is developed on the basis of MALDI-MS by replacing the organic matrix with inorganic materials. Thus, SALDI-MS is an organic matrix-free technology, using inorganic materials to assist desorption/ionization of analytes by transferring the absorbed energy to analyte molecules. The matrix signals in low mass range could be significantly eliminated and the noisy background could be reduced, which are crucial for small molecule analysis. Compared with MALDI-MS, SALDI-MS has been recognized with the following advantages: (a) simple and flexible sample preparation; (b) reduced background signals in the low  $m/z$  region owing to decreased chemical noise; (c)

possibility to selectively capture and preconcentrate analytes by particles modification; (d) application in a wide wavelength range with different laser types. Until now, many kinds of micro- and nano- structured materials have been used in SALDI-MS, including metal materials (for example, Au, Ag, Pa and Pt), metallic oxides, carbon materials, silicon materials, and the others [44–50]. According to previous reports, both the chemical composition and structure of the materials have great effects on the DIE of analytes in SALDI-MS. In the following, applications of these materials in SALDI-MS will be described.

#### **4.2.1 Metal nanomaterials**

Metal nanomaterials are well-known matrices in SALDI-MS for biological analysis because of their unique optical, thermal and electrical properties. Owing to the ease of preparation and good biocompatibility, Au nanomaterials are widely applied in SALDI-MS [51, 52]. As reported in recent studies, Au nanomaterials have been used for analysis of a wide range of small molecules, including amino acids, peptides, synthetic polymers, aminothiols, drugs, oligosaccharides and chinese herbal medicine granules [53–59]. Au nanomaterials exhibit strong interactions with thiol and amino groups. Thus, they can capture biomolecules with thiol and amino groups via the thiol-gold and amine-gold interactions, which can concentrate the analytes from sample solutions to achieve a lower detection limit for biomolecules. Nile red-adsorbed AuNPs (NR-AuNPs) were reported as selective probes for analysis of aminothiols in SALDI-MS [57] (Figure 4.4). Three aminothiols including glutathione (GSH), cysteine (Cys) and homocysteine (HCys) and a non-thiol amino acid (arginine) were used in this work. The aminothiols could induce aggregation of AuNPs, indicated by the sample precipitation. With pre-concentration, the LOD for three aminothiols in SALDI-MS were improved to 40, 20, and 30-fold lower, respectively.

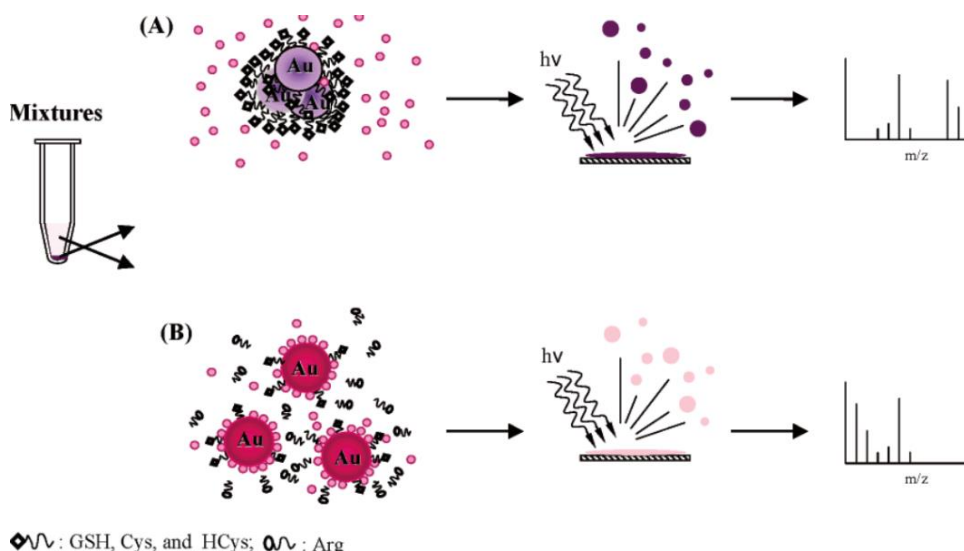


**Figure 4.4** Schematic illustration of workflow of SALDI-MS with AuNPs as matrix for analysis of aminothiols. Reproduced with permission from reference [57]. Copyright (2006) American Chemical Society.

The size, structure and the surface chemistry of nanoparticles are crucial parameters for detection sensitivity, selectivity and high DIE in SALDI-MS. Mixed AuNPs with two different diameters of 3 and 14 nm were used in SALDI-MS to detect amino-thiol compounds [60]. The authors found that larger AuNPs could selectively capture amino-thiol on the AuNPs' surface and smaller AuNPs could improve the signal sensitivity. With this protocol, glutathione, cysteine, and homocysteine were detected with limit of detection (LOD) of 2, 20 and 44 nM, respectively. As reported in the recent studies, gold nanoclusters, nanowires, nanorods and nanoflowers have been successfully used in SALDI-MS, for analysis of biomolecules within a wide range of molecular weight and different polarities [44, 60–63]. For example, flower-like AuNPs were applied as matrix to enhance ionization of peptides [44]. The author illustrated that the peak intensities of peptides were improved up to 7.5 times higher by using gold nanoflowers as matrix over the classical CHCA matrix.

Gold nanomaterials are usually synthesized with surface ligands which are unfavorable for desorption/ionization of analytes. Eliminating of ligands would help to increase the quality of mass spectra and detection sensitivity in SALDI-MS. Chemical-free AuNPs were synthesized by using a laser ablation method and used as matrix in SALDI-MS[61]. Contrary to citrate stabilized AuNPs (citrate-AuNPs) as matrix, these chemical-free AuNPs generate reduced background in the low-mass region (<500 Da). This allowed better quality of mass spectra and lower LOD for analytes including arginine, fructose, atrazine, anthracene and paclitaxel

in picomole detection. By designing the ligands, AuNPs could be used to detect some special compounds in SALDI-MS. For example, 4-mercaptophenylboronic acid functionalized AuNPs (4-MPBA-AuNPs) were synthesized and successfully used for enrichment and detection of glycopeptides [64]. The boronic acid group on the surface of 4-MPBA could react with cis-1,2-diols groups of glycopeptides and form reversible covalent bonds, which facilitates the successful isolation and selection of the analyte molecules.

As mentioned above, the gold nanomaterials have shown good performance as matrices in SALDI-MS, especially in detecting small molecules. Meanwhile, it is realized that such materials have limits in analysis of large molecules such as large peptides and proteins. Take proteins as an example, the interactions between gold nanomaterials and thiols are so strong that the molecules could not be desorbed from AuNPs with laser agitation. One exception is the binary mixture of AuNPs and organic matrix that was reported as the matrices of detecting large proteins in SALDI-MS [65, 66]. For example, hybrid materials of AuNPs and organic matrix molecule, like AuNCS@SA (gold nanocluster as core and sinapic acid as ligand), were synthesized and used to analyse large proteins such as myoglobin [66].

Like the gold nanomaterials, silver nanomaterials are also widely used matrices in SALDI-MS [67]. They have been successfully used for analysis of different kinds of analytes, including fatty acids, amino acids, oligosaccharides, oestrogens, peptides, olefins, drugs and imaging lipids in animal tissues [68–77]. By choosing a suitable composite partner, a binary mixture of Ag nanomaterials would show special characters in SALDI-MS. For example, AgNPs covered with zeolite were developed as matrix in SALDI-MS for analysis of low molecular weight analytes including acetylsalicylic acid, l-histidine, glucose, urea, cholesterol, and those in human serum [78]. The introduction of zeolite prevents the destruction of AgNPs after the photoexcitation, which permits Ag to work as efficient, long-living and stable ion supply. Ag–Au alloy NPs were prepared and used for imaging of latent fingerprints (LFPs) in SALDI-MSI [79]. With this Ag–Au hybrid nanoparticle, several endogenous fatty acids were detected unambiguously. Compared with pure AgNPs or AuNPs, these Ag–Au alloy NPs have better performance in stability and image contrast. In addition, it has been illustrated that the Ag–Au alloy NPs with certain composition of 60:40 wt % have the best SALDI-MS performance. Similar with AuNPs, AgNPs could also be used to concentrate analytes in solution and get better sensitivity in SALDI-MS, by careful designing of the ligands [80–83].

Except for the coinage metals mentioned above, the platinum (Pt) and palladium (Pd) nanomaterials have also been used in the SALDI-MS. For example, with Pt nanoparticles

(PtNPs) as substrates, peptides and proteins with molecular weights from 1200 to 25000 Da could be detected effectively [84]. PtNPs were reported as matrix as well as probe in SALDI-MS for analysis of natural and denatured (microwave-digested) proteins (lysozyme and bovine serum albumin) [85]. High quality mass spectra of target molecules were obtained in optimized condition and higher numbers of peptides sequence were obtained for digested lysozyme protein. Except for analyzing large molecules, PdNPs are also used as matrix in SALDI-MS for analysis of small molecules, such as free acids and triacylglycerides (TAG) from vegetable oil [86].

#### **4.2.2 Metallic oxide nanomaterials**

Among all the metallic oxides, TiO<sub>2</sub> nanomaterials attracted most interest and were considered as one category of the most promising candidate matrices in SALDI-MS, because of their special optical properties, i.e., strong absorption in the UV range. In the previous studies, different crystalline types of TiO<sub>2</sub> (i.e., anatase, rutile and brookite) were investigated as matrix in SALDI-MS for analysis of low molecular weight compounds [83]. The results showed that neat anatase or rutile TiO<sub>2</sub> nanomaterial showed better SALDI-MS performance than a commercial TiO<sub>2</sub> with mixed anatase/rutile structure, indicating the crystalline form played an important role in the application of TiO<sub>2</sub> as matrix. TiO<sub>2</sub> nanocrystals with different shapes and sizes were used as substrates in SALDI-MS for analysis of physiologically relevant small molecules such as steroid hormones, amino acids and carbohydrates [87]. The results showed that all TiO<sub>2</sub> nanocrystals, regardless of their shape and size, had great potential in detection of small molecules. However, the quality of mass spectra, repeatability and sensitivity varied greatly. Popović *et al.* reported that size and shape of nanocrystals influenced the packing way of carbohydrates onto the sample plate [88], which later affected the homogeneity and reproducibility of analytes. Larger TiO<sub>2</sub> nanocrystals generated higher reproducible signals of analytes.

For most SALDI-MS matrices, they are one-time used, causing the waste of the materials. Preparing re-useable matrices always have promising future. A 50 nm thick TiO<sub>2</sub> layer was coated directly on surface of steel target plates and was used as matrix in SALDI-MS for analysis of amino acids, sugars, poly (ethylene glycol) (PEG) 200, and real sample of extracts from *Cynara scolymus* leaves [89]. Compared with TiO<sub>2</sub> nanopowder as matrix, the TiO<sub>2</sub> nanolayer showed a better performance for PEG 200, with around 30-fold improvement in signal intensity. Besides, this kind of TiO<sub>2</sub> nanolayer could be reused for many times,

promising for the scalable detection. Moreover, the hybrid nanomaterials of  $\text{TiO}_2$  are also good candidates for SALDI-MS materials. For example, core/shell nanoparticles of  $\text{Fe}_3\text{O}_4/\text{TiO}_2$  ( $\text{Fe}_3\text{O}_4/\text{TiO}_2$  NPs) were synthesized and used as affinity probes for the analysis of phosphor peptide in SALDI-MS [90] (Figure 4.5). Compared with micro  $\text{TiO}_2$  materials that have no well-designed nanostructure,  $\text{Fe}_3\text{O}_4/\text{TiO}_2$  NPs have a higher surface area ratio and better trapping capacities for phosphopeptides. In addition, by employing a magnetic field,  $\text{Fe}_3\text{O}_4/\text{TiO}_2$  NPs could be isolated from samples because of the magnetic property of  $\text{Fe}_3\text{O}_4$  core. These NPs were used to selectively pre-concentrate phosphor peptide from protein digests and the detection limit was as low as 500 pM for a digest solution of beta-casein (100  $\mu\text{L}$ ).

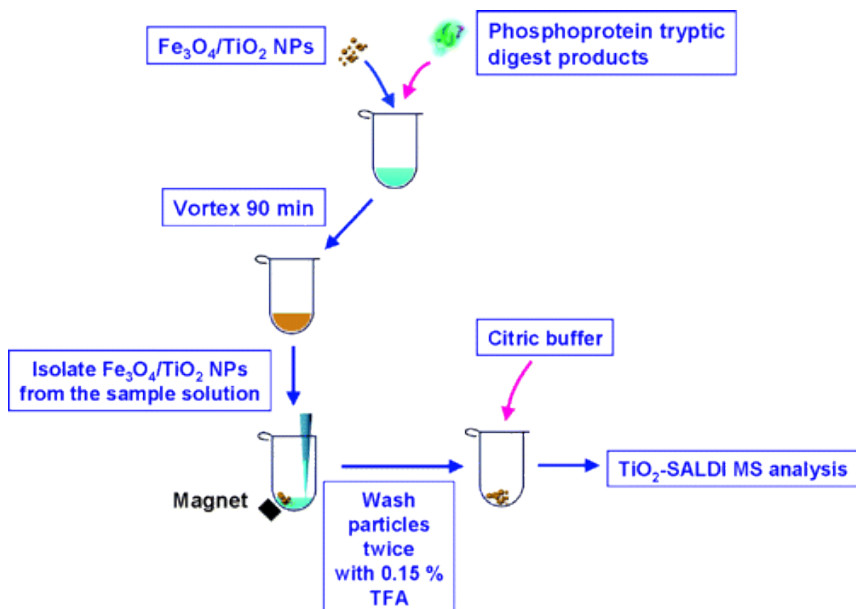


**Figure 4.5** Schematic illustration of workflow of SALDI-MS with  $\text{Fe}_3\text{O}_4/\text{TiO}_2$  NPs as the trapping adsorbents as well as matrix for analysis of aminothiols. Reproduced with permission from reference [90]. Copyright (2005) American Chemical Society.

Except for  $\text{TiO}_2$ , some other metal oxides have also been used as SALDI-MS matrix and showed that the structure (e.g., surface porosity and shape) of the metal oxides has strong influence on the DIE in SALDI-MS. For example, mesostructured tungsten titanium oxides (MTTO) were synthesized and applied as matrices in SALDI-MS [91]. With the as-prepared porous MTTO, the signal intensity of peptide, i.e., gramicidin S, was improved about 100

times in comparison with nonporous MTTO. The intensity improvement may be attributed to the coupling effect of porous structure and the strong ultraviolet absorption of MTTO. In addition, zinc oxide nanoparticles (ZnO NPs) with anisotropic shapes were prepared and used in SALDI-MS for analysis of polypropylene glycol (PPG) (average molecular weight 400) [92]. The results showed that ZnO NPs had high sensitivity to synthetic polymers, which is comparable to MALDI with DHB as matrix.

#### **4.2.3 Carbon nanomaterials**

Carbon materials consist a large family of carbon based materials, including fullerenes, carbon NPs, carbon nanotubes (CNTs), graphene, graphite oxide (GO) and carbon nanodots (C dots). These materials have strong optical absorption at wavelength range of 250-350 nm [93, 94], which are ideal materials for several lasers widely used in SALDI including N<sub>2</sub> (337 nm) laser and Nd:YAG lasers (266 and 355 nm). Because of such superior optical absorption as well as good thermal and electrical conductivity, these materials attracted great interests of scientists and are widely applied in SALDI-MS to analyze both small and large molecules [42, 95–98]. Fullerene C<sub>60</sub> [99] was first used as SALDI-MS matrix in 1994 to analyze phosphotungstic acid. In 1995, graphite particles with size ranging from 2 to 150 μm dispersed in glycerol were applied in SALDI-MS for analysis of peptides and proteins, as well as the other low molecular weight analytes [42]. The results showed that best spectra of the larger molecules were observed under dry condition and a sensitivity in the pico- to nano-mole range, which was as good as that in conventional MALDI. Because of the high surface area ratio and thermal conductivity, CNTs have been considered as excellent matrices for SALDI-MS. For example, CNTs were used as matrices in SALDI-MS for analysis of low molecular weight compounds [100]. The results showed that CNTs could reduce background interference and improve sensitivity and reproducibility of analyte signals, because the analytes such as peptides, organic compounds and beta-cyclodextrin could be trapped and enriched by CNTs. Moreover, CNTs could lower the laser threshold for desorption/ionization and avoid the fragmentation of the analytes. However, poor solubility of CNTs in both water and organic solvent make them aggregate easily which greatly suppresses the DIE of analytes in SALDI-MS. To overcome the obstacle, several strategies have been developed mainly by well-design of the chemical structure towards as-demand synthesis. For example, water-dispersible multiwall carbon nanotubes (MWCNTs) @polydopamine core-shell composites were synthesized and used as matrix for SALDI-MS for analysis of various water-soluble

small molecules [101]. The SALDI-MS results showed high peak intensities and good detection sensitivity could be obtained with LOD at 1 ng/mL for histidine.

Except for high surface area and thermal conductivity, graphene materials have excellent absorb ability in extraction and enrichment for a wide range of analytes, which make them particularly suitable as probes of analytes in SALDI-MS [102–108]. For example, Tang *et al.* [107] reported that graphene was an ultrahighly efficient platform for preconcentration and detection of single-stranded DNA (Figure 4.6). DNA-adsorbed graphene could be used directly for surface selected laser desorption/ionization (SELDI) TOF MS. The binding force of graphene with biomolecules (DNA and proteins) improved the extraction efficiency and detection sensitivity. Like the CNTs, pristine graphene also has the water soluble problem. Meanwhile, chemical oxidation of graphene (graphite oxide, GO) has improved water dispersibility and avoids the self-agglomeration. A lot of literatures have reported that GO could be good matrix for SALDI and SELDI-MS [102–104, 106, 108]. For example, GO was utilized as a dual-platform to enrich and detect tetracyclines (TCs) in SALDI-MS with free background interference in low mass range [108]. Due to the large surface area and strong interaction with TCs, GO served as an excellent matrix in SALDI-MS and the LOD of TCs was as low as 2 nM.

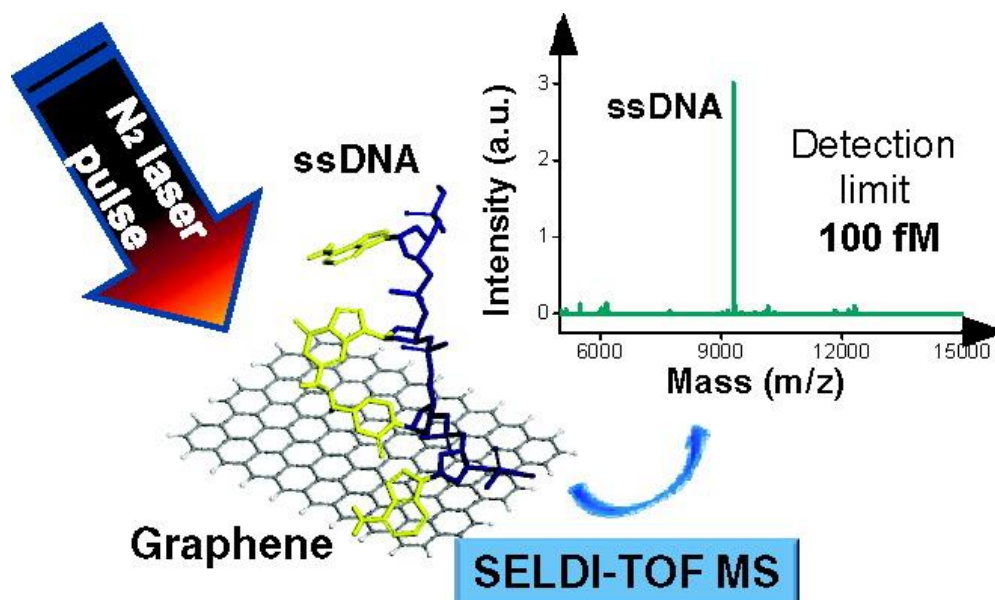


**Figure 4.6** Schematic illustration of workflow of SELDI-MS with graphene as matrix for analysis of DNA. Reproduced with permission from reference [107]. Copyright (2010)

American Chemical Society.

Recently emerged C dots are new family members in carbon nanomaterial. They have ultrafine dimensions, isotropic shapes and tunable surface functionalities and good biocompatibility. C dots were reported as matrix for the analysis of small molecules such as amino acids and beta-agonists by SALDI-TOF MS in both positive and negative ion modes [109]. The LOD of octadecanoic acid could be as low as 0.2 fmol.

#### **4.2.4 Silicon nanomaterials**

Silicon materials have high UV absorptivity and good thermal conductivity that fit well with the demanding of SALDI-MS matrix. In 1999, desorption/ionization on silicon (DIOS) was first reported for analysis of small molecules by Siuzdak and his co-workers [110], which opened a new era in detection of small molecules. Since then, silicon nanomaterials including silicon NPs, porous silicon, silicon films, silicon nanoarrays, silicon nanowires and silicon nanocomposites, were used as matrices for SALDI-MS to analyze all kinds of biomolecules [111–120].

Silicon materials are easy to be treated to get porous structures, providing great surface area of contact. Surface porosity could reduce the required thermal energy for effective analytes desorption by confining the heat and laser energy in the porous structure [121]. Therefore, by increasing porosity of silicon could increase surface roughness and ion yield [122]. Nanostructure-initiator mass spectrometry (NIMS) is one of the silicon porous structure substrates in SALDI-MS, which is very popular in recent studies [123–125]. NIMS uses a nanostructured or ‘clathrate’ surface to trap liquid (‘initiator’) compounds which will be subsequently released by laser irradiation for mass analysis. With NIMS, small molecules, drugs, lipids, carbohydrates and peptides could be adsorbed on its surface and then detected with low background and high sensitivity. Moreover, NIMS could also be used to analyze complex samples such as cells and bio fluids [125]. A study of the relationship between NIMS surface morphology and analyte selectivity was reported by Siuzdak *et al.* [124] (Figure 4.7). The results showed that the sensitivity of NIMS was affected by surface morphology significantly. The sensitivity of small molecules increased with porosity, whereas higher sensitivity for large molecules could be obtained with the NIMS with low surface porosity and small pore size. It is estimated that this transition occurred when the pore size is 3 times smaller than the maximum of molecular dimensions.

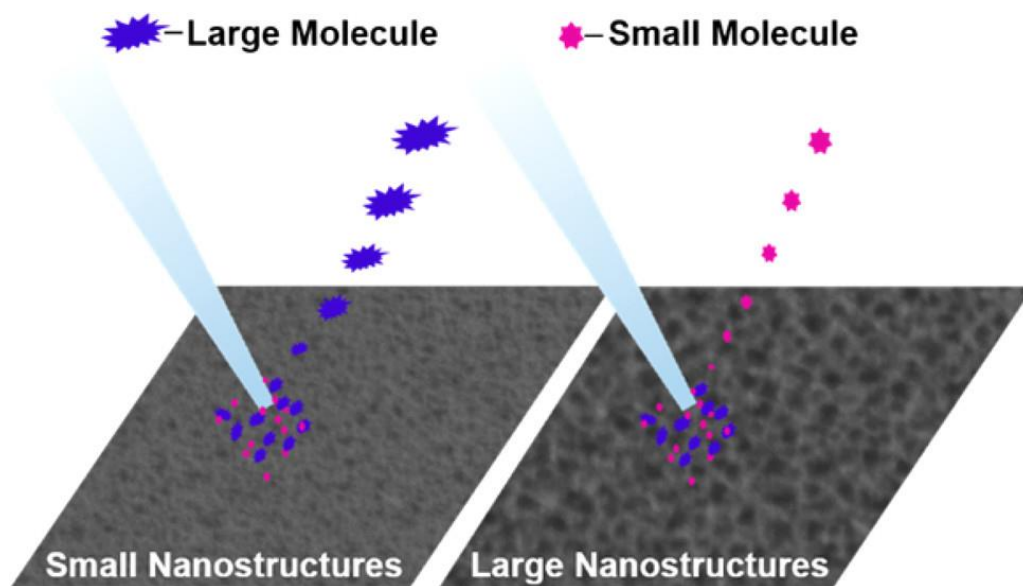


**Figure 4.7** Schematic illustration of the relationship between NIMS surface morphology and analyte selectivity. Reproduced with permission from reference [124]. Copyright (2017) American Chemical Society.

In addition, surface modification could further improve the DIE of porous silicon in SALDI-MS. There are plenty of works focusing on the surface functionalization of silica materials to help the extraction of analytes for better selectivity and sensitivity [126, 127]. For example, through layer-by-layer assembly, hyaluronic acid functionalized  $\text{Fe}_3\text{O}_4@ \text{SiO}_2$  nanoparticles ( $\text{Fe}_3\text{O}_4@ \text{SiO}_2@ \text{HA}$ ) with different sizes have been synthesized for facile extraction, detection and profiling serum biomarkers via ligand-protein interactions in SALDI-MS [126]. HA is easy to be bonded with silica shell, which is otherwise difficult to be functionalized directly on  $\text{Fe}_3\text{O}_4$ . With this method, HA-CD44 binding was achieved in both standard solutions and diluted serum samples; in the latter case, a detection limit of 0.6 ng/mL was reported.

Except for porous structure, silicon is easy to be fabricated to a lot of other nanostructures. Nanofabricated silicon nanopost arrays (NAPAs) were reported as effective matrix in SALDI-MS for analysis of metabolite extracts, peptides, drugs, explosives and tissue imaging [128–132]. Compared to other nanostructures, NAPAs offered dramatic increase of the ion yield, high reproducibility and controllable fabrication [133]. Under optimized condition, the LOD of verapamil from the NAPAs in SALDI-MS was as low as 6 amol. Moreover, after a long

period storage such as 1.5 years, the NAPA structures will not change their performance in mass spectra, indicating the potential for reusability of these structures.

Silicon materials have the advantages of cheap, stable and easy to modify. Therefore, it is convenient to make them into commercial substrates for SALDI-MS. In 2003, Waters Corp. released a commercial DIOS<sup>TM</sup> chip based on porous silicon. Modification of DIOS leads these substrates more functionalities for special analysis with low limit of detection. In a recent work [134], the detection limit of des-Arg9-bradykinin with 480 molecules (800 ymol) was obtained with pentafluorophenyl-functionalized DIOS chip. In 2007, the SiNWs substrates were made commercially available under the name NALDI<sup>TM</sup> from Nanosys, Inc. and Bruker Daltonics, Inc.. This substrate was specially designed for instruments of Bruker Daltonics Flex<sup>TM</sup> series and for the detection of low molecular weight compounds with  $m/z$  from 50 to 1500. A comparison between NALDI<sup>TM</sup> MS and conventional MALDI-MS for detection of small molecules was made, about 10 times more sensitivity was achieved with NALDI<sup>TM</sup> MS [135].

### **4.3 Quantitative analysis in MALDI-MS and SALDI-MS**

New discoveries in fundamental, industrial and clinical researches always demand quantitative data of the target molecules, either relatively or absolutely. In some sub-fields of biochemistry, such as proteomics, the project cannot move on without quantitative molecular analysis. It is a pity that many MS methods are not suitable or available for quantitative analysis. To address this issue, many efforts have been made on technological and methodological improvements. Currently, liquid chromatography with electrospray (LC-ESI) and gas chromatography (GC) are the best choices for quantitative analysis in MS. However, there are many limitations for these methods; for example, the procedure is complex and time-consuming, and not suitable for throughput measurements. While MALDI has the merits of high throughput, simple sample preparation and sensitive analysis, which attract many scientists. Although it still has some problems in quantitative analysis, including ion suppression and signal fluctuation, these problems tend to be less burdensome with the development of MALDI.

### 4.3.1 Quantitative analysis in MALDI-MS

MALDI-MS is notoriously known for its poor shot-to-shot and sample-to-sample signal reproducibility, limiting its application in quantitative analysis. The main reason for the poor signal reproducibility is the inhomogeneous recrystallization of matrix and analyte molecules, generating “sweet spot” and coffee-ring like structure during sample deposition and solvent evaporation [136]. Because of this drawback, MALDI-MS is usually used as a semi-quantitative analysis technique. To make MALDI to be suitable for reliable quantitative analysis, great endeavour has been made in the past decades. For example, the signal reproducibility could be improved by using a fourier transform ion cyclotron resonance (FTICR) or a triple-quadrupole (qqq) mass spectrometer in a multi reaction monitoring (MRM) or a selected reaction monitoring (SRM) mode [137, 138]. In addition, the use of internal standard (IS) could also overcome some part of this limitation. For example, Emilia Szajli *et al.* [139] investigated the reliability of MALDI for quantitative analysis by using a statistical calculation of the inverse confidence limit. They reported that the use of isotope-labeled IS led to dramatic increase in precision. However, the isotope-labelled IS are quite expensive and not available for common use. Therefore, the compounds which have similar structure with that of analytes were proposed as IS. Volmer *et al.* [140] assessed the performance of different small molecules as IS in quantitative analysis in MALDI-MS. The results showed that closely matched molecular weight and structural similarities between analyte and IS are essential parameters for acceptable quantitative analysis data. Moreover, signal reproducibility could also be improved by using high frequency laser to create massive data and doing data average [141, 142]. A high repetition rate laser, with a 100 fold increase of the pulse frequency as compared to the standard one, was introduced in MALDI source which created massive accumulated data [141]. By increasing the reproducibility and intensity, the RSD of sample signal was greatly decreased to be lower than 5% after taking into account of the area ratio of analyte to IS. The magnitude of the dynamic range of the calibration curves was increased at least two and three orders by using a qqTOF and qqq platforms, respectively.

By introducing some other designs, such as novel matrix or special target plate [143–147], the signal reproducibility in MALDI could also be improved. However, most significant improvements in quantitative analysis in MALDI-MS were from modified sample preparation. Some strategies, including fast solvent evaporation [21], electrospray techniques [22, 148], seed layer approaches [149, 150], hydrophobic target coatings [23, 24], and so on [151–153], have been employed to improve the sample preparation and most of which

showed improvement in the signal reproducibility. For example, Avinash Patil *et al.* [153] produced homogeneous layer of samples for MALDI with a simple forced dried droplet method. The author found that signal reproducibility was improved with RSD of 16%, which is acceptable for quantitative analysis. Russell Hensal *et al.* [148] used electrospray method to deposit samples on surface of target plate that have significantly improved the sample homogeneity. The improved homogeneity in electrosprayed samples decreased not only the short-to-short but also the sample-to-sample variability, in which lead to a decrease in coefficient of variation (CV) of MS signal (15.1% or better as compared to 49.6% for the drop-dried samples). Onnerfjord *et al.* [149] prepared homogeneous samples for MALDI-MS with a seed layer method which is also called a two-layer method. With this method, the surface homogeneity and sample-to-sample reproducibility were highly improved with variations within-sample and between-sample at a 95% confidence level. A linear calibration curve of human insulin was obtained within one order of magnitude using bovine insulin as IS ( $R^2 > 0.996$ ). Martin Pabst *et al.* developed a platform based on microarray for mass spectrometry (MAMS) technology and the parallel lanes of hydrophilic reservoirs to prepare homogeneous sample for MALDI-MS [154] (Figure 4.8). Due to the interplay of hydrophobic/hydrophilic interaction, the samples were rapidly and automatically aliquoted into sample spot. With this device, a few microliters of sample could be aliquoted up to 40 replicates within seconds, and each aliquot contains only 10 nL. The evaporation of the solvent was very fast and sample was dispersed quite homogeneously. The quantitative analysis of [Glu<sup>1</sup>]-fibrin peptide B with CHCA as matrix was successfully achieved with calibration range of 0.2–2  $\mu\text{g/mL}$  and  $R^2$  higher than 0.99.

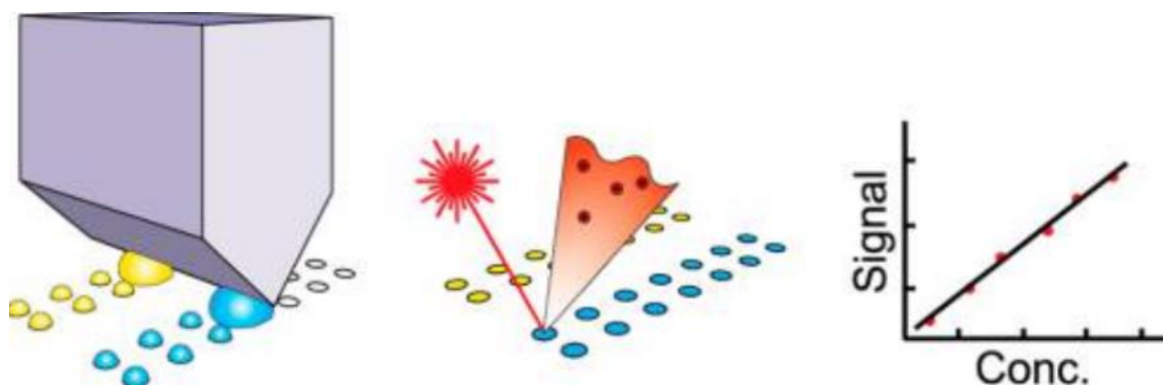


**Figure 4.8** Schematic illustration of workflow with a self-aliquoting microarray plate for quantitative analysis. Reproduced with permission from reference [154]. Copyright (2013) American Chemical Society.

Except for the method mentioned above, adjusting solution pH and solvent composition can also alter the crystallization behaviour and then improve the sample homogeneity [8, 155, 156]. However, the sweet spot issue remains. To overcome this problem more effectively, liquid matrix such as ionic liquids have been used. Ionic liquids have showed great potential to make homogeneous sample for quantitative analysis of biomolecules with higher sensitivity [25, 26, 157, 158]. Li *et al.* tested several CHCA-based ionic liquids (1-methyl imidazolium-CHCA, diethyl ammonium-CHCA and pyridinium-CHCA) as matrices in MALDI for quantitative analysis of different molecules including peptides, small proteins and oligodeoxynucleotides [26]. With homogeneous sample preparation, high signal reproducibility was obtained with RSD from 2% to 6% and good calibration curve were achieved with  $R^2$  from 0.992 to 0.998 for Tyr-bradykinin. The authors found that the slopes of the calibration curves had an inverse relation with the peptide molecular weights, which could be used to predict the relative sensitivities for similar analytes.

#### **4.3.2 Quantitative analysis in SALDI-MS**

In SALDI-MS, there is no co-crystallization of analytes and inorganic nanomaterials. Therefore, the homogeneity of inorganic nanomaterials and analytes would be improved in some level. The increased homogeneity of samples would increase signal reproducibility of analytes in SALDI-MS [55, 60, 71, 159–163]. For example, Shoji Okuno *et al.* made a comparison about quantitative analysis of polypropylene glycol (PPG) mixtures between MALDI (using DHB and CHCA as matrices) and SALDI (using DIOS as matrix) [159]. By a systematic study of the factors influencing signal reproducibility, the authors found that DIOS was more suitable for quantitative analysis. Furthermore, the sample homogeneity could be improved by using nanomaterials with smaller size. Ultrathin graphitic carbon nitride (g-C<sub>3</sub>N<sub>4</sub>) nanosheets were used as novel matrices for negative ion mode in SALDI-MS for detection of small molecules [163]. The homogeneity of sample dispersion was improved because of the small size of this g-C<sub>3</sub>N<sub>4</sub> nanosheets. By analysing histidine, good reproducibility was achieved with RSD of shot-to-shot variation less than 19.3% (n=5) and sample-to-sample variation less than 13.3% (n=10).

Selective absorption of analytes on nanomaterials surface could increase the signal reproducibility in SALDI-MS [55, 57, 164, 165]. Using ligands of inorganic materials as IS has been developed for quantitative analysis of analytes with high accuracy and precision in SALDI-MS [166, 167]. As mentioned in the previous section, due to the special Au-S

interaction, AuNPs were used to selectively capture amino thiols to achieve a sensitive and reproducible detection [57]. For example, N-2-mercaptopropionylglycine capped AuNPs were designed as extractor, IS as well as matrix in SALDI-MS to detect amino thiols like cysteine, GSH and homocysteine [167]. The results showed that this approach provided good quantitative linearity with  $R^2$  around 0.99 and reproducibility with RSD less than 10 %. In addition, CdS quantum dots (QD) were synthesized as matrix for SALDI-MS to quantify carbohydrates [164]. The carbohydrates could be selectively absorbed on surface of CdS due to hydrogen bond, which leads to the sensitivity and reproducibility of SALDI-MS measurements greatly improved. The relative error for eight individual measurements was less than 4% for measurement of glucose in human serum.

To achieve quantitative analysis in SALDI-MS, some other designs have been developed. Ordered nanostructures of inorganic materials were taken as superior matrix for quantitative analysis in SALDI-MS. For example, vertically aligned silicon nanopillar arrays were fabricated as matrix for SALDI-MS to detect methadone and peptides [168]. Under optimized condition, good calibration curve with  $R^2 > 0.99$  and linear rang of 20–2000 ng/mL were obtained. As a real sample application, the quantitative analysis of methadone in Milli-Q water was achieved with a high sensitivity of 32 ng/mL. Controlling sample size to be smaller than the diameter of laser spot enables all analytes to be desorbed/ionized in one laser shot, which minimizes the signal variation in SALDI-MS [117, 169]. The ordered hydrophobic silicon nanocone arrays with hydrophilic spot of 50  $\mu\text{m}$  was designed as matrix in SALDI to increase signal reproducibility[169] (Figure 4.9). All the analytes were concentrated in the hydrophilic spot which is smaller than the laser spot, making it possible to desorb and ionize all the analytes in one spot. Good reproducibility was obtained with RSD lower than 12.6 %. Quantitative analysis of R6G was achieved with good linear dependence ( $R^2 > 0.98$ ), in a wide concentration range from 1nM to 1  $\mu\text{M}$  and low LOD of 1 fmol.

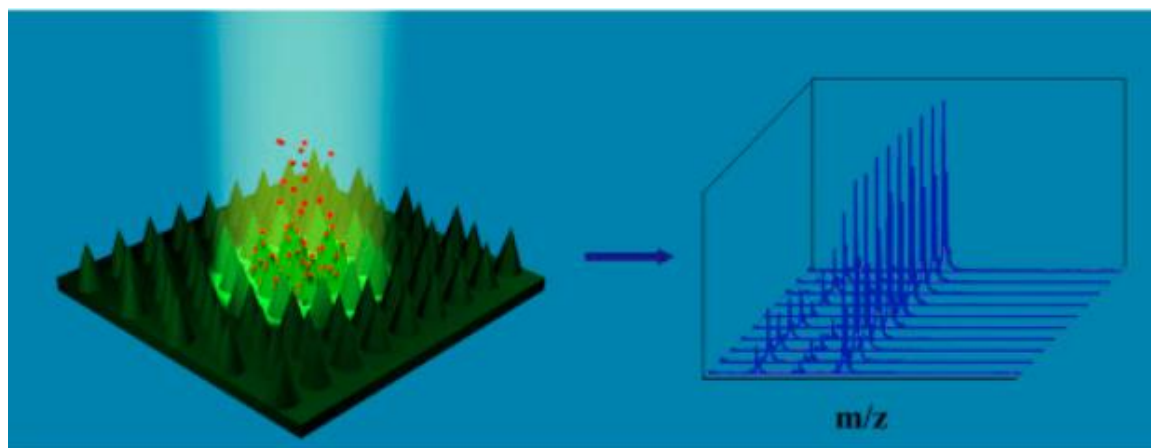


**Figure 4.9** Schematic illustration of SALDI-MS with silicon nanocone array as matrix for quantitative analysis. Reproduced with permission from reference [169].

Recent studies showed that homogeneous distribution of nanomaterials to form continuous film-like substrates decreased sweet spot formation and increased signal reproducibility in SALDI-MS [9, 170–176]. For example, multilayer thin films of alternating reduced graphene oxide (rGO) and AuNP [LBL rGO/AuNP] were fabricated by spin coating method and applied as platform for effective quantitative analysis in SALDI-MS [174]. By optimizing the layer number of rGO and AuNPs, the signal stability and reproducibility were highly improved as compared to standard single layer sample. The RSD for glutathione signal in SALDI-MS was less than 15%. Multi-layered AuNP thin films (MTF-AuNPs) were fabricated and used in SALDI-MS to detect a bone biomarkers for assessment of osteoporosis at the early stage [170]. The MTF-AuNPs had highly ordered and homogeneous structure, which allowed the detection of hydroxyproline (HYP) with high sensitivity and excellent reproducibility, i.e., with RSD of 9.3%. Choi *et al.* used a large area graphene film as interacting target surface, on which matrix and analytes were drop-casted and an optically uniform sample layer spontaneously formed [172]. The mass measurements showed that signal reproducibility over the entire sample was highly improved (RSD <10%) and the sweet spots were effectively suppressed. With this method, good linear responses of ion intensity of small peptides (angiotensin II and glu-fibrinopeptide B) were achieved. Electrospray deposition (ESD) technique was used to deposit analytes on DIOS in SALDI-MS for quantitative analysis of amino acids and peptide [177]. With this technique, the analytes were homogeneously dispersed on surface of porous silicon. Compared with traditional drop-dried method, the ESD prepared samples exhibited significantly improved sample to sample reproducibility, with typical RSD values less than 7%. A homogeneous and highly oriented

cuboctahedra AgNPs films were prepared with a Langmuir-Blodgett (LB) method and used as effective sample plate for SALDI-MS to analyze glucose [76] (Figure 4.10). Moreover, the sweet spot issue was eliminated that benefited the quantitative analysis. In comparison with traditional MALDI matrices like CHCA, the absolute ion intensities, signal-to-noise ratios, background noise and reproducibility were highly improved by using LB films as sample plate. For the signal of  $[\text{glucose} + \text{Na}]^+$ , the RSD was only 5.7% because of the improved homogeneity of the sample. Au-nanobowl arrays were prepared as matrix for SALDI-MS to improve signal reproducibility, and enabled quantitative analysis of oligonucleotides and polypeptides [171]. The RSD for measurements of oligonucleotide ( $6.6 \mu\text{M}$ ) was as low as 3.3%. For this kind of substrates, it is not necessary to select measurement location because of homogeneous distribution of the sample.

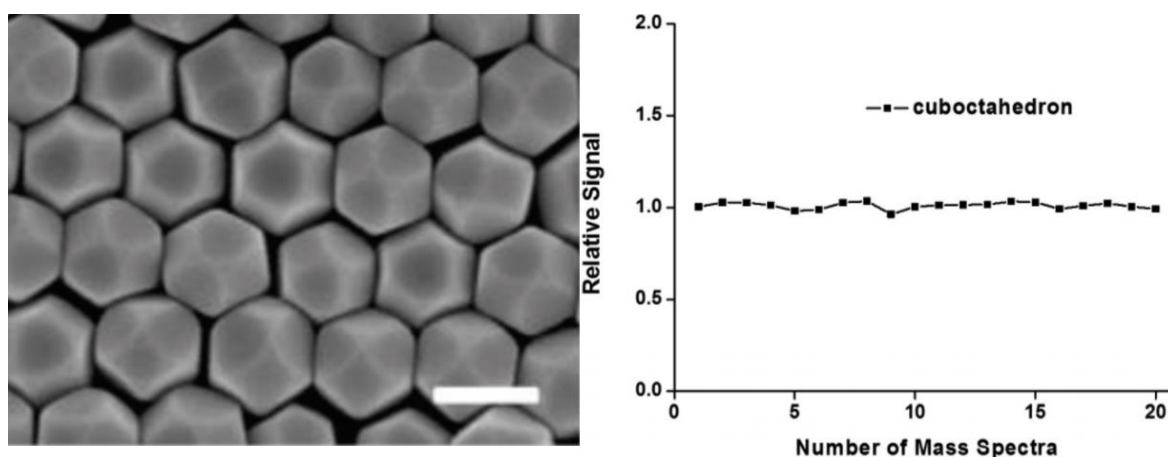


**Figure 4.10** Scanning electron microscopy data of silver cuboctahedra film (left) prepared with Langmuir-Blodgett (LB) method and reproducibility of glucose with the as-prepared LB film as matrix in SALDI-MS (right). Reproduced with permission from reference [76].

#### 4.4 Objective

MALDI and SALDI are powerful techniques in bioanalytical analysis and attract lots of attention in the past decades. As indicated by the closely related studies mentioned above, the signal fluctuation and bad signal reproducibility caused by inhomogeneous deposition have been taken as the main obstacles in restricting their applications in quantitative analysis. The aim of this work is to develop novel methods that are easy-to-operate, low-cost, and high-throughput to prepare samples with well-controlled structure for quantitative analysis of small biomolecules including lipids and endogenous metabolites in MALDI-MS and SALDI-MS.

To achieve this goal, a channel target plate has been designed for MALDI-MS measurements, to inhibit the inhomogeneity issue of organic matrices triggered by coffee-ring effect during solvent evaporation. Moreover, AuNP layers with well-controlled layer thickness and homogeneity, prepared with a home-made device inspired by Langmuir-Blodgett trough, have been used as the SALDI-MS substrates to improve the analytes' signal reproducibility. Besides, to further improve the sensitivity and availability, the AuNPs with well-designed structure, including capping ligand and particles' size, have been systematically used as the matrix in SALDI-MS to study the affecting parameters on DIE.

The simplicity, sensitivity and real sample application, which are common criteria to judge the quality of the MS method, are employed in this thesis for evaluating the methods mentioned above. Moreover, important factors influencing desorption/ionization efficiency (DIE) and signal reproducibility of analytes have been investigated to improve detection sensitivity and reliability. We believe that our new methods contribute to quantitative analysis of biomolecules with MALDI-MS and SALDI-MS, because of their simplicity, low detection limit and also improved signal reproducibility.

## V List of publications

**The results of the dissertation have been published in the following peer-reviewed journals:**

1. **Zhen Liu**, Peng Zhang, Lars Kaestner, Dietrich A Volmer, A simple MALDI target plate with channel design to improve detection sensitivity and reproducibility for quantitative analysis of biomolecules, **Journal of Mass Spectrometry**, 2019, 54, 878–884.
2. **Zhen Liu**, Peng Zhang, Thomas Kister, Tobias Kraus, Dietrich A. Volmer, Ultra-thin homogeneous AuNP monolayers as tunable functional substrates for surface-assisted laser desorption/ionization of small biomolecules, **Journal of the American Society for Mass Spectrometry**, 2020, 31, 1, 47-57.
3. **Zhen Liu**, Peng Zhang, Andrea Pyttlik, Tobias Kraus, Dietrich A. Volmer, Influence of core size and capping ligand of gold nanoparticles on the desorption/ionization efficiency of small biomolecules in AP-SALDI-MS, **Analytical Science Advances**, 2020, in press ([doi.org/10.1002/ansa.202000002](https://doi.org/10.1002/ansa.202000002)).

## **Publication 1**

# **A simple MALDI target plate with channel design to improve detection sensitivity and reproducibility for quantitative analysis of biomolecules**

Zhen Liu, Peng Zhang, Lars Kaestner, Dietrich A Volmer,

*Journal of mass spectrometry*, 2019, 54, 878–884, <https://doi.org/10.1002/jms.4447>

This article is open access and permits to use with proper citation.

## RESEARCH ARTICLE

# A simple MALDI target plate with channel design to improve detection sensitivity and reproducibility for quantitative analysis of biomolecules

Zhen Liu<sup>1</sup> | Peng Zhang<sup>2</sup>  | Lars Kästner<sup>3</sup> | Dietrich A. Volmer<sup>4</sup> 

<sup>1</sup>Institute of Bioanalytical Chemistry, Saarland University, Saarbrücken, Germany

<sup>2</sup>School of Materials Science and Engineering, Sun Yat-sen University, Guangzhou, China

<sup>3</sup>Department of Anatomy and Cell Biology, Saarland University, Homburg, Germany

<sup>4</sup>Department of Chemistry, Humboldt University of Berlin, Berlin, Germany

**Correspondence**

Prof. Dr. Dietrich A. Volmer, Department of Chemistry, Humboldt University of Berlin, Brook-Taylor-Str. 2, Berlin 12489, Germany. Email: dietrich.volmer@hu-berlin.de

**Funding information**

China Scholarship Council

**Abstract**

Overcoming the detrimental effects of sweet spots during crystallization is an important step to improve the quantitative abilities of matrix-assisted laser desorption/ionization (MALDI) mass spectrometry. In this study, we introduce MALDI targets, which exhibit a channel design to reduce sweet spot phenomena and improve reproducibility. The size of the channels was 3.0 mm in length, 0.35 mm in depth, and 0.40 mm in width, adjusted to the width of the implemented laser beam. For sample deposition, the matrix/sample mixture was homogeneously deposited into the channels using capillary action. To demonstrate the proof-of-principle, the novel plates were used for the quantification of acetyl-L-carnitine in human blood plasma using a combined standard addition and isotope dilution method. The results showed that the reproducibility of acetyl-L-carnitine detection was highly improved over a conventional MALDI-MS assay, with RSD values of less than 5.9% in comparison with 15.6% using the regular MALDI method. The limits of quantification using the new plates were lowered approximately two-fold in comparison with a standard rastering approach on a smooth stainless-steel plate. Matrix effects were also assessed and shown to be negligible. The new assay was subsequently applied to the quantification of acetyl-L-carnitine in human plasma samples.

**KEYWORDS**

acetyl L carnitine, channel plates, MALDI-MS, plasma, quantification

## 1 | INTRODUCTION

During the sample preparation for MALDI-MS, the analytes are co-crystallized with a chemical matrix such as  $\alpha$ -cyano-4-hydroxycinnamic acid (CHCA) or 2,5-dihydroxybenzoic acid (DHB). Because of commonly observed heterogeneous co-crystallization of matrix and analytes, ion signals usually fluctuate strongly from laser shot to shot and from sample spot to spot, as dried matrix/analyte mixtures form

sweet spots on the sample targets. MALDI-MS is therefore often dismissed as a quantitative technique.

There are, however, multiple methods to improve the reproducibility of MALDI-MS to levels similar to LC-MS techniques.<sup>1,2</sup> For example, using an internal standard for the analytes that matches solution phase and ionization properties has been shown to strongly improve reproducibility.<sup>3-5</sup> The obvious choices for this purpose are stable isotope standards, but unfortunately, often these standards are not

This is an open access article under the terms of the Creative Commons Attribution License, which permits use, distribution and reproduction in any medium, provided the original work is properly cited.

© 2019 The Authors. Journal of Mass Spectrometry published by John Wiley & Sons Ltd

commercially available or very expensive. Alternatively, methods that improve the sample preparation procedures to force a homogenous distribution of matrix and analytes have been shown to significantly improve signal homogeneity. Methods that achieve these homogenous crystallizations include hydrophobic target coatings,<sup>6,7</sup> fast evaporation methods,<sup>8</sup> electrospraying techniques,<sup>9,10</sup> or seed layer approaches.<sup>11,12</sup> In addition, Zenobi and coworkers developed a self-aliquoting microarray plate that contains parallel lanes of hydrophilic reservoirs into which the samples were deposited using a metal sliding device. These arrays reduced sample requirements to just 10  $\mu\text{L}$  per aliquot and exhibited excellent quantitative abilities, as demonstrated for angiotensin II and [Glu<sup>1</sup>] fibrinopeptide B.<sup>13</sup> Finally, large-area graphene films were used as target surface to improve reproducibility of matrix/analytes preparation for quantification of biomolecules in MALDI-MS.<sup>14</sup>

The downside of many of these techniques is that they require specialized hardware and that they are not as simple and convenient to use as conventional metal target plates. In this article, we describe a simple channel plate design to improve the reducibility of MALDI quantification, by forcing the matrix/analyte to dry within a narrowly confined cuboid of a few microliter internal volume on the steel target plates and subsequent scanning of the entire crystallized area using the MALDI laser beam. The quantitative abilities of this design were demonstrated for the analysis of acetyl-L-carnitine in human blood plasma matrices.

## 2 | EXPERIMENTAL

### 2.1 | Chemicals and materials

CHCA (alpha-cyano-4-hydroxycinnamic acid), acetyl-L-carnitine, and *d*<sub>3</sub>-acetylcarnitine were purchased from Sigma-Aldrich (Steinheim, Germany); trifluoroacetic acid (TFA) was from Fisher Scientific (Schwerte, Germany); acetonitrile, methanol, and isopropanol were from VWR (Darmstadt, Germany). Deionized water was generated by a Millipore (Bedford, Massachusetts) water purification system.

### 2.2 | Blood plasma samples

Human plasma was prepared from blood samples from two healthy volunteers (with ethical permission, local research ethics committee, Ärztekammer des Saarlandes, ref. no. 51/18).

### 2.3 | Sample preparation

CHCA was prepared in methanol (TFA, 0.1% v/v) at 10 mg/mL. Acetyl-L-carnitine and *d*<sub>3</sub>-acetyl-L-carnitine were dissolved in water at 1 mM as stock solutions. All stock solutions were stored at  $-20^{\circ}\text{C}$  and diluted to the required concentration prior to use.

Samples were prepared from 100  $\mu\text{L}$  of plasma and 100  $\mu\text{L}$  of internal standard solution (20.00  $\mu\text{M}$ ). To this mixture, 5 mL of acetonitrile/methanol (3:1 v/v) were added, and the combined mixture

vortexed for 10 seconds, followed by centrifugation at 13 000 rpm (5 min); the supernatant was transferred into a new plastic tube. Centrifugation was repeated once more, and the combined supernatants were evaporated under vacuum in a homemade system; 100  $\mu\text{L}$  of water was added, followed by vortexing for 5 minutes at  $35^{\circ}\text{C}$  and centrifugation at 13 000 rpm (5 min).

### 2.4 | Calibration curves based on isotope dilution and standard addition

Acetyl-L-carnitine at different concentrations was added to plasma and vortexed for 30 seconds, followed by addition of CHCA solution. A volume of 0.40  $\mu\text{L}$  of this mixture was pipetted into the channels and dried under ambient environments.

For calibration, standard solutions of acetyl-L-carnitine at 0.50  $\mu\text{M}$ , 1.00  $\mu\text{M}$ , 2.00  $\mu\text{M}$ , 5.00  $\mu\text{M}$ , 10.00  $\mu\text{M}$ , 20.00  $\mu\text{M}$ , 37.50  $\mu\text{M}$ , and 50.00  $\mu\text{M}$  were used. Calibration curves were obtained by using a combined standard addition/isotope dilution method as described by Lee et al, to improve accuracy and precision<sup>15</sup>:  $y = b \times (c_{\text{sample}} + x)$ , where  $y$  = isotope ratio  $IR_{\text{sample}}$ ,  $b = k \times / (c_{\text{is,sol}} \times V_{\text{is,sol}}/V_{\text{sample}})$  and  $x = (V_{\text{s,sol}} \times c_{\text{s,sol}})/V_{\text{sample}}$ .  $k$  is the response factor of the instrument. In our experiments,  $c_{\text{is,sol}}$ ,  $V_{\text{is,sol}}$  and  $V_{\text{sample}}$  were always invariant; therefore, both  $b$  and  $k$  were constants;  $c_{\text{sample}}$  = concentration of native acetylcarnitine in the sample,  $IR_{\text{sample}}$  = intensity ratio of acetylcarnitine to *d*<sub>3</sub>-acetylcarnitine,  $c_{\text{is,sol}}$  concentration of standard *d*<sub>3</sub>-acetylcarnitine solution,  $V_{\text{is,sol}}$  volume of standard *d*<sub>3</sub>-acetylcarnitine solution,  $V_{\text{sample}}$  volume of sample,  $V_{\text{s,sol}}$  volume of standard acetylcarnitine solution, and  $c_{\text{s,sol}}$  concentration of standard acetylcarnitine solution. The sample concentration ( $c_{\text{sample}}$ ) was obtained from the negative  $x$  intercept value by plotting experimental data as  $y$  versus  $x$  after least-squares fitting. An 8-point calibration curve was used (with 10 technical replicates at each concentration level). As a comparison, the calibration curve of acetyl-L-carnitine from a conventional smooth stainless-steel target plate was used, with identical concentrations as those used on the channel target plate.

### 2.5 | Evaluation of matrix effects

To evaluate matrix effects, a calibration curve of acetylcarnitine from spiked pure solvent (water) was used, with identical concentrations as those used in human plasma. We assessed plasma matrix effects by comparing the signals of acetyl-L-carnitine in water with that in plasma. The relative ratio of the slopes  $b_{\text{serum}}/b_{\text{water}}$  was used as indicator for matrix effects.

### 2.6 | Trueness and precision

For trueness evaluation, 3 three quality controls (1.00  $\mu\text{M}$ , 5.00  $\mu\text{M}$  and 20.00  $\mu\text{M}$ ) were incorporated into each calibration curve and measured five times.

Precision was assessed by repeatability (intraday) and intermediate (interday) precision. Precision was determined from five same-day

replicates and daily measurements over a period of 5 days. The results were expressed as % RSD.

## 2.7 | MALDI channel plates and sample preparation

Custom channel plates were made in the university workshop using commercial stainless steel plates (Figure 1). Length, width, and depth of the channels were 3.0, 0.35, and 0.40 mm, respectively.

## 2.8 | Mass spectrometry

MS experiments were performed with a Bruker Esquire HCT+ 3-D ion trap (Bremen, Germany) coupled with a MassTech (Burtonsville, Maryland) atmospheric pressure MALDI source. An Nd:YAG laser with wavelength of 355 nm was used as the light source. Laser energy was set to 50% and repetition rate at 200 Hz. Mass spectra were acquired in positive ionization mode. The mass spectrometer was set to smart mode with drying gas temperature at 300°C and flow rate at 5.0 L/min. Acetyl-L-carnitine and  $d_3$ -acetyl-L-carnitine were detected in multiple reaction monitoring (MRM) using a relative collision energy of 0.50. Two transitions per analyte were monitored, viz,  $m/z$  204  $\rightarrow$  145 and 204  $\rightarrow$  85 for acetyl-L-carnitine, and  $m/z$  207  $\rightarrow$  145 and 207  $\rightarrow$  85 for the  $d_3$  isotope standard. For data acquisition, horizontal rastering was used to cover the entire sample area for each channel at a speed of approximately 40 mm/min, resulting in 30-second-long signal profiles per sample channel (approximately 6000 laser shots were averaged per channel; individual data points along the channel were acquired for 4 s in 0.4 mm steps; data acquisition started 0.25 mm before each channel and stopped 0.25 mm after).

## 2.9 | SEM and light microscope images

The morphologies of CHCA/acylcarnitine co-crystals within the channels and on the surface of the conventional target plates were characterized by secondary electron microscopy (DEI Quanta 400, Hillsboro, Oregon) and Moticam 3.0 (Motic Deutschland, Wetzlar, Germany).

## 3 | RESULT AND DISCUSSION

In this study, we introduced a new target plate with customized channels to improve sample homogeneity and reproducibility in quantitative MALDI-MS. As shown in Figure 1, the channels were milled into the center of the sample spots of a regular MALDI plate, giving an 8  $\times$  12 matrix of 96 channel wells. The length, width, and depth of each of the cuboid channels were 3.0, 0.35, and 0.40 mm, respectively. The width was marginally narrower than the diameter of the used laser beam, which was 0.40 mm, making sure that the beam covered the entire width of the channel, while the beam was moved along the length of the channel during data acquisition.

We used acetyl-L-carnitine in human plasma as analyte to demonstrate the abilities of the new plate. Acylcarnitine is an essential endogenous metabolite in mammals, usually at concentration levels in the range of 3 to 14  $\mu$ mol/L in plasma.<sup>16-18</sup> As the metabolism of acetyl-L-carnitine is closely linked to a variety of metabolic problems, it is routinely monitored in clinical diagnostics, usually by using LC-MS techniques. As LC-MS methods typically include a time-consuming chromatography step, MALDI-MS was investigated here as a potentially faster alternative to LC-MS.<sup>19</sup> It has been previously demonstrated that MALDI-MS provided quantitative abilities comparable with ESI-based LC-MS/MS for pharmaceutical drugs and biological fluids,<sup>20-22</sup> with comparable analytical figures of merit, but analysis times of up to 100 times faster.

### 3.1 | Comparison between channel and conventional target plates

The most desired feature of the new channel plate was to improve the quantitative reproducibility of MALDI analysis, by introducing constant volumes of sample and matrix solution into each of the well-defined channels and by illuminating the entire sampling surface with the laser light. In order to fill the channels with a well-defined, constant amount of sample solution, a 0.4  $\mu$ L of the sample solution was pipetted into the channels (Figure 2A). The solutions spontaneously and evenly distributed within the channels by means of capillary action (a short video clip of this procedure is shown in the Supporting

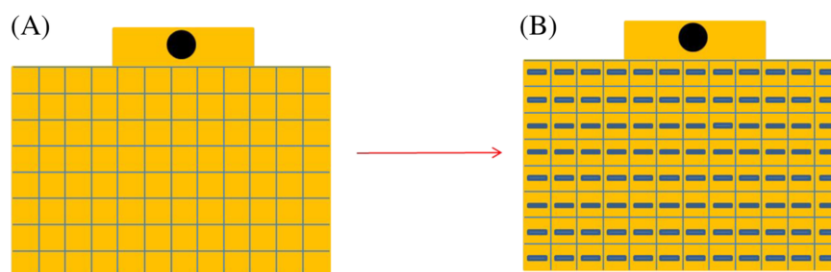


**FIGURE 1** Schematic diagram of the MALDI target plates: (A) original target and (B) customized channel target. The channel size is as follows: length, 3.00 mm; width, 0.35 mm; depth, 0.40 mm. Matrix is added to channels using capillary action, and the analytes are added using a micropipette

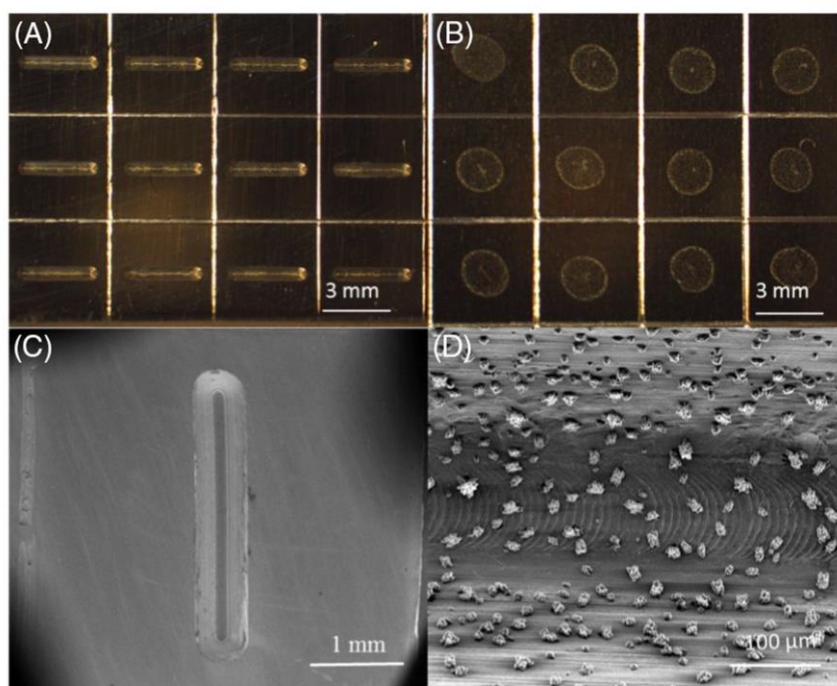


**FIGURE 2** Light microscope images of samples on (A) channel plates and (B) smooth conventional stainless steel MALDI plates. (C) and (D) are scanning electron microscopy (SEM) images of sample/matrix mixtures deposited into the channels at different magnification levels [Colour figure can be viewed at [wileyonlinelibrary.com](http://wileyonlinelibrary.com)]

Information, with added methyl orange dye to improve visibility). As the solvent evaporates, co-crystals of analytes/matrix readily formed within the channels without the possibility for a coffee ring effect, similar to the forced co-crystallization of analyte/matrix on hydrophobic surfaces.<sup>7,13</sup> For comparison, the same solution was pipetted onto a conventional stainless-steel target plate, resulting in the well-known coffee ring effect (Figure 2B).

The homogenous nature of the sample matrix crystals within channels, without any coffee ring formation, was further illustrated at higher magnifications using SEM (Figures 2C,D). According to Wong et. al, there is a minimal size for coffee ring structures for different materials.<sup>23</sup> The authors point out that for suspended particles of about 100nm size, the minimum diameter of the coffee ring structures is around 10 μm. In our channels, the surface is very rough, effectively dividing the channel surface into smaller subcompartments of few micrometers size or even smaller. We hypothesize that these small compartments are individually filled with CHCA and acetyl-L-carnitine crystals, preventing the formation of coffee ring structures in the channels such as those seen on the smooth regular steel surfaces.

### 3.2 | Reproducibility

Under optimized MALDI-MS/MS condition, we evaluated the reproducibility of the acetyl-L-carnitine signal produced from different channels across the plate. A plot of relative intensity (analyte/internal

standard) of acetyl-L-carnitine from 10 different channels is shown in Figure 3. The relative standard deviation in these experiments was less

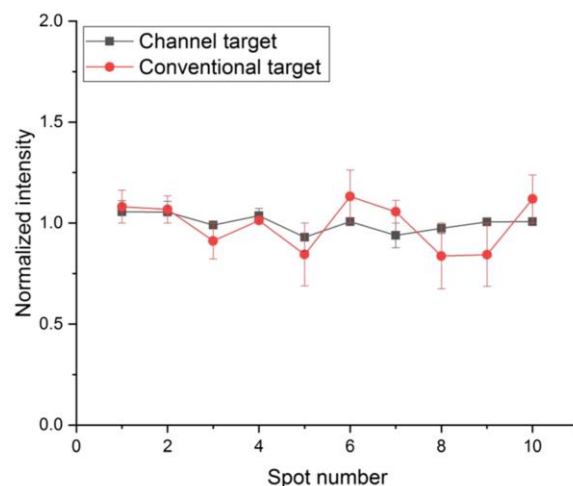


**FIGURE 3** Reproducibility of measurement of acetyl-L-carnitine across 10 different samples from a channel plate in comparison with a conventional plate at equal concentration levels (analyte and internal standard, 20.00 μM each). The intensity ratio of acetyl-L-carnitine to  $d_3$ -acetyl-L-carnitine was normalized and displayed on the y axis [Colour figure can be viewed at [wileyonlinelibrary.com](http://wileyonlinelibrary.com)]

than 5.9%. In comparison, the relative standard deviation from a conventional target plate was 15.6%.

The improved signal reproducibility largely resulted from the complete consumption of the sample/matrix crystals within the channels, which effectively removed sweets spots issues. Complete laser ablation during quantitative MALDI has previously been shown to greatly improve precision.<sup>2,13</sup> In our experiments, the channels were 0.35 mm wide, while the laser beam's diameter was slightly larger, viz, 0.40 mm, thus enabling the entire width of the channel to be irradiated.

### 3.3 | Calibration curves

Standard addition method is commonly used to quantify endogenous compounds in complex biological samples, when no blank sample matrix is available. Here, we used this technique for the quantification of acylcarnitine in human plasma. The calibration curve was obtained by plotting the intensity ratio of acetyl-L-carnitine to  $d_3$ -acetyl-L-carnitine against the added concentration (Table 1). In comparison, a calibration curve of acetyl-L-carnitine from a conventional smooth target plate was used. Table 1 clearly shows, however, that all investigated analytical figures of merit obtained from the channel plate were superior to the conventional plate.

### 3.4 | Limits of quantification

LOQ was defined as the lowest concentration from the calibration curves that could be readily quantified with a precision of 20% RSD or better. From our experiments, the LOQ of acylcarnitine from the channel target plate was 0.50  $\mu\text{M}$ , which was twofold lower than the LOQ from the conventional plate (Table 1).

### 3.5 | Matrix effects

We evaluated the effect of the plasma matrix by comparing the relative signal intensities in plasma and in pure solvent (water). The resulting calibration plots are illustrated in Figure 4. The slopes for acetyl-L-carnitine from plasma and water were 0.046 and 0.040, respectively. These values were used as indicators for matrix effects as described in experimental part. From these results, it could be seen

**TABLE 1** Quantification results for acetyl-L-carnitine using the standard addition method on both channel and conventional target plates

Target Plate	Spiked Concentration, $\mu\text{M}$	$y = b \times c_{\text{sample}} + bx$	$R^2$	LOQ, $\mu\text{M}^a$
Channel target	0.50-50.00	$y = 0.189 + 0.046x$	0.9989	0.50
Conventional target	0.50-10.00	$y = 0.226 + 0.043x$	0.9798	1.00

<sup>a</sup>LOQ was defined as the lowest concentration that could be quantified with a precision of 20% RSD or better.

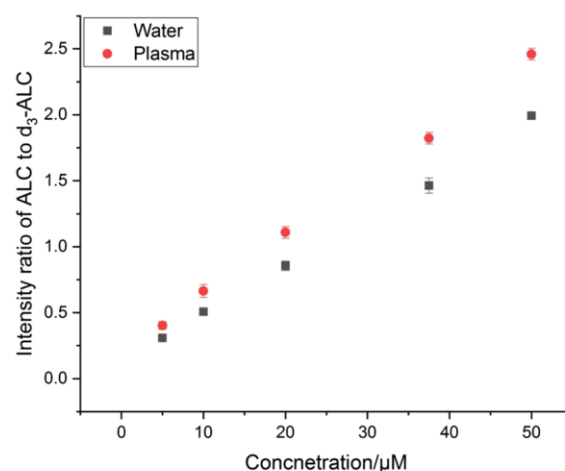


**FIGURE 4** Calibration plots from spiked plasma and pure solvent (water). The concentration of  $d_3$ -acetyl-L-carnitine was 20.00  $\mu\text{M}$  [Colour figure can be viewed at wileyonlinelibrary.com]

that the matrix strongly influenced the acetyl-L-carnitine signal in plasma, requiring a combination of the standard addition method and isotope dilution analysis for correction.

### 3.6 | Human samples

Samples from two volunteers were analyzed using the developed method, and concentrations levels of 4.11  $\mu\text{M}$  and 8.48  $\mu\text{M}$  were determined (Table 2), which are comparable with levels typically seen in other studies.<sup>16</sup>

### 3.7 | Trueness and precision

Trueness was assessed by analyzing quality control samples at low, medium, and high concentration levels in plasma (Table 3). The

**TABLE 2** Measurement precision in human plasma using the standard addition method

	AC concentration, $\mu\text{M}$	Intraday (RSD, %)	Interday (RSD, %)
Sample 1	4.11	3.72	4.0
Sample 2	8.47	2.86	6.0

**TABLE 3** Recovery rates at three different concentrations in plasma

Spiked Concentration ( $\mu\text{M}$ )	Detected Concentration, $\mu\text{M}$ (RSD, %)	Recovery, %
1.00	1.07 (7.94)	107.0
5.00	4.91 (5.74)	98.2
20.00	20.63 (3.11)	103.2

recovery rates for each concentration were in range of 98.2% to 107.0% with RSD less than 8.0%. Precision was determined from intraday and interday experiments, ranging from 2.9% to 6.0%, respectively (Table 2).

#### 4 | CONCLUSIONS

We have developed a simple technique to produce homogenous crystals of matrix and sample using a novel channel sampling plate for MALDI-MS. The channel design afforded very good reproducibility of the measurements across different sample spots, while at the same time improving detection sensitivity over regular MALDI plates. The applicability of the new plates was demonstrated by developing a quantitative assay for the measurement of acetyl-L-carnitine in human plasma. The new technique is inexpensive, does not require specialized sample deposition techniques, and has the potential for full automation and thus high throughput quantitative measurements.

#### ACKNOWLEDGEMENTS

The authors thank Jun Feng (Leibniz Institute for New Materials, Saarbrücken, Germany) for the SEM measurements. Z.L. acknowledges the China Scholarship Council for financial support.

#### ORCID

Peng Zhang  <https://orcid.org/0000-0003-1695-360X>

Dietrich A. Volmer  <https://orcid.org/0000-0003-2820-1480>

#### REFERENCES

- Duncan MW, Roder H, Hunsucker SW. Quantitative matrix-assisted laser desorption/ionization mass spectrometry. *Brief Funct Genomic Proteomic*. 2008;7(5):355-370.
- Sleno L, Volmer DA. Some fundamental and technical aspects of the quantitative analysis of pharmaceutical drugs by matrix-assisted laser desorption/ionization mass spectrometry. *Rapid Commun Mass Spectrom*. 2005;19(14):1928-1936.
- Sleno L, Volmer DA. Assessing the properties of internal standards for quantitative matrix-assisted laser desorption/ionization mass spectrometry of small molecules. *Rapid Commun Mass Spectrom*. 2006;20(10):1517-1524.
- Pirman DA, Yost RA. Quantitative Tandem Mass Spectrometric Imaging of Endogenous Acetyl-L-Carnitine from Piglet Brain Tissue Using an Internal Standard. *Anal Chem*. 2011;83(22):8575-8581.
- Szájli E, Fehér T, Medzihradsky KF. Investigating the quantitative nature of MALDI-TOF MS. *Mol Cell Proteomics*. 2008;7(12):2410-2418.
- Chen CJ, Lai CC, Tseng MC, Liu YC, Lin SY, Tsai FJ. Simple fabrication of hydrophobic surface target for increased sensitivity and homogeneity in matrix-assisted laser desorption/ionization time-of-flight mass spectrometry analysis of peptides, phosphopeptides, carbohydrates and proteins. *Anal Chim Acta*. 2013;783:31-38.
- Owen SJ, Meier FS, Brombacher S, Volmer DA. Increasing sensitivity and decreasing spot size using an inexpensive, removable hydrophobic coating for matrix-assisted laser desorption/ionization plates. *Rapid Commun Mass Spectrom*. 2003;17(21):2439-2449.
- Vorm O, Roepstorff P, Mann M. Improved resolution and very high sensitivity in MALDI TOF of matrix surfaces made by fast evaporation. *Anal Chem*. 1994;66(19):3281-3287.
- Li S, Zhang Y, Liu J, et al. Electrospray deposition device used to precisely control the matrix crystal to improve the performance of MALDI MSI. *Sci Rep*. 2016;6:1-10.
- Hensel RR, King RC, Owens KG. Electrospray sample preparation for improved quantitation in matrix-assisted laser desorption/ionization time-of-flight mass spectrometry. *Rapid Commun Mass Spectrom*. 1997;11(16):1785-1793.
- Önnerfjord P, Ekström S, Bergquist J, Nilsson J, Laurell T, Marko-Varga G. Homogeneous sample preparation for automated high throughput analysis with matrix-assisted laser desorption/ionisation time-of-flight mass spectrometry. *Rapid Commun Mass Spectrom*. 1999;13(5):315-322.
- Ho YC, Tseng MC, Lu YW, Lin CC, Chen YJ, Fuh MR. Nanoparticle-assisted MALDI-TOF MS combined with seed-layer surface preparation for quantification of small molecules. *Anal Chim Acta*. 2011;697(1-2):1-7.
- Pabst M, Fagerer S. R, Köhling, R, Küster, SK, Steinhoff, R, Badertscher, M, Wahl, F, Dittrich, PS, Jefimovs, K, Zenobi, R. Self-aliquoting microarray plates for accurate quantitative matrix-assisted laser desorption/ionization mass spectrometry. *Anal Chem*. 2013;85(20):9771-9776.
- Choi YK, Oh JY, Han SY. Large-Area Graphene Films as Target Surfaces for Highly Reproducible Matrix-Assisted Laser Desorption Ionization Suitable for Quantitative Mass Spectrometry. *J Am Soc Mass Spectrom*. 2018;29(10):2003-2011.
- Lee J, Jang ES, Kim B. Development of isotope dilution-liquid chromatography/mass spectrometry combined with standard addition techniques for the accurate determination of tocopherols in infant formula. *Anal Chim Acta*. 2013;787:132-139.
- Rosca MG, Lemieux H, Hoppel CL. Mitochondria in the elderly: is acetylcarnitine a rejuvenator? *Adv Drug Deliv Rev*. 2009;61(14):1332-1342.
- Isaguirre AC, Olsina RA, Martinez LD, Lapiere AV, Cerutti S. Rapid and sensitive HILIC-MS/MS analysis of carnitine and acetylcarnitine in biological fluids. *Anal Bioanal Chem*. 2013;405(23):7397-7404.
- Hirche F, Fischer M, Keller J, Eder K. Determination of carnitine, its short chain acyl esters and metabolic precursors trimethyllysine and  $\gamma$ -butyrobetaine by quasi-solid phase extraction and MS/MS detection. *J Chromatogr B*. 2009;877(22):2158-2162.
- Manna JD, Reyzer ML, Latham JC, Weaver CD, Marnett LJ, Caprioli RM. High-throughput quantification of bioactive lipids by MALDI mass spectrometry: application to prostaglandins. *Anal Chem*. 2011;83(17):6683-6688.
- Volmer DA, Sleno L, Bateman K, et al. Comparison of MALDI to ESI on a Triple Quadrupole Platform for Pharmacokinetic Analyses. *Anal Chem*. 2007;79(23):9000-9006.
- Gode D, Schmitt C, Engel M, Volmer DA. Screening Dyrk1A inhibitors by MALDI-QqQ mass spectrometry: systematic comparison to established radiometric, luminescence, and LC-UV-MS assays. *Anal Bioanal Chem*. 2014;406(12):2841-2852.
- Koulman A, Petras D, Narayana VK, Wang L, Volmer DA. Comparative high-speed profiling of carboxylic acid metabolite levels by differential isotope-coded MALDI mass spectrometry. *Anal Chem*. 2009;81(18):7544-7551.

23. Shen XY, Ho CM, Wong TS. Minimal size of coffee ring structure. *J Phys Chem B*. 2010;114(16):5269-5274.

### SUPPORTING INFORMATION

Additional supporting information may be found online in the Supporting Information section at the end of the article.

**How to cite this article:** Liu Z, Zhang P, Kästner L, Volmer DA. A simple MALDI target plate with channel design to improve detection sensitivity and reproducibility for quantitative analysis of biomolecules. *J Mass Spectrom*. 2019;54:878-884. <https://doi.org/10.1002/jms.4447>

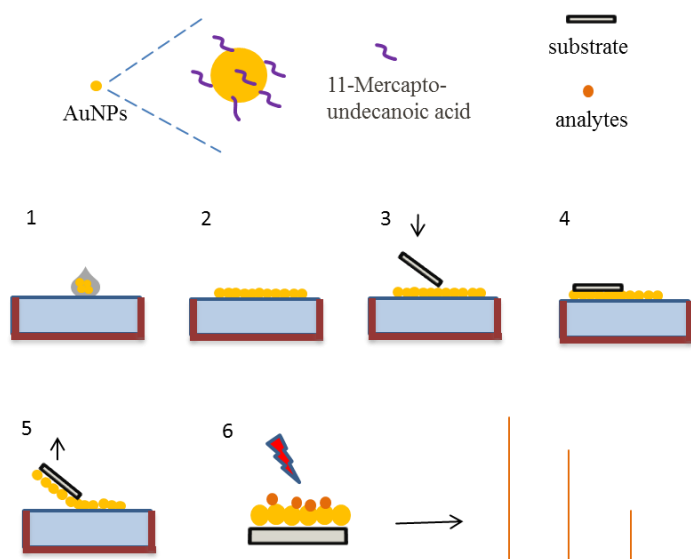
## Publication 2

## Ultra-thin homogenous AuNP monolayers as tunable functional substrates for surface-assisted laser desorption/ionization of small biomolecules

Zhen Liu, Peng Zhang, Thomas Kister, Tobias Kraus, Dietrich A. Volmer

Journal of the American Society for Mass Spectrometry, 2020, 31, 1, 47-57,

<https://doi.org/10.1021/jasms.9b00038>



Reprinted with permission from American Chemical Society Copyright (2020).

# Ultrathin Homogenous AuNP Monolayers as Tunable Functional Substrates for Surface-Assisted Laser Desorption/Ionization of Small Biomolecules

 Zhen Liu,<sup>†</sup> Peng Zhang,<sup>‡</sup> Thomas Kister,<sup>§</sup> Tobias Kraus,<sup>§,||</sup> and Dietrich A. Volmer<sup>\*,†,⊥</sup>
<sup>†</sup>Institute of Bioanalytical Chemistry, Saarland University, 66123 Saarbrücken, Germany

<sup>‡</sup>School of Materials Science and Engineering, Sun Yat-sen University, Guangzhou 510275, China

<sup>§</sup>INM-Leibniz Institute for New Materials, 66123 Saarbrücken, Germany

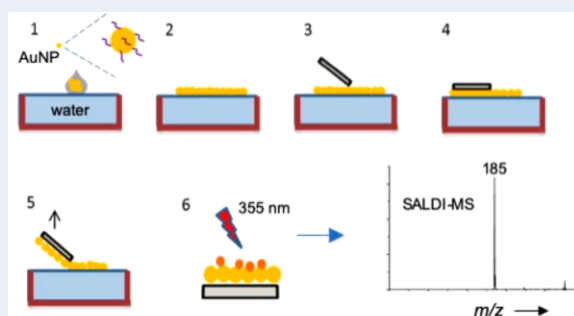
<sup>||</sup>Institute of Colloid and Interface Chemistry, Saarland University, 66123 Saarbrücken, Germany

<sup>⊥</sup>Department of Chemistry, Humboldt University of Berlin, Brook-Taylor-Strasse 2, 12489 Berlin, Germany

## Supporting Information

**ABSTRACT:** A series of ultrathin, homogenous gold nanoparticle (AuNP) substrates for surface-assisted laser desorption/ionization mass spectrometry (SALDI-MS) were prepared using a simple air/water interface approach. These SALDI substrates enabled soft ionization and provided significant improvements in terms of signal intensities and reduced background levels in comparison to other AuNP morphologies for different analytes such as fatty acids, peptides, amino acids, saccharides, and drugs. Through different microscopic and spectroscopic methods, we determined that the packing homogeneity of the [AuNP]<sub>n</sub> substrates played a vital role in the efficiency of the SALDI process. We demonstrated that the signal intensities of the investigated analytes were readily optimized by manipulating the thickness of the [AuNP]<sub>n</sub> substrates. The desorption/ionization efficiency increased as a function of the number of layers and then reached a saturation point. The optimized [AuNP]<sub>n</sub> substrates not only exhibited high SALDI-MS desorption/ionization efficiencies but also showed excellent reproducibilities of the analyte signals.

**KEYWORDS:** gold nanoparticles (AuNP), surface-assisted laser desorption/ionization (SALDI), mass spectrometry (MS), biomolecules, soft ionization



## INTRODUCTION

Matrix-assisted laser desorption/ionization (MALDI)-MS has been widely used in biological applications because of its soft desorption and ionization conditions and its broad application range.<sup>1,2</sup> However, the requirement of a chemical matrix severely limits MALDI in the detection of small molecules at lower  $m/z$  ranges < 500, owing to matrix interferences. Surface-assisted laser desorption/ionization (SALDI) is frequently used as a matrix-free alternative to MALDI. Recent advances in the SALDI field are mainly due to the availability of efficient nanoparticulate substrates. A wide variety of different nanomaterials including carbon,<sup>3–6</sup> silicon,<sup>7–9</sup> metal (Au, Ag, Pt, etc.),<sup>10–13</sup> metal oxides,<sup>14–17</sup> and other nanomaterials<sup>18–21</sup> have been successfully implemented for SALDI. Compared with MALDI, SALDI offers distinct advantages,<sup>22–24</sup> namely its simple and flexible sample preparation, limited background signals in the low  $m/z$  range, and its ability to modify nanoparticles to selectively capture and ionize analytes. The desorption and ionization efficiency in SALDI is highly

dependent on physical (size, surface roughness, electrical conductivity, light absorption, and melting point) and chemical properties (surface modification, binding energy to analytes) of the nanomaterials.<sup>25,26</sup> Generally, rapid laser-induced heating of the substrates and slow energy dissipation,<sup>27</sup> leading to desorption and ionization of analytes, is widely accepted as the primary mechanism of function.

Owing to the unique optical, thermal, and electrical properties, gold nanomaterials are promising candidates for SALDI-MS analysis of biomolecules.<sup>28,29</sup> Mclean *et al.*<sup>30</sup> used AuNP with different sizes (2–10 nm) to detect peptides. They found a size effect of AuNP on desorption and ionization efficiencies of peptides, where larger AuNP showed better performance. Amendlac *et al.*<sup>31</sup> reported that chemical-free AuNP exhibited low background levels for  $m/z$  < 500 as

**Received:** May 27, 2019

**Accepted:** November 2, 2019

**Published:** November 21, 2019

compared to AuNP with surface-protected agents, providing picomolar level detection of small molecules. Gold nanorods<sup>32</sup> were used to detect biomolecules after irradiation with an IR laser. Havel *et al.*<sup>33</sup> used flowerlike gold nanoparticle as mediator to enhance ionization of peptides. Finally, fluorinated AuNP<sup>34</sup> were synthesized for comprehensive analysis of metabolites in biological tissues with high sensitivity and minimal background noise levels. Lower laser energy was required during this process, which led to gentle desorption/ionization.

While the above inorganic nanomaterials were shown to be effective SALDI substrates for small molecules, signal fluctuations and poor reproducibility of analyte measurement remain a major problem. There are multiple reasons for this, including hot spot formation during sample deposition and solvent evaporation, leading to poor shot-to-shot and spot-to-spot reproducibility.<sup>35,36</sup> Furthermore, the morphology of the substrate is often highly inhomogeneous, resulting in significant variations of ion signals. Recent studies<sup>37–41</sup> showed that homogenous distribution of nanomaterials to form continuous thin films decreased sweet spot formation and increased signal intensity and reproducibility in SALDI-MS. Multilayered AuNP thin films<sup>37</sup> were used to detect a bone biomarker (hydroxyproline) for assessment of osteoporosis with excellent reproducibility of 9.3 % RSD. Gold nanoporous films,<sup>38</sup> modified by cysteine, were easily prepared to detect a wide range of compounds including amino acids, drugs, cyclodextrins, peptides, and polyethylene glycols with good reproducibility (<10% RSD). Kawasaki *et al.*<sup>39</sup> used a layer-by-layer (LBL) method to obtain multilayer films of AuNP on a silicon wafer for SALDI, to detect angiotensin I at low concentration levels. The author showed that the sensitivity for angiotensin improved as the number of layers was increased; it reached a plateau for 5 layers. The same material was also used to extract and directly identify environmental pollutants at very low concentration levels (<100 pg/L). Choi *et al.*<sup>40</sup> attached a homogenous layer of graphene foil on a target plate, and samples were deposited onto this foil. Sweet spots were effectively eliminated and reproducibility highly improved (<10% RSD). The new method exhibited good linear response for small peptides (angiotensin II and Glu-fibrinopeptide B). Kuo *et al.*<sup>41</sup> used spin coating to prepare an LBL thin film of reduced graphene oxide (rGO) and AuNP, which was shown to be very efficient for SALDI. By using this LBL film, substrate homogeneity and mass spectral signal reproducibility were highly improved as compared to routine sample preparation. The authors also used a Langmuir-Blodgett (LB) film made of cuboctahedral silver as effective surface for SALDI-MS to analyze glucose. The absolute ion intensities, signal-to-noise ratios, and reproducibilities were superior to traditional MALDI matrices.<sup>35</sup>

There are multiple methods to prepare packed monolayer films, *e.g.*, spin coating,<sup>42</sup> physical deposition,<sup>43</sup> controlled drying,<sup>44</sup> or preassembly at air/water interfaces.<sup>45–47</sup> The predominant air/water method is a Langmuir-based process, which enables the nanoparticles to preassemble in highly-ordered structures over large areas. This method is time-consuming, however, and requires specialized equipment. Nagel *et al.*<sup>48</sup> introduced a much simpler method to produce high quality monolayers, where the colloidal nanoparticles were directly assembled at a water/air interface and a monolayer formed automatically without any additional compression. The monolayers of nanoparticles on the water

surface are subjected to isothermal compression and undergo phase transition from liquid to solid as a function of the increase of surface pressure. Under optimal conditions, continuous layers of nanoparticles are formed and evenly arranged with sufficient density and space. These monolayer films can then be transferred to any substrate or surface.

In this study, a new method was developed to prepare homogenous monolayers of small AuNP. Each monolayer was ultrathin ( $\approx 2.5$  nm), and multilayer AuNP substrates ( $[\text{AuNP}]_n$ ) were prepared by transferring individual monolayers of AuNP for  $n$  times on the substrate. In previous reports, LBL,<sup>39,49</sup> controlled drying,<sup>37</sup> and spin coating<sup>41</sup> were used to prepare multilayer films for SALDI-MS. These methods were not as simple to use as our new method, however, and did not always provide the necessary homogeneity.<sup>50</sup> For example, LBL nanomaterials can only be deposited onto specific substrates (*e.g.*, silicon wafers or glass). Also, as electrostatic interactions are utilized to form the continuous layers, an equivalent counterpart is needed for the nanoparticles. Finally, the preparation process is very time-consuming, often requiring hours to complete. Compared to these methods, the approach presented here is very simple and fast (<10 min) and can be implemented on a variety of different substrates. In our experiments,  $[\text{AuNP}]_n$  substrates were used as functional substrates for SALDI-MS to detect small molecules, including fatty acids, amino acids, drugs, small peptides, and saccharides. These substrates offered several advantages: (1) the small AuNP provided a large surface areas for improved contact with the analyte and increased LDI efficiency; (2) the  $[\text{AuNP}]_n$  substrates were homogeneous over extended areas, which avoided sweet spot formation and enhanced reliability; (3) there was almost exclusive formation of potassium adducts during ionization, which increased sensitivity for quantitative applications; and (4) the ionization efficiency for the analytes could be adjusted by changing the number of layers ( $n$ ) of the  $[\text{AuNP}]_n$  substrates.

## ■ EXPERIMENTAL SECTION

**Chemicals and Reagents.** CHCA ( $\alpha$ -cyano-4-hydroxycinnamic acid), palmitic acid, stearic acid, oleic acid, linoleic acid, erythromycin A, cysteine, phenylalanine, and 4-amino-1-benzylpyridinium bromide (ABP) were purchased from Sigma-Aldrich (Steinheim, Germany). Flumequine, peometon, D-fructose, L-sorbose, D-maltose, and D-sucrose were from Merck (Darmstadt, Germany). Timolol maleate, glutathione, and Leu-enkephalin were from Cayman Chemicals (Hamburg, Germany). Acetonitrile (ACN) and methanol were from VWR Chemicals (Darmstadt, Germany). Deionized water was generated by a Millipore (Bedford, MA, USA) water purification system.

Stock solutions of analytes were prepared as follows: fatty acids (palmitic acid, stearic acid, oleic acid, and linoleic acid) and drugs (erythromycin, flumequine, peometon, and timolol maleate) were dissolved in methanol at 1 mM; amino acids (cysteine and phenylalanine), small peptides (glutathione and Leu-enkephalin), and saccharides (D-fructose, L-sorbose, D-maltose, and D-sucrose) were dissolved in water at 10 mM; ABP was dissolved in methanol at 10 mM. All stock solutions were stored at  $-20$  °C and diluted to the required concentration prior to use. If not otherwise specified, fatty acids, drugs, amino acids, small peptides, saccharides, and ABP were diluted to 100  $\mu\text{M}$  in methanol. Sodium and potassium salt were added to analytes solutions if needed.

**Preparation of Small Gold Nanoparticles.** Stock AuNP solutions were prepared according to a modified protocol, which was previously published.<sup>51</sup> Ligand exchange from oleylamine to 11-mercaptoundecanoic acid was performed as follows: 10 mL of AuNP, dispersed in toluene, was heated to 80 °C at 200 rpm. 200 mg of 11-mercaptoundecanoic acid was dissolved in 5 mL of toluene and heated to 80 °C until the 11-mercaptoundecanoic acid was fully dissolved. Afterwards, the dissolved 11-mercaptoundecanoic acid was added to the AuNP solution. During ligand exchange, the AuNP agglomerate (11-mercaptoundecanoic acid capped AuNP do not disperse in toluene). Subsequently, the AuNP dispersion was centrifuged for 3 min at 3000 rpm. To remove excess ligand, the sedimented AuNP were dispersed in 5 mL of toluene (at this state, the AuNP were still agglomerated). The suspension was sonicated for 5 min, followed by centrifugation (3 min at 3000 rpm) and removal of the supernatant. This was repeated 5 times. Finally, the AuNP were dispersed in 10 mL of methanol. The AuNP solution was stored at room temperature.

**Preparation and Characterization of [AuNP]<sub>n</sub> Substrates.** A homemade microtrough (130 × 80 × 30 mm, Figure 1) was used to prepare the AuNP substrates. Deionized

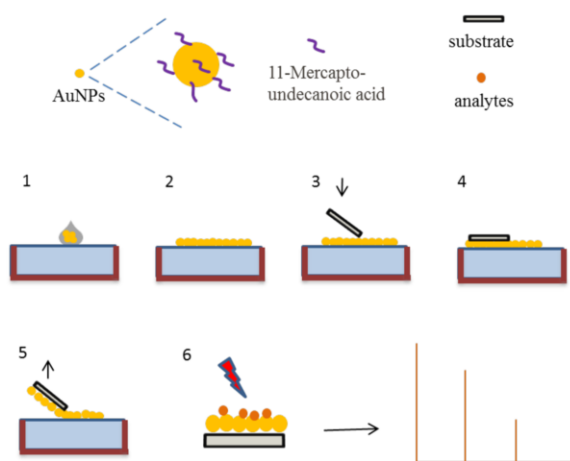


**Figure 1.** Schematic illustration of the process of AuNP film preparation and SALDI-MS (11-mercaptoundecanoic is the ligand of the AuNP).

water was first filled into the trough. Then 10  $\mu\text{L}$  of the AuNP solution was deposited onto the water using a microsyringe, by allowing the needle of the syringe to contact the water surface of water and gently pushing out the AuNP solution. The amphiphilic ligand of the AuNP (11-mercaptoundecanoic acid) automatically enabled the formation of an AuNP monolayer on the water surface. A clean steel target plate was then placed onto the water surface at an angle of ca. 45° and slowly “rolled” onto the water surface for full contact, held in that position for 10 s, then lifted up again to a 45° angle, and pulled out. The substrate was subsequently dried at ambient conditions. [AuNP]<sub>n</sub> substrates, where *n* denotes the number of layers, were prepared by placing additional layers on top of the previous layer.

UV/Vis experiments of films on glass were performed with a Lambda 750 spectrometer (Perkin Elmer, Shelton, CT, USA). The AuNP monolayer was carefully transferred to a carbon-coated copper TEM grid (Plano, Wetzlar, Germany), and

TEM experiments were undertaken with a JEM-2010 microscope (Jeol GmbH, Munich, Germany) operated at an accelerating voltage of 200 kV. For X-ray scattering measurements, the AuNP films were carefully transferred to the thin rectangular glass substrates (borosilicate,  $170 \pm 5 \mu\text{m}$  thick, Thorlabs GmbH, Germany). X-ray scattering was performed with a Xeuss 2.0 setup (Xenocs, Sassenage, France) equipped with a GeniX Low Divergence Cu-K $\alpha$  source. The X-ray wavelength was 1.54 Å. The scattering signal was collected with a Dectris Pilatus 1M detector, and the sample to detector distance was calibrated with silver behenate. A horizontal scanning of the sample was achieved with fixing its height position while moving the sample along the direction normal to the beam at a step of 5 mm. The conversion of 2D image to the 1D curve was done with Foxtrot software.

A scanning electron microscope (FEI Quanta 400F, FEI Europe, Eindhoven, The Netherlands) was used at an operating voltage of 10 kV to characterize the surface structures of the [AuNP]<sub>n</sub> thin films. The contact angle and its change with time was determined for aqueous dispersions (volume 2  $\mu\text{L}$ ) of the [AuNP]<sub>n</sub> films on cleaned silicon wafers with a OCA 20 contact angle measuring system (Data Physics Instruments, Filderstadt, Germany) at room temperature using the sessile drop method. The frequency for the contact angle data collection was 25 Hz. The video images were processed with the OCA 20 instrument software to obtain the contact angle values.

**Preparation of MALDI and SALDI Samples.** MALDI samples were prepared using the dried droplet method. CHCA solution (10 mg/mL in acetonitrile/water 70/30 v/v) was first mixed with the analytes, 1.0  $\mu\text{L}$  of the mixture was deposited on the surface of the target plate using a micropipette, and the droplet was dried at ambient conditions.

[AuNP]<sub>n</sub> films were transferred and dried on steel target plates, and 0.5  $\mu\text{L}$  of the analyte solutions was deposited onto the steel surface and dried at ambient conditions. Two comparisons were made: (1) 0.5  $\mu\text{L}$  of the original AuNP solution was pipetted onto the steel target. After the solvent evaporated, 0.5  $\mu\text{L}$  of the analyte solution was placed onto the AuNP and dried; (2) the original AuNP solution was mixed with the analyte solution. Then, 1  $\mu\text{L}$  of the mixture was pipetted onto a steel target and dried at ambient conditions.

**Mass Spectrometry.** MS experiments were performed using a Bruker Esquire HCT<sup>+</sup> ion trap mass spectrometer (Bremen, Germany) coupled with a MassTech (Burtonsville, MD, USA) atmospheric pressure (AP) MALDI source. A Nd:YAG laser emitting at 355 nm was used as the light source. Laser energy was set to 50%, and the repetition rate was set to 200 Hz. Mass spectra were acquired in positive ion mode from *m/z* 50 to 500 using a raster motion of the target plate. Ion currents were accumulated as follows: velocity, 40.0 mm/min; scan length, 2.0 mm; scan height, 2.0 mm; spacing, 0.5 mm; step size, 0.5 mm; raster direction, horizontal. A drying gas temperature of 50 °C at a flow rate of 5.0 L/min was used.

## RESULTS AND DISCUSSION

In this study, small AuNP were used to prepare ultrathin films as functional substrates for SALDI-MS. By using a simple air/water interfacial approach, homogenous monolayer AuNP films were formed by adding AuNP colloidal onto the surface of water as shown in Figure 1. [AuNP]<sub>n</sub> substrates were prepared by repeatedly (*n*-fold) transferring the monolayer

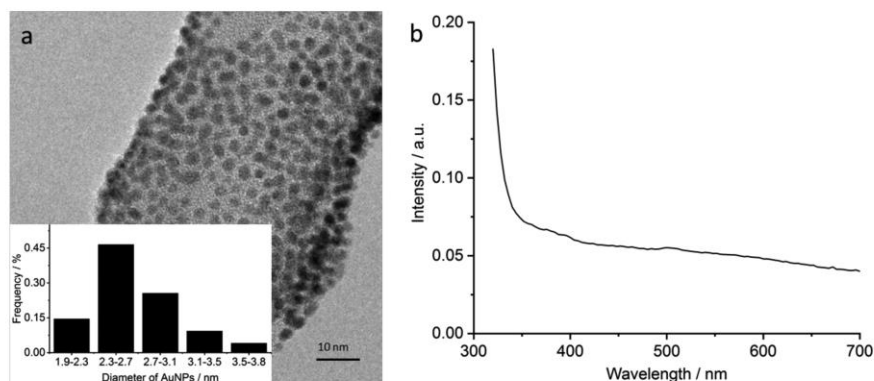


**Figure 2.** (a) TEM image of a single layer of an AuNP film and (b) UV/Vis absorption of the  $[\text{AuNP}]_1$  substrate. The mean diameter of the AuNP is ca. 2.5 nm; that is, the thickness of one layer of the AuNP film is also approx. 2.5 nm. The insert (left) shows the size distribution of the AuNP.

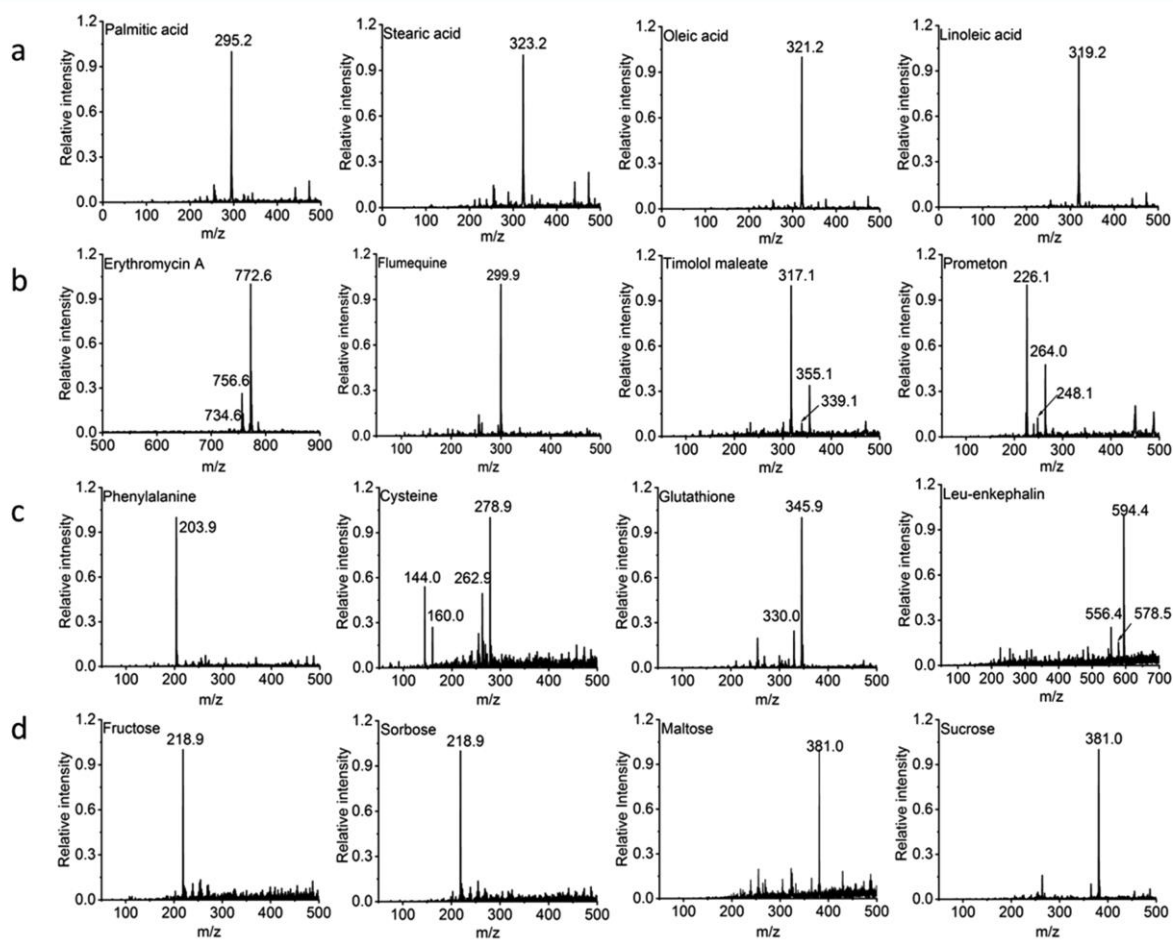


**Figure 3.** SALDI-MS spectra of (a) fatty acids, (b) drugs, (c) amino acids and small peptides, and (d) saccharides on  $[\text{AuNP}]_1$  films at concentrations of  $100 \mu\text{M}$  each.

AuNP films, followed by drying them under ambient conditions.

In all experiments described here, an atmospheric pressure (AP) MALDI source was implemented for SALDI-MS. AP-MALDI allows for much quicker and easier sample handling and often provides softer ionization conditions with reduced

fragmentation levels,<sup>52,53</sup> which is ideal for molecules that are unstable under vacuum conditions.<sup>54</sup> While sometimes the mass range is not as wide as for vacuum MALDI and the ion transmission efficiency from ion source to analyzer is lower,<sup>55,56</sup> the signal-to-noise ratios for analytes in AP-MALDI are usually comparable to vacuum MALDI.<sup>57</sup> In our

**Table 1.** SALDI-MS Ion Currents of Linoleic Acid Using Mixtures of AuNP and Linoleic Acid, Linoleic Acid Deposited onto AuNP, or Linoleic Acid Deposited onto  $[\text{AuNP}]_1$  Film<sup>a</sup>

state	$[\text{M}_1 + \text{H}]^+$ ( <i>m/z</i> 281)	$[\text{M}_1 + \text{Na}]^+$ ( <i>m/z</i> 303)	$[\text{M}_1 + \text{K}]^+$ ( <i>m/z</i> 319)	$[\text{M}_2 + \text{H}]^+$ ( <i>m/z</i> 441)	$[\text{M}_2 + \text{Na}]^+$ ( <i>m/z</i> 457)	$[\text{M}_2 + \text{K}]^+$ ( <i>m/z</i> 473)
mixture of AuNP and analyte	22	1842	1551	1076	4451	2628
deposited onto AuNP	99	1538	2597	4559	6683	14328
deposited onto $[\text{AuNP}]_1$ film	29	201	10938	641	131	473

<sup>a</sup> $\text{M}_1$  and  $\text{M}_2$  represent linoleic acid and 11-mercaptoundecanoic acid, respectively.

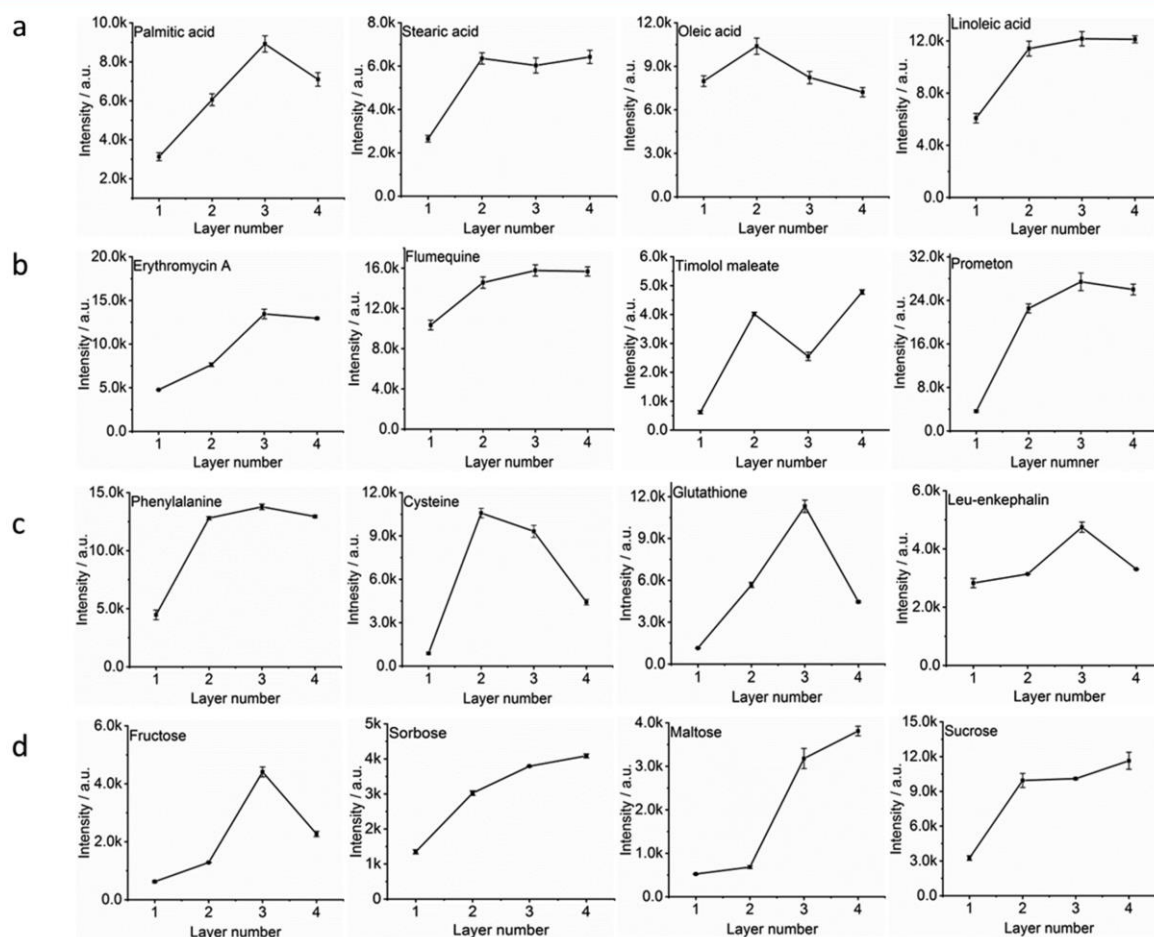


**Figure 4.** SALDI-MS of (a) fatty acids, (b) drugs, (c) amino acids and small peptides, and (d) saccharides on  $[\text{AuNP}]_n$  for different layer numbers at concentrations of 100  $\mu\text{M}$  each.

exploratory SALDI-MS study, AP ionizations conditions were ideal for conducting the method optimization. AP conditions also avoided ablation with subsequent ionization of the AuNP substrate material and thus interference signals in the SALDI mass spectra, which will be further described below.

**Characterization of the  $[\text{AuNP}]_1$  Films.** The structures of the  $[\text{AuNP}]_1$  films were initially characterized by TEM and UV/Vis spectroscopy (Figure 2). The TEM images clearly showed single AuNP within the  $[\text{AuNP}]_1$  films. The AuNP exhibited uniform spherical shapes with narrow size distribution of diameters between 1.9 and 3.8 nm. We calculated the statistical mean diameter of the AuNP as 2.5 nm (see insert of Figure 2a). Considering that the  $[\text{AuNP}]_1$  film is a single layer,

we inferred the thickness of the single  $[\text{AuNP}]_1$  film to be *ca.* 2.5 nm. In Figure 2b, the UV/Vis spectra showed several absorption peaks at 510, 395, 380, and 360 nm. The peak at 510 nm can be rationalized by the surface plasmon band of AuNP, while peaks below 400 nm were due to metal-centered (interband) transitions and/or ligand-metal charge-transfer transitions.<sup>58,59</sup> Considering that these small AuNP exhibited strong absorption under 400 nm and that a laser wavelength of 355 nm was used for the MS experiments, we anticipated that photons would be readily absorbed by the AuNP for enhanced desorption/ionization efficiency of organic molecules. To further characterize the batch-to-batch reproducibility of the  $[\text{AuNP}]_1$  films, four further batches were prepared and

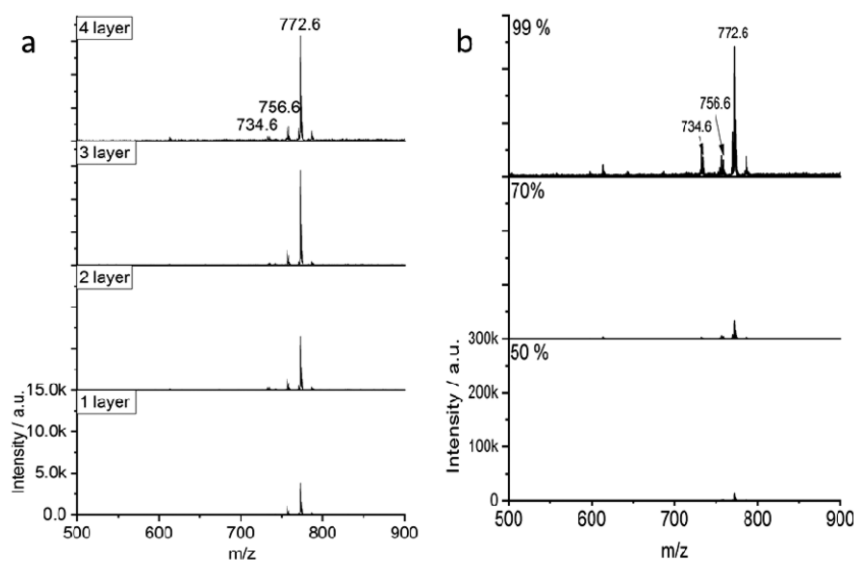


**Figure 5.** SALDI-MS spectra of erythromycin A using (a)  $[\text{AuNP}]_n$  for different layer numbers  $n$  and (b)  $[\text{AuNP}]_4$  for different laser energies (concentration, 100  $\mu\text{M}$ ).

characterized by TEM and UV/Vis spectroscopy (Supporting Information, Figures S1 and S2), readily showing the excellent reproducibility of  $[\text{AuNP}]_1$  film preparation.

**$[\text{AuNP}]_1$  Substrate-Assisted LDI-MS of Small Molecules.** To demonstrate the ionizing abilities of the  $[\text{AuNP}]_1$  substrates, they were evaluated for SALDI-MS analysis of different low molecular weight compounds. Different small molecules were investigated to demonstrate the proof-of-concept: fatty acids (palmitic acid, stearic acid, oleic acid, linoleic acid), synthetic drugs (erythromycin A, flumequine, peometon, timolol maleate), amino acids (cysteine, phenylalanine), small peptides (glutathione, Leu-enkephalin), and saccharides (D-fructose, L-sorbose, D-maltose, and D-sucrose). As shown in Figure 3, all investigated analytes were clearly detected as protonated molecules, sodium and/or potassium adducts with very limited background signals from the  $[\text{AuNP}]_1$  substrate. These initial results clearly revealed the potential of the  $[\text{AuNP}]_1$  films as versatile substrates for SALDI-MS analysis. As SALDI-MS spectra are usually dominated by cation adducts,<sup>60</sup> 0.5  $\mu\text{M}$  sodium or 0.5  $\mu\text{M}$  potassium ions were added to all analyte solutions, to further promote adduct formation. Except for some low intensity noise from the AuNP, no fragmentation of analytes was observed, suggesting that the  $[\text{AuNP}]_1$  films provided soft ionization abilities during SALDI-MS.

**Comparison to Other Morphologies of AuNP.** In SALDI-MS, both structure and aggregate state of nanomaterials have a profound effect on the desorption/ionization process.<sup>26,28,29</sup> Here, comparisons between different AuNP states were made using linoleic acid as the test analyte (Table 1). The SALDI spectra exhibited linoleic acid's  $[\text{M} + \text{Na}]^+$  and  $[\text{M} + \text{K}]^+$  ions, as well as signals from the AuNP ligands (11-mercaptoundecanoic acid). Importantly, signal intensities of linoleic acid from  $[\text{AuNP}]_1$  films were much higher than those generated from deposited AuNP or mixtures of AuNP and linoleic acid. This is likely the result of the improved contact of linoleic acid and AuNP in the films as well as the homogeneity of the  $[\text{AuNP}]_1$  substrates.

**$[\text{AuNP}]_n$  Films and Their Application in SALDI-MS.** To optimize the desorption and ionization efficiency of the analytes,  $[\text{AuNP}]_n$  ( $n = 1-4$ ) substrates of different thickness were prepared. When transferred onto a glass surface,  $[\text{AuNP}]_n$  films visually appeared in purple color (Figure S3a). As the number of layers increased, the color of the  $[\text{AuNP}]_n$  substrates deepened.  $[\text{AuNP}]_n$  films were also characterized by UV/Vis spectroscopy as shown in Figure S3b. From this figure, it can be seen that the absorption of the  $[\text{AuNP}]_n$  films at 355 nm increased with the number of layers (the quantitative increase is shown in the Supporting Information, Figure S4), allowing increasing energy absorption of the  $[\text{AuNP}]_n$  substrates. The  $[\text{AuNP}]_n$  films were then used to analyze different analytes by SALDI-MS (Figure 4). For some compounds, e.g., fatty acids, signal intensities reached a plateau at two layers. For other analytes, such as drugs, three-layer substrates provided maximum ion currents. These results clearly showed that there was an optimal thickness of  $[\text{AuNP}]_n$  substrates for different compounds, which are in agreement with previous reports on  $\text{MoS}_2$  thin films and graphene oxide films.<sup>49,61</sup> There was no linear increase of signal intensity with the increased layer number, however, which might be related to the water contact angle changes of the AuNP substrates (Supporting Information, Figure S5). The contact angle on  $[\text{AuNP}]_n$  substrates decreased and gradually leveled out as the layer number increased. From SEM experiments of the  $[\text{AuNP}]_n$  substrates (Supporting Information, Figure S6), it can be seen that the surface of  $[\text{AuNP}]_n$  films was already very smooth after two layers.

Considering the above results, we believe that the AuNP on the surface of the target plate reach approximate saturation after two (or three) layers; beyond this, oversaturation appears, with reduced energy uptake and less favorable desorption and ionization conditions, because of ligand restrictions of the AuNP. As the energy thresholds for desorption/ionization are compound dependent, it is possible to adjust and optimize the number of layers of the  $[\text{AuNP}]_n$  substrates for different analytes to meet their individual energy requirements. We

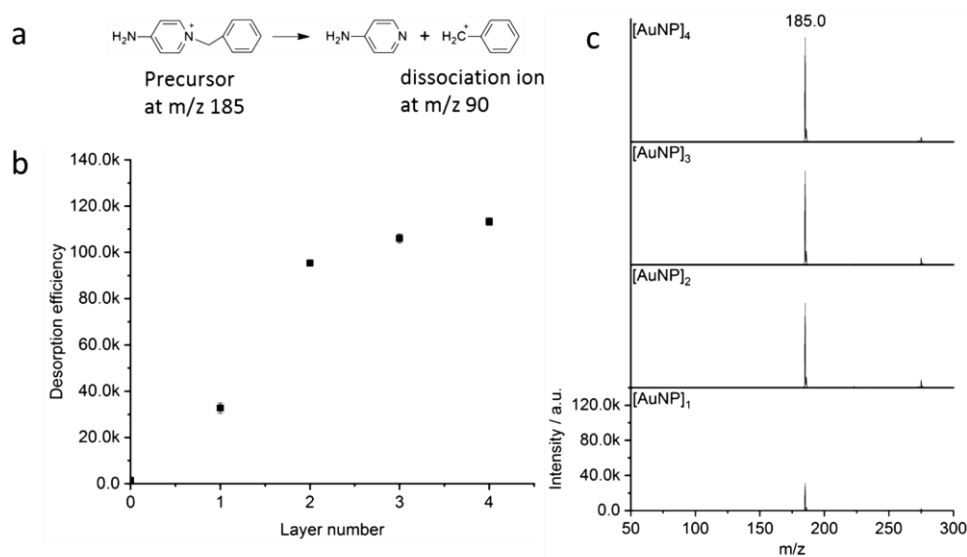


**Figure 6.** (a) Dissociation process of ABP, (b) desorption efficiency of ABP ions, and (c) SALDI mass spectrum of ABP from  $[\text{AuNP}]_n$  substrates (concentration, 100  $\mu\text{M}$ ).

hypothesize that the ability to control the energy uptake of the  $[\text{AuNP}]_n$  substrates would also allow the control of the internal energy and fragmentation behavior of labile ions and the possibility to reduce (or induce) fragmentations if needed.

#### Soft Desorption/Ionization from $[\text{AuNP}]_n$ Substrates.

Both MALDI and SALDI generally exhibit soft ionization characteristics, mostly producing intact molecule-related ions without fragments for most analytes. We chose erythromycin A as a “thermometer ion” to evaluate our new materials, as the ionized erythromycin A molecule is prone to losing a water molecule upon ion activation. Under MALDI conditions using CHCA as matrix, erythromycin A exhibited a protonated molecule at  $m/z$  734, with strong accompanying dissociations leading to fragment ions at  $m/z$  716, 698, 576, 558, 540, and 522 from water and sugar losses (Supporting Information, Figure S7a). This is very similar to the MS/MS spectrum after ion activation of  $m/z$  734 (Figure S7b). Under SALDI conditions using  $[\text{AuNP}]_1$  films, only molecule-related ions at  $m/z$  734, 756, and 772 were generated, however, corresponding to  $[\text{M} + \text{H}]^+$ ,  $[\text{M} + \text{Na}]^+$ , and  $[\text{M} + \text{K}]^+$  (Figure 5). As the layer number of the  $[\text{AuNP}]_n$  substrates increased from  $n = 1$ –4, the intensity of these molecule-related ions increased and gradually reached a plateau, without any fragmentation. Based on these observations, we conclude that the  $[\text{AuNP}]_n$  films provide soft ionization abilities during SALDI, much softer than MALDI using CHCA. The laser energy was adjusted to see whether higher laser energy induces fragmentation of erythromycin A in SALDI. The laser energy was varied from 50% to 99%. The ion intensities increased sharply with increasing laser energy as shown in Figure 5b, without any fragmentation at the highest laser energy available on the used instrument. Fragmentations under SALDI therefore appear to be induced by energy transfer to or from the substrate materials to the analyte rather than to the analyte directly.<sup>62</sup>

**Desorption of Thermometer Benzylpyridinium Ions from  $[\text{AuNP}]_n$  Substrates.** To further explore the SALDI process on the  $[\text{AuNP}]_n$  substrates, benzylpyridinium thermometer ions were used to describe the desorption efficiency

and survival yields.<sup>63,64</sup> Precursor 4-amino-1-benzylpyridinium (ABP) ions were utilized here, and the desorption efficiency was described using the total intensity of the precursor ABP ions,  $[\text{ABP}]^+$  at  $m/z$  185, and the dissociation product of ABP,  $[\text{ABP-pyridine}]^+$ , at  $m/z$  90. The survival yield of ABP was defined as the fraction of remaining precursor ABP ion intensity relative to the total ABP ion current. A plot of desorption efficiency of ABP ions against the layer number of the  $[\text{AuNP}]_n$  substrates is illustrated in Figure 6. The desorption efficiency of ABP ions from the  $[\text{AuNP}]_1$  substrate was 32726 counts and significantly increased to 95374 for  $[\text{AuNP}]_2$ , 106058 for  $[\text{AuNP}]_3$  substrates, and 113292 counts for  $[\text{AuNP}]_4$  substrates. This increase was in accordance with the increased UV/Vis absorption, indicating that a thermally-driven desorption/ionization process might play an important role in the ion desorption process. In addition, this increase of desorption efficiency corresponded to a decreased water contact angle and a general increase of intensities with the layer number for small molecules on the  $[\text{AuNP}]_n$  substrates. From the mass spectrum of ABP, it can be seen that the intensity of the fragment ion at  $m/z$  90 was very low (Supporting Information, Figure S8). Therefore, the survival yield of ABP from 4 different substrates was less sensitive to the layer number of  $[\text{AuNP}]_n$  substrates and generally very high ( $\geq 99.9\%$ ). The reason for this is that ABP tended to be desorbed directly off the  $[\text{AuNP}]_n$  substrates as an intact precursor ion rather than as a dissociation product. As previously reported,<sup>63,64</sup> high survival yields of ABP correspond to a small internal energy transfer from  $[\text{AuNP}]_n$  substrates under SALDI conditions, indicating that the higher survival yields of ABP are insensitive to internal energy transfers. This behavior cannot be explained by a thermal desorption mechanism, suggesting that some other nonthermal process occurs that dissipates the absorbed energy.

For the AuNP (diameter, 2.5 nm) used in our experiment, the melting point is only approx. 835 K.<sup>63,65</sup> The nanoparticles therefore melt relatively easily. Gold ions are thus common in vacuum SALDI mass spectra.<sup>30</sup> This was confirmed for our

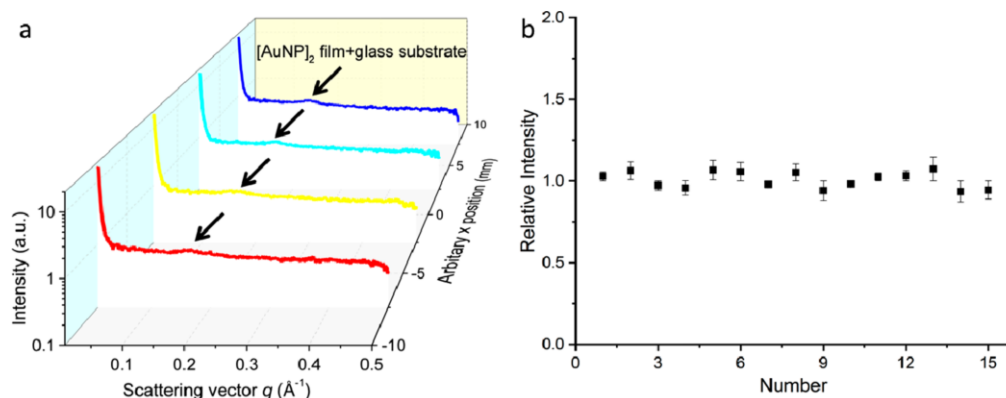


**Figure 7.** (a) Homogeneity of two-layer  $[\text{AuNP}]_2$  films characterized by SAXS. (b) Stability of SALDI signal intensities of linoleic acid for an  $[\text{AuNP}]_2$  film (linoleic acid,  $80 \mu\text{M}$ ).

AuNP, by investigating linoleic acid on  $[\text{AuNP}]_2$  substrates using vacuum MALDI (Supporting Information, Figure S9), clearly showing gold ions in both positive and negative modes (e.g.,  $\text{Au}^+$ ,  $\text{Au}_2^+$ ,  $\text{Au}_3^+$ ,  $\text{Au}_2^-$ ,  $\text{Au}_3^-$ , ...) under vacuum MALDI conditions, indicating ablation of AuNP during laser irradiation. However, under AP-MALDI conditions, no gold-related ions were observed (Supporting Information, Figure S9), suggesting insufficient energy for ablation and ionization of gold ions from the  $[\text{AuNP}]_2$  substrates. We hypothesize that during the laser irradiation, the local temperature rise on the surface of the  $[\text{AuNP}]_2$  substrate was not as pronounced under AP conditions as under vacuum conditions. Even the highest laser energy available on the AP-MALDI instrument provided no gold-related ions, while the vacuum MALDI instrument gave abundant gold ions, even at very low laser energies. This may be related to the effects of surface destruction, phase transitions, the air environment in the AP ion source, *etc.*; that is, processes that may help to dissipate the energy. We therefore believe that the local temperature of the  $[\text{AuNP}]_2$  substrates in AP-SALDI was not as high as the melting point of the AuNP but sufficient for desorption and ionization of the analytes.

**Structural Homogeneity of  $[\text{AuNP}]_n$  Films and Its Influence on Signal Reproducibilities and Detection Sensitivities.** The structural homogeneity of  $[\text{AuNP}]_n$  substrates was characterized by SAXS (Figure 7a). SAXS is a well-established protocol to evaluate the particles' structure (size, shape, and assembly), and the scattering intensity is proportional to the particles' number, form, and assembly.<sup>66,67</sup> As seen from the TEM data, the AuNP have well-defined structures, *i.e.*, narrow size distribution and uniform spherical shape. As the  $[\text{AuNP}]_n$  films were prepared by packing different numbers of the same single layers on top of each other, we used the intensity of this scattering peak for qualitative analysis of the structural homogeneity of the AuNP films. Moreover, we attributed the indicated peak in Figure 7a to the scattering signal of AuNP because a similar scattering peak was not observed for the neat glass substrate (Supporting Information, Figure S10a). As shown in Figure 7a, the peak intensities were virtually identical at different locations of the  $[\text{AuNP}]_2$  substrates covering a horizontal space of 15 mm, indicating a homogenous structure in the  $[\text{AuNP}]_2$  film. Similar homogeneity was found in the scattering curves of

other  $[\text{AuNP}]_n$  substrates with different thickness (Supporting Information, Figure S10).

Next, we characterized the analytes' homogeneity of dispersion on the  $[\text{AuNP}]_2$  substrates (Supporting Information, Figure S11). From the SEM images, it can be seen that the analytes were almost homogeneously distributed on the surface of the  $[\text{AuNP}]_2$  substrate, except for a minor coffee-ring effect.

We then assessed the signal reproducibility by evaluating the signal intensities for linoleic acid deposited onto an  $[\text{AuNP}]_2$  substrate (Figure 7b), showing fluctuations of <8% RSD. These low numbers agreed well with the homogenous distribution of AuNP in the  $[\text{AuNP}]_2$  films and also indirectly demonstrate the absence of major sweets spots for deposited analytes. In addition, signal reproducibilities of linoleic acid from different batches of  $[\text{AuNP}]_2$  films were also assessed (Supporting Information, Figure S12), showing comparable variations with RSD < 10 % RSD.

Finally, we investigated fatty acids for  $[\text{AuNP}]_2$  films at lower concentrations (Supporting Information, Figure S13). The approximate limits of detection for palmitic acid, stearic acid, oleic acid, and linoleic acid were  $2.0 \mu\text{M}$ ,  $2.0 \mu\text{M}$ ,  $0.5 \mu\text{M}$ , and  $0.5 \mu\text{M}$ , respectively. While these numbers are relatively high, they are mainly the result of the utilized quadrupole ion trap instrument, which was a less sensitive, older generation instrument used for the development work here. In addition, this instrument also did not allow high duty cycle data acquisition such as SIM or SRM, which could lower LOD 100–1000 $\times$  further.

## CONCLUSIONS

In this study,  $[\text{AuNP}]_n$  substrates were prepared by using a simple air/water approach. TEM and SAXS data showed that the resulting substrates were ultrathin and homogenous in terms of nanoparticle packing density. The  $[\text{AuNP}]_n$  substrates were successfully implemented for the SALDI-MS analysis of various small molecules, including fatty acids, drugs, amino acids, small peptides, and saccharides. The generated ion currents from the  $[\text{AuNP}]_1$  films were much higher than those from other aggregate states of AuNP. The signal intensities depended on the number of layers of the  $[\text{AuNP}]_n$  films and gradually reached a plateau for  $[\text{AuNP}]_2$  or  $[\text{AuNP}]_3$ . The  $[\text{AuNP}]_n$  substrates provide soft ionization characteristics with no observed fragmentations for the investigated analytes. We

utilized benzylpyridinium ions as thermometer ions to further describe the desorption and ionization process. The data showed that the desorption/ionization efficiency of ABP reached saturation for  $[\text{AuNP}]_2$ , directly correlating with the saturation of AuNP on the surface of the substrates. The  $[\text{AuNP}]_n$  substrates exhibited no distinct sweet spots, and the generated signals under SALDI-MS conditions were very stable, readily allowing quantitative analyses.

## ■ ASSOCIATED CONTENT

### Supporting Information

The Supporting Information is available free of charge at <https://pubs.acs.org/doi/10.1021/jasms.9b00038>.

Figure S1, TEM images; Figure S2, UV/vis spectra; Figure S3, visual image of  $[\text{AuNP}]_n$  substrates and corresponding UV/vis absorption spectra; Figure S4, UV/vis absorption of  $[\text{AuNP}]_n$  films; Figure S5, contact angle of multilayer AuNP films; Figures S6 and S11, SEM images; Figure S7, MALDI-MS and MS/MS spectra; Figure S8, SALDI mass spectrum; Figure S9, mass spectra; Figure S10, waterfall diagrams; Figure S12, stability of SALDI signal intensities; and Figure S13, signal-to-noise ratios (PDF)

## ■ AUTHOR INFORMATION

### Corresponding Author

\*Phone: +49 30 2093 7588. E-mail: [dietrich.volmer@huberlin.de](mailto:dietrich.volmer@huberlin.de).

### ORCID

Peng Zhang: 0000-0003-1695-360X

Thomas Kister: 0000-0002-9827-1380

Tobias Kraus: 0000-0003-2951-1704

Dietrich A. Volmer: 0000-0003-2820-1480

### Notes

The authors declare no competing financial interest.

## ■ ACKNOWLEDGMENTS

The authors would like to thank Nils Steinbruck (Saarland University) for UV/Vis spectra. Z.L. acknowledges the China Scholarship Council for financially supporting her Ph.D. studies.

## ■ REFERENCES

- (1) Karas, M.; Bachmann, D.; Hillenkamp, F. Influence of the Wavelength in High-Irradiance Ultraviolet Laser Desorption Mass Spectrometry of Organic Molecules. *Anal. Chem.* **1985**, *57*, 2935–2939.
- (2) Cole, R. B. *Electrospray and MALDI Mass Spectrometry: Fundamentals, Instrumentation, Practicalities, and Biological Applications*, 2nd ed.; 2010; DOI: 10.1002/9780470588901.
- (3) Cha, S.; Yeung, E. S. Colloidal graphite-assisted laser desorption/ionization mass spectrometry and MSn of small molecules. I. Imaging of cerebroside directly from rat brain tissue. *Anal. Chem.* **2007**, *79*, 2373–2385.
- (4) Xu, S.; Li, Y.; Zou, H.; Qiu, J.; Guo, Z.; Guo, B. Carbon Nanotubes as Assisted Matrix for Laser Desorption/Ionization Time-of-Flight Mass Spectrometry. *Anal. Chem.* **2003**, *75*, 6191–6195.
- (5) Lee, G.; Bae, S. E.; Huh, S.; Cha, S. Graphene oxide embedded sol-gel (GOSG) film as a SALDI MS substrate for robust metabolite fingerprinting. *RSC Adv.* **2015**, *5*, 56455–56459.
- (6) Lin, Z.; Wu, J.; Dong, Y.; Xie, P.; Zhang, Y.; Cai, Z. Nitrogen and Sulfur Co-doped Carbon-Dot-Assisted Laser Desorption/Ionization Time-of-Flight Mass Spectrometry Imaging for Profiling Bisphenol S Distribution in Mouse Tissues. *Anal. Chem.* **2018**, *90*, 10872–10880.
- (7) Wen, X.; Dagan, S.; Wysocki, V. H. Small-molecule analysis with silicon-nanoparticle-assisted laser desorption/ionization mass spectrometry. *Anal. Chem.* **2007**, *79*, 434–444.
- (8) Go, E. P.; Apon, J. V.; Luo, G.; Saghatelian, A.; Daniels, R. H.; Sahi, V.; Dubrow, R.; Cravatt, B. F.; Vertes, A.; Siuzdak, G. Desorption/ionization on silicon nanowires. *Anal. Chem.* **2005**, *77*, 1641–1646.
- (9) Wei, J.; Buriak, J. M.; Siuzdak, G. Desorption – ionization mass spectrometry on porous silicon. *Nature* **1999**, *399*, 243–246.
- (10) Marsico, A. L. M.; Creran, B.; Duncan, B.; Elci, S. G.; Jiang, Y.; Onasch, T. B.; Wormhoudt, J.; Rotello, V. M.; Vachet, R. W. Inkjet-Printed Gold Nanoparticle Surfaces for the Detection of Low Molecular Weight Biomolecules by Laser Desorption/Ionization Mass Spectrometry. *J. Am. Soc. Mass Spectrom.* **2015**, *26*, 1931–1937.
- (11) Silina, Y. E.; Meier, F.; Nebolsin, V. A.; Koch, M.; Volmer, D. A. Novel galvanic nanostructures of Ag and Pd for efficient laser desorption/ionization of low molecular weight compounds. *J. Am. Soc. Mass Spectrom.* **2014**, *25*, 841–851.
- (12) Kawasaki, H.; Yonezawa, T.; Watanabe, T.; Arakawa, R. Platinum nanoflowers for surface-assisted laser desorption/ionization mass spectrometry of biomolecules. *J. Phys. Chem. C* **2007**, *111*, 16278–16283.
- (13) Ding, F.; Qian, Y.; Deng, Z.; Zhang, J.; Zhou, Y.; Yang, L.; Wang, F.; Wang, J.; Zhou, Z.; Shen, J. Size-selected silver nanoparticles for MALDI-TOF mass spectrometry of amyloid-beta peptides. *Nanoscale* **2018**, *10*, 22044–22054.
- (14) Kim, K.; Um, K.; Yoon, C.; Ryoo, W. S.; Lee, K. Wafer-level detection of organic contamination by ZnO-rGO hybrid-assisted laser desorption/ionization time-of-flight mass spectrometry. *Talanta* **2018**, *182*, 273–278.
- (15) Lee, K.H.; Chiang, C.K.; Lin, Z.H.; Chang, H.T. Determining enediol compounds in tea using surface-assisted laser desorption/ionization mass spectrometry with titanium dioxide nanoparticle matrices. *Rapid Commun. Mass Spectrom.* **2007**, *21*, 2023–2030.
- (16) Kailasa, S. K.; Wu, H. F. Multifunctional ZrO<sub>2</sub> nanoparticles and ZrO<sub>2</sub>-SiO<sub>2</sub> nanorods for improved MALDI-MS analysis of cyclodextrins, peptides, and phosphoproteins. *Anal. Bioanal. Chem.* **2010**, *396*, 1115–1125.
- (17) Komori, H.; Hashizaki, R.; Osaka, I.; Hibi, T.; Katano, H.; Taira, S. Nanoparticle-assisted laser desorption/ionization using synaptic acid-modified iron oxide nanoparticles for mass spectrometry analysis. *Analyst* **2015**, *140*, 8134–8137.
- (18) Northen, T. R.; Yanes, O.; Northen, M. T.; Marrinucci, D.; Uritboonthai, W.; Apon, J.; Golledge, S. L.; Nordström, A.; Siuzdak, G. Clathrate nanostructures for mass spectrometry. *Nature* **2007**, *449*, 1033–1036.
- (19) Coffinier, Y.; Szunerits, S.; Drobecq, H.; Melnyk, O.; Boukherroub, R. Diamond nanowires for highly sensitive matrix-free mass spectrometry analysis of small molecules. *Nanoscale* **2012**, *4*, 231–238.
- (20) Lu, T.; Olesik, S. V. Electrospun nanofibers as substrates for surface-assisted laser desorption/ionization and matrix-enhanced surface-assisted laser desorption/ionization mass spectrometry. *Anal. Chem.* **2013**, *85*, 4384–4391.
- (21) Wang, H.; Wu, Y.; Guo, B.; Sun, W.; Ding, L.; Chen, B. Quantification of low-polar small molecules using room temperature ionic liquids matrix-assisted desorption corona beam ionization. *Analyst* **2012**, *137*, 3982–3988.
- (22) Silina, Y. E.; Volmer, D. A. Nanostructured solid substrates for efficient laser desorption/ionization mass spectrometry (LDI-MS) of low molecular weight compounds. *Analyst* **2013**, *138*, 7053.
- (23) Chiang, C. K.; Chen, W. T.; Chang, H. T. Nanoparticle-based mass spectrometry for the analysis of biomolecules. *Chem. Soc. Rev.* **2011**, *40*, 1269–1281.
- (24) Guinan, T.; Kirkbride, P.; Pigou, P. E.; Ronci, M.; Kobus, H.; Voelcker, N. H. Surface-assisted laser desorption ionization mass

- spectrometry techniques for application in forensics. *Mass Spectrom. Rev.* **2015**, *34*, 627–640.
- (25) Song, K.; Cheng, Q. Desorption and ionization mechanisms and signal enhancement in surface assisted laser desorption/ionization mass spectrometry (SALDI-MS). *Appl. Spectrosc. Rev.* **2019**, 1–23.
- (26) Stolee, J. A.; Walker, B. N.; Zorba, V.; Russo, R. E.; Vertes, A. Laser-nanostructure interactions for ion production. *Phys. Chem. Chem. Phys.* **2012**, *14*, 8453–8471.
- (27) Tanaka, K. The Origin of Macromolecule Ionization by Laser Irradiation (Nobel Lecture). *Angew. Chem., Int. Ed.* **2003**, *42*, 3860–3870.
- (28) Unnikrishnan, B.; Chang, C. Y.; Chu, H. W.; Anand, A.; Huang, C. C. Functional gold nanoparticles coupled with laser desorption/ionization mass spectrometry for bioanalysis. *Anal. Methods*. **2016**, *8*, 8123–8133.
- (29) Abdelhamid, H. N.; Wu, H. F. Gold nanoparticles assisted laser desorption/ionization mass spectrometry and applications: from simple molecules to intact cells. *Anal. Bioanal. Chem.* **2016**, *408*, 4485–4502.
- (30) McLean, J. A.; Stumpo, K. A.; Russell, D. H. Size-selected (2–10 nm) gold nanoparticles for matrix assisted laser desorption/ionization of peptides. *J. Am. Chem. Soc.* **2005**, *127*, 5304–5305.
- (31) Amendola, V.; Litti, L.; Meneghetti, M. LDI-MS assisted by chemical-free gold nanoparticles: Enhanced sensitivity and reduced background in the low-mass region. *Anal. Chem.* **2013**, *85*, 11747–11754.
- (32) Castellana, E.T.; Gamez, R.C.; Gómez, M.E.; Russell, D.H. Longitudinal surface plasmon resonance based gold nanorod biosensors for mass spectrometry. *Langmuir* **2010**, *26*, 6066–6070.
- (33) Kolářová, L.; Kučera, L.; Vanhara, P.; Hampl, A.; Havel, J. Use of flower-like gold nanoparticles in time-of-flight mass spectrometry. *Rapid Commun. Mass Spectrom.* **2015**, *29*, 1585–1595.
- (34) Palermo, A.; Forsberg, E. M.; Warth, B.; Aisporna, A. E.; Billings, E.; Kuang, E.; Benton, H. P.; Berry, D.; Siuzdak, G. Fluorinated Gold Nanoparticles for Nanostructure Imaging Mass Spectrometry. *ACS Nano* **2018**, *12*, 6938–6948.
- (35) Kuo, T.R.; Chen, Y.C.; Wang, C.I.; Shen, T.H.; Wang, H.Y.; Pan, X.Y.; Wang, D.Y.; Liou, C.C.; Chang, Y.H.; Chen, Y.C.; Wu, Y.H.; Liu, Y.R.; Lin, Y.H.; Hu, C.C.; Chen, C.C. Highly oriented Langmuir-Blodgett film of silver cuboctahedra as an effective matrix-free sample plate for surface-assisted laser desorption/ionization mass spectrometry. *Nanoscale* **2017**, *9*, 11119–11125.
- (36) Wu, H. P.; Su, C. L.; Chang, H. C.; Tseng, W. L. Sample-first preparation: A method for surface-assisted laser desorption/ionization time-of-flight mass spectrometry analysis of cyclic oligosaccharides. *Anal. Chem.* **2007**, *79*, 6215–6221.
- (37) Pan, X. Y.; Chen, C. H.; Chang, Y. H.; Wang, D. Y.; Lee, Y. C.; Liou, C. C.; Wang, Y. X.; Hu, C. C.; Kuo, T. R. Osteoporosis risk assessment using multilayered gold-nanoparticle thin film via SALDI-MS measurement. *Anal. Bioanal. Chem.* **2019**, *411*, 2793–2802.
- (38) Liu, R.; Liu, J. F.; Zhou, X.X.; Jiang, G. Bin: Cysteine modified small ligament au nanoporous film: An easy fabricating and highly efficient surface-assisted laser desorption/ionization substrate. *Anal. Chem.* **2011**, *83*, 3668–3674.
- (39) Kawasaki, H.; Sugitani, T.; Watanabe, T.; Yonezawa, T.; Moriwaki, H.; Arakawa, R. Layer-by-layer self-assembled multilayer films of gold nanoparticles for surface-assisted laser desorption/ionization mass spectrometry. *Anal. Chem.* **2008**, *80*, 7524–7533.
- (40) Choi, Y. K.; Oh, J. Y.; Han, S. Y. Large-Area Graphene Films as Target Surfaces for Highly Reproducible Matrix-Assisted Laser Desorption Ionization Suitable for Quantitative Mass Spectrometry. *J. Am. Soc. Mass Spectrom.* **2018**, *29*, 2003–2011.
- (41) Kuo, T. R.; Wang, D. Y.; Chiu, Y. C.; Yeh, Y. C.; Chen, W. T.; Chen, C. H.; Chen, C. W.; Chang, H. C.; Hu, C. C.; Chen, C. C. Layer-by-layer thin film of reduced graphene oxide and gold nanoparticles as an effective sample plate in laser-induced desorption/ionization mass spectrometry. *Anal. Chim. Acta* **2014**, *809*, 97–103.
- (42) Mihi, A.; Ocaña, M.; Míguez, H. Oriented colloidal-crystal thin films by spin-coating microspheres dispersed in volatile media. *Adv. Mater.* **2006**, *18*, 2244–2249.
- (43) Malaquin, L.; Kraus, T.; Schmid, H.; Delamar, E.; Wolf, H. Controlled particle placement through convective and capillary assembly. *Langmuir* **2007**, *23*, 11513–11521.
- (44) Weekes, S. M.; Ogrin, F. Y.; Murray, W. A.; Keatley, P. S. Macroscopic arrays of magnetic nanostructures from self-assembled nanosphere templates. *Langmuir* **2007**, *23*, 1057–1060.
- (45) Retsch, M.; Zhou, Z.; Rivera, S.; Kappl, M.; Zhao, X. S.; Jonas, U.; Qin, L. Fabrication of large-area, transferable colloidal monolayers utilizing self-assembly at the air/water interface. *Macromol. Chem. Phys.* **2009**, *210*, 230–241.
- (46) Bardosova, M.; Pemble, M. E.; Povey, I. M.; Tredgold, R. H. The langmuir-blodgett approach to making colloidal photonic crystals from silica spheres. *Adv. Mater.* **2010**, *22*, 3104–3124.
- (47) Denkov, N. D.; Velev, O. D.; Kralchevsky, P. A.; Ivanov, I. B.; Yoshimura, H.; Nagayama, K. Two-dimensional crystalization. *Nature* **1993**, *361*, 26.
- (48) Vogel, N.; Goerres, S.; Landfester, K.; Weiss, C. K. A convenient method to produce close- and non-close-packed monolayers using direct assembly at the air-water interface and subsequent plasma-induced size reduction. *Macromol. Chem. Phys.* **2011**, *212*, 1719–1734.
- (49) Kim, Y.-K. K.; Min, D.-H. H. Mechanistic study of laser desorption/ionization of small molecules on graphene oxide multilayer films. *Langmuir* **2014**, *30*, 12675–12683.
- (50) Vogel, N.; Retsch, M.; Fustin, C. A.; Del Campo, A.; Jonas, U. Advances in Colloidal Assembly: The Design of Structure and Hierarchy in Two and Three Dimensions. *Chem. Rev.* **2015**, *115*, 6265–6311.
- (51) Kister, T.; Mravlak, M.; Schilling, T.; Kraus, T. Pressure-controlled formation of crystalline, Janus, and core-shell supraparticles. *Nanoscale* **2016**, *8*, 13377–13384.
- (52) Laiko, V. V.; Moyer, S. C.; Cotter, R. J. Atmospheric pressure MALDI/Ion trap mass spectrometry. *Anal. Chem.* **2000**, *72*, 5239–5243.
- (53) Schulz, E.; Karas, M.; Rosu, F.; Gabelica, V. Influence of the Matrix on Analyte Fragmentation in Atmospheric Pressure MALDI. *J. Am. Soc. Mass Spectrom.* **2006**, *17*, 1005–1013.
- (54) Keller, C.; Maeda, J.; Jayaraman, D.; Chakraborty, S.; Sussman, M. R.; Harris, J. M.; Ané, J. M.; Li, L. Comparison of vacuum maldi and ap-maldi platforms for the mass spectrometry imaging of metabolites involved in salt stress in medicago truncatula. *Front. Plant Sci.* **2018**, *9*, 1238.
- (55) Tan, P. V.; Laiko, V. V.; Doroshenko, V. M. Atmospheric Pressure MALDI with Pulsed Dynamic Focusing for High-Efficiency Transmission of Ions into a Mass Spectrometer. *Anal. Chem.* **2004**, *76*, 2462–2469.
- (56) Schneider, B. B.; Lock, C.; Covey, T. R. AP and vacuum MALDI on a QqLIT instrument. *J. Am. Soc. Mass Spectrom.* **2005**, *16*, 176–182.
- (57) Miller, C. A.; Yi, D.; Perkins, P. D. An atmospheric pressure matrix-assisted laser desorption/ionization ion trap with enhanced sensitivity. *Rapid Commun. Mass Spectrom.* **2003**, *17*, 860–868.
- (58) Huang, C. C.; Yang, Z.; Lee, K. H.; Chang, H. T. Synthesis of highly fluorescent gold nanoparticles for sensing mercury(II). *Angew. Chem., Int. Ed.* **2007**, *46*, 6824–6828.
- (59) Jin, R. Atomically precise metal nanoclusters: Stable sizes and optical properties. *Nanoscale* **2015**, *7*, 1549–1565.
- (60) Gámez, F.; Plaza-Reyes, A.; Hurtado, P.; Guillén, E.; Anta, J. A.; Martínez-Haya, B.; Pérez, S.; Sanz, M.; Castillejo, M.; Izquierdo, J. G.; Bañares, L. Nanoparticle TiO<sub>2</sub> films prepared by pulsed laser deposition: Laser desorption and cationization of model adsorbates. *J. Phys. Chem. C* **2010**, *114*, 17409–17415.
- (61) Kim, Y.-K. K.; Wang, L.-S. S.; Landis, R.; Kim, C. S.; Vachet, R. W.; Rotello, V. M. A layer-by-layer assembled MoS<sub>2</sub> thin film as an efficient platform for laser desorption/ionization mass spectrometry analysis of small molecules. *Nanoscale* **2017**, *9*, 10854–10860.

(62) Lee, C.; Ni, C. K. Soft Matrix-Assisted Laser Desorption/Ionization for Labile Glycoconjugates. *J. Am. Soc. Mass Spectrom.* **2019**, *30*, 1455–1463.

(63) Ng, K. M.; Chau, S. L.; Tang, H. W.; Wei, X. G.; Lau, K. C.; Ye, F.; Ng, A. M. C. Ion-Desorption Efficiency and Internal-Energy Transfer in Surface-Assisted Laser Desorption/Ionization: More Implication(s) for the Thermal-Driven and Phase-Transition-Driven Desorption Process. *J. Phys. Chem. C* **2015**, *119*, 23708–23720.

(64) Tang, H.-W.; Che, C.-M. Ion Desorption Efficiency and Internal Energy Transfer in Carbon Based SALDI-MS: Desorption Mechanisms and the Design of Substrates. *Anal. Chem.* **2009**, *81*, 4720–4729.

(65) Shim, J. H.; Lee, B. J.; Cho, Y. W. Thermal stability of unsupported gold nanoparticle: A molecular dynamics study. *Surf. Sci.* **2002**, *512*, 262–268.

(66) Liu, D.; Pallon, L. K. H.; Pourrahimi, A. M.; Zhang, P.; Diaz, A.; Holler, M.; Schneider, K.; Olsson, R.T.; Hedenqvist, M.S.; Yu, S.; Gedde, U.W. Cavitation in strained polyethylene/aluminium oxide nanocomposites. *Eur. Polym. J.* **2017**, *87*, 255–265.

(67) Zhang, P.; Kraus, T. Anisotropic nanoparticles as templates for the crystalline structure of an injection-molded isotactic polypropylene/TiO<sub>2</sub> nanocomposite. *Polymer* **2017**, *130*, 161–169.

*Supplementary Material*

**Ultra-thin homogenous AuNP monolayers as tunable functional substrates for surface-assisted laser desorption/ionization of small biomolecules**

Zhen Liu, Peng Zhang, Thomas Kister, Tobias Kraus, Dietrich A. Volmer

Journal of the American Society for Mass Spectrometry, 2020, 31, 1, 47-57,

<https://doi.org/10.1021/jasms.9b00038>

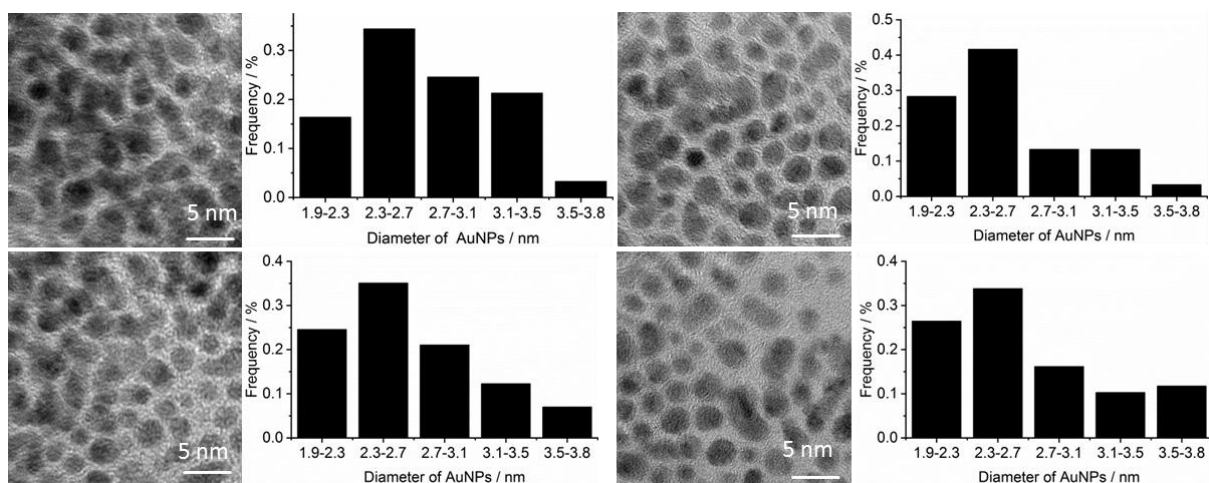


**Figure S1.** TEM images of single layers of AuNP films from 4 different batches along with corresponding size distributions of the AuNP.

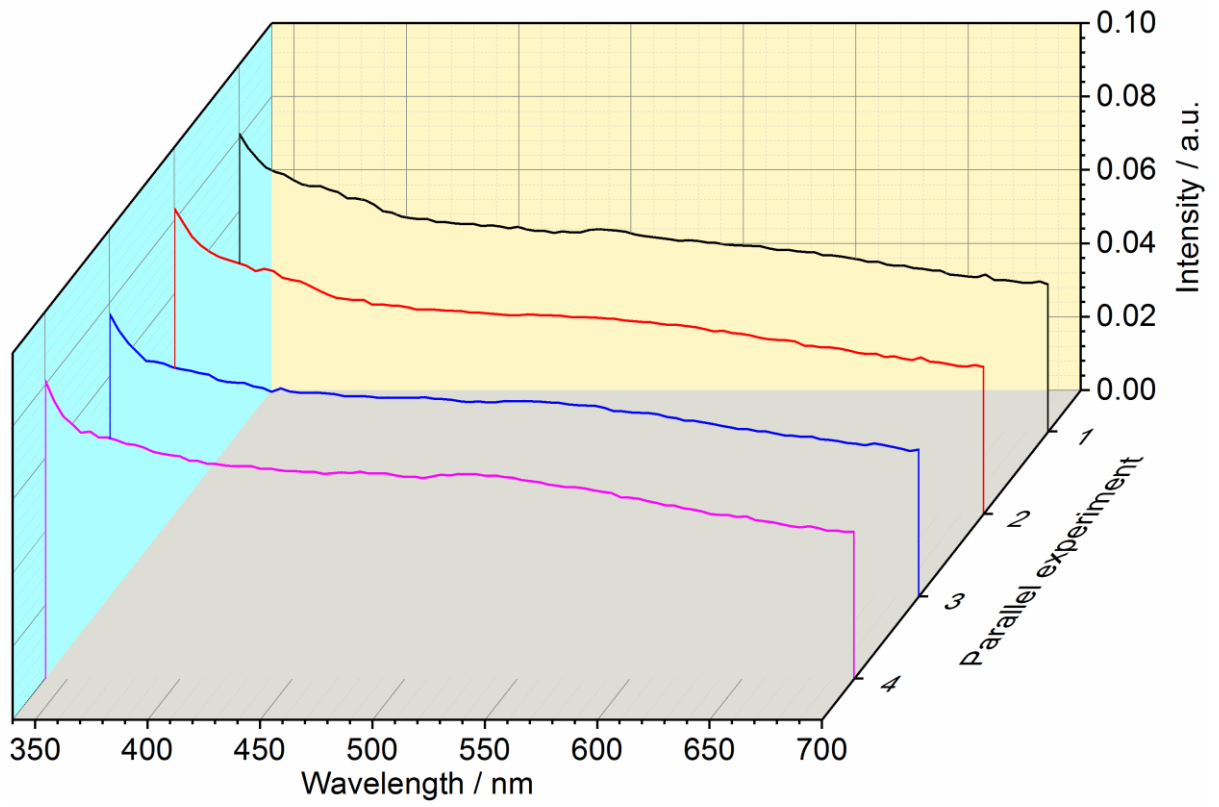


**Figure S2.** UV/Vis spectra of single layers of AuNP films from four different batches.

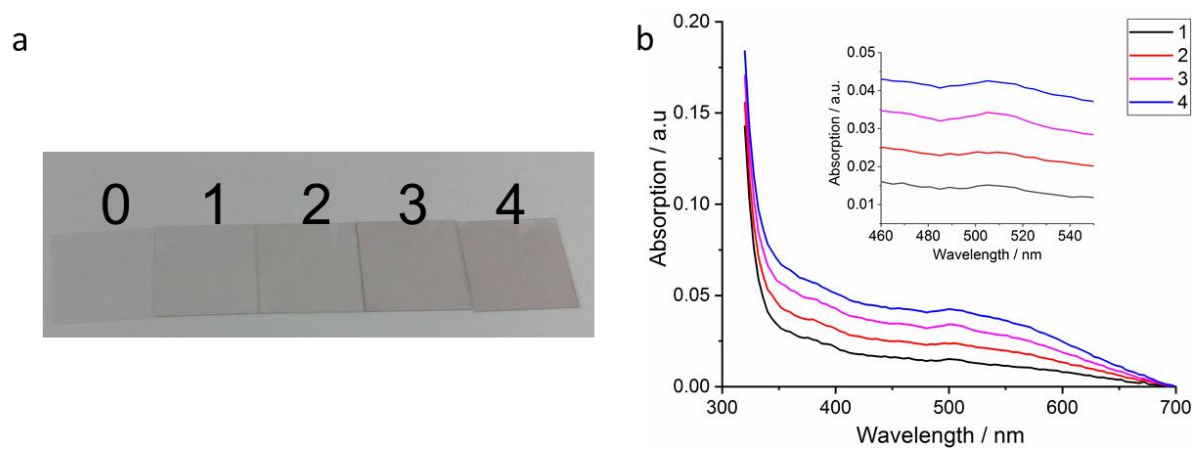


**Figure S3.** (a) Visual image of  $[\text{AuNP}]_n$  substrates and (b) corresponding UV/Vis absorption spectra.

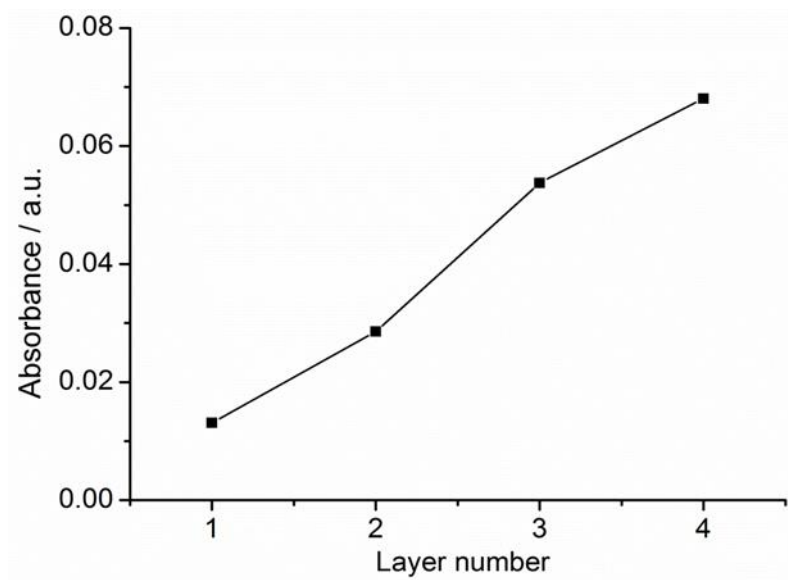


**Figure S4.** UV/Vis absorption of [AuNP]<sub>n</sub> films at 355 nm.

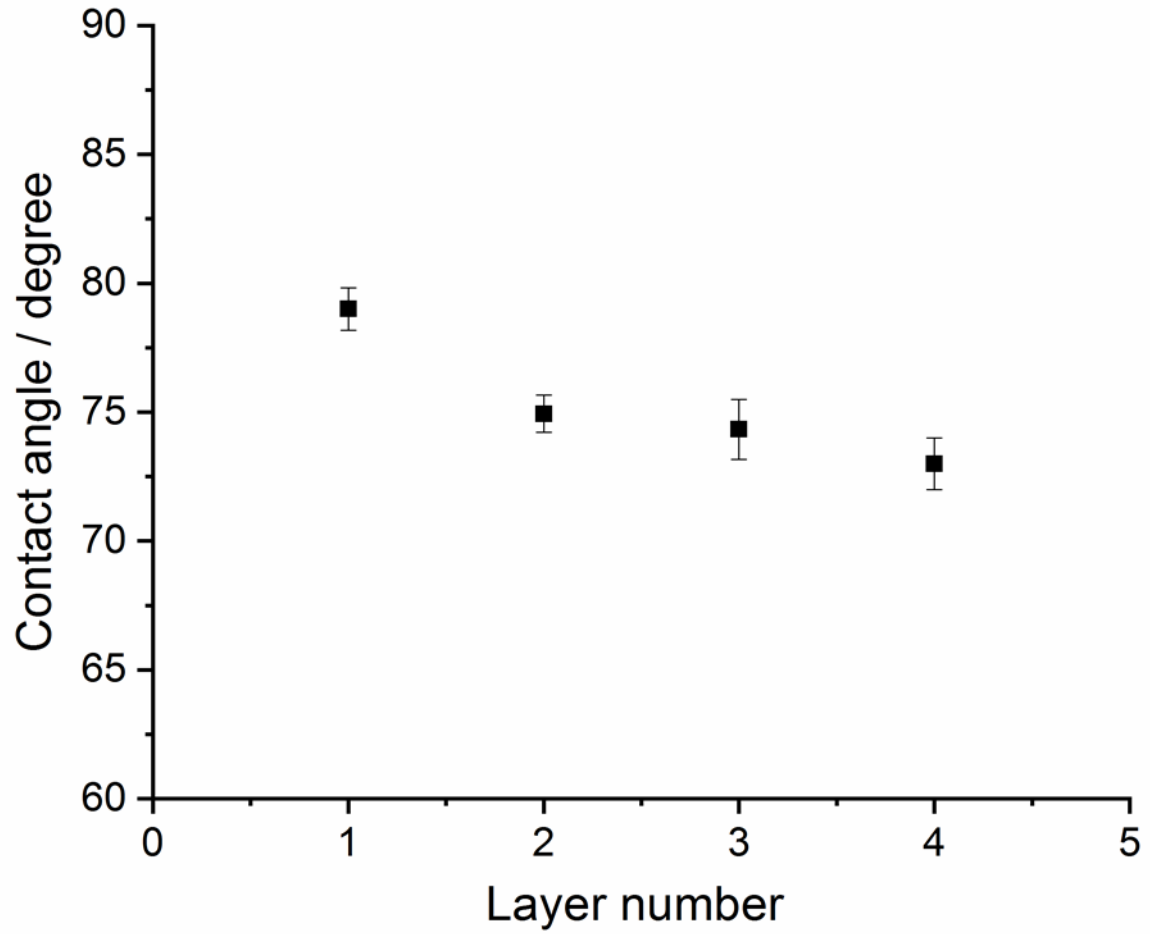


**Figure S5.** Contact angle of multilayer AuNP films.

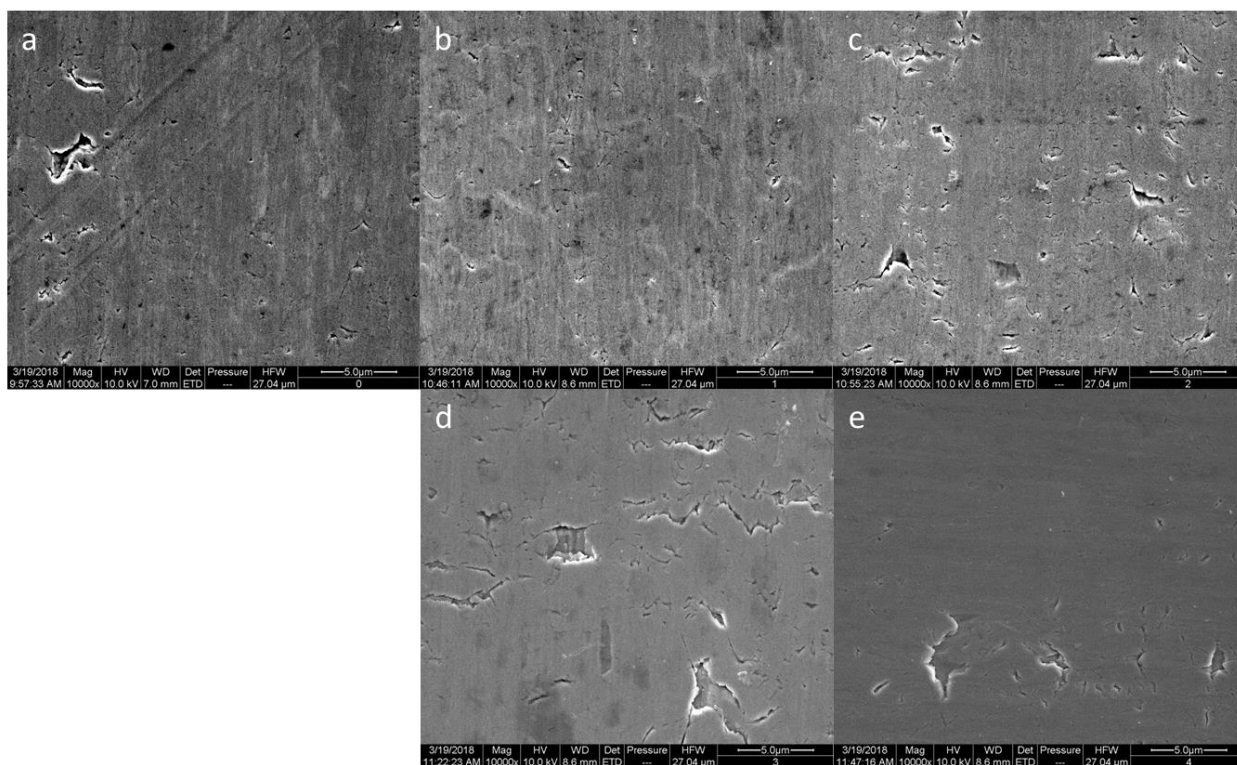


**Figure S6.** SEM images of [AuNP]<sub>n</sub> films:  $n =$  (a) 0, (b) 1, (c) 2, (d) 3 and (e) 4 layers.

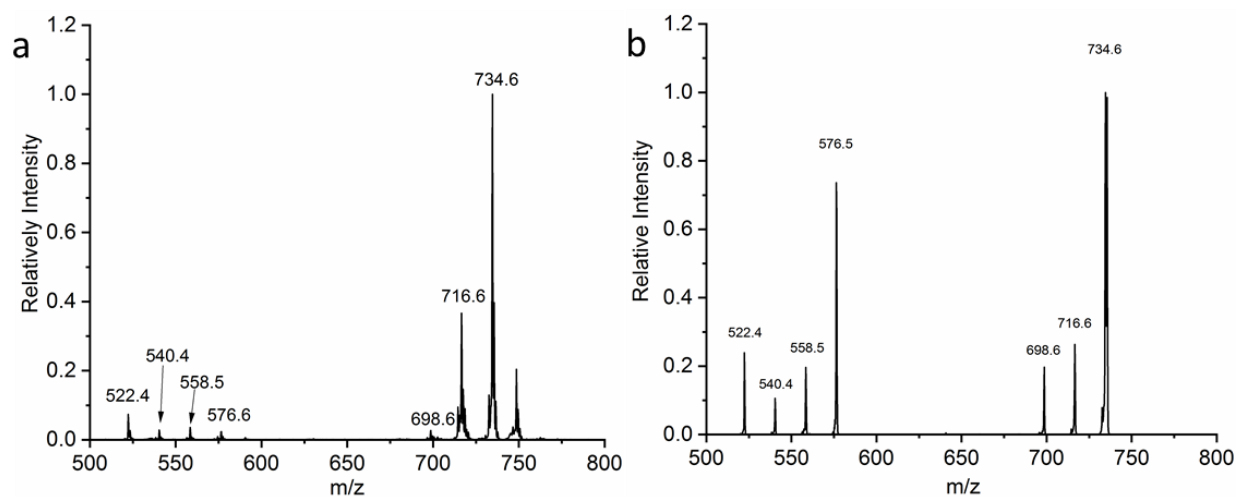


**Figure S7.** (a) MALDI-MS and (b) MS/MS spectrum of erythromycin A using CHCA as matrix (CHCA, 10 mg/mL; erythromycin A, 100  $\mu$ M).

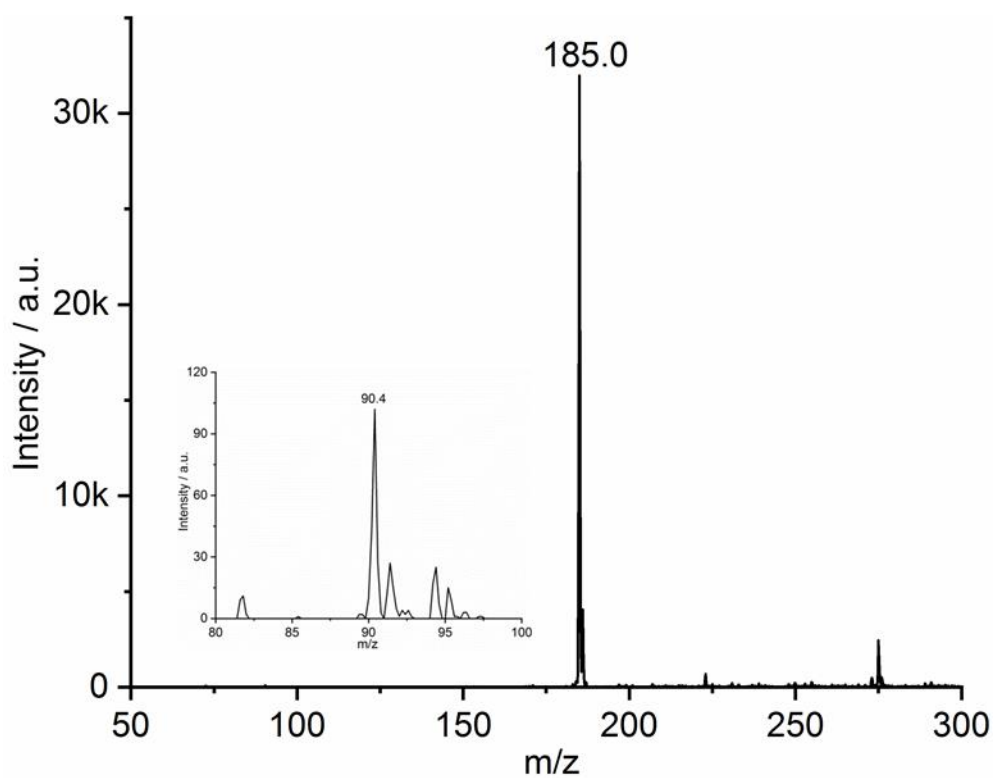


**Figure S8.** SALDI mass spectrum of 4-amino-1-benzylpyridinium (ABP) ions from an  $[\text{AuNP}]_1$  substrate.

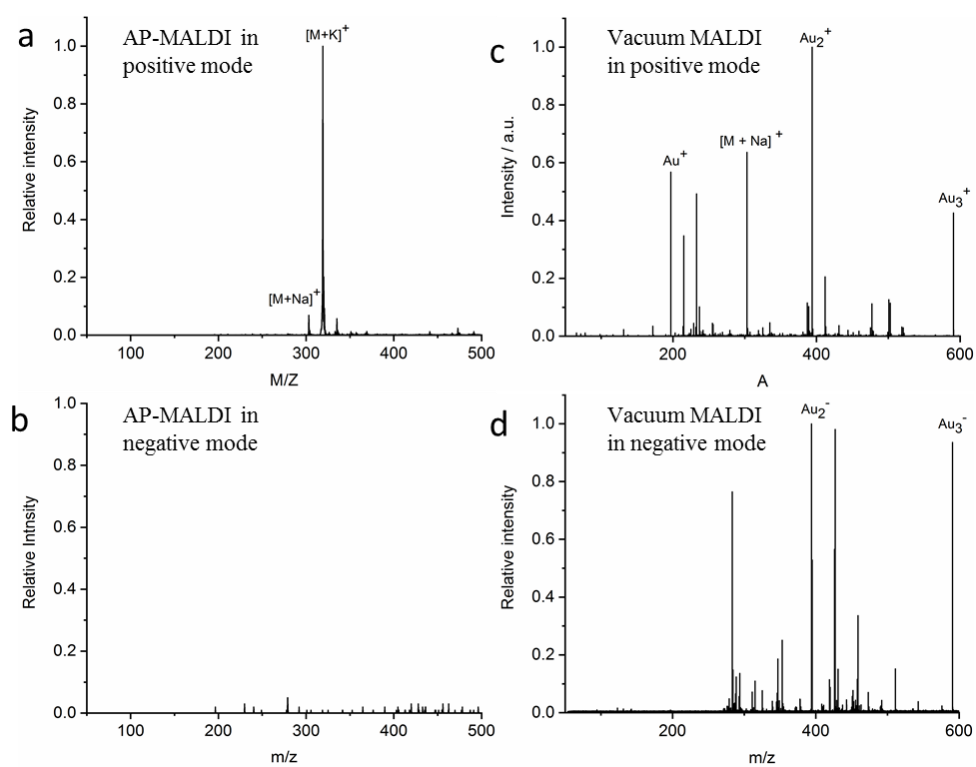


**Figure S9.** Panels (a) and (b) show mass spectra of linoleic acid under positive and negative ionization from AP-SALDI analysis; (c) and (d) illustrate mass spectra in positive and negative ion mode from vacuum MALDI analysis (concentration of linoleic acid, 100  $\mu$ M; M denotes the monoisotopic mass of linoleic acid).

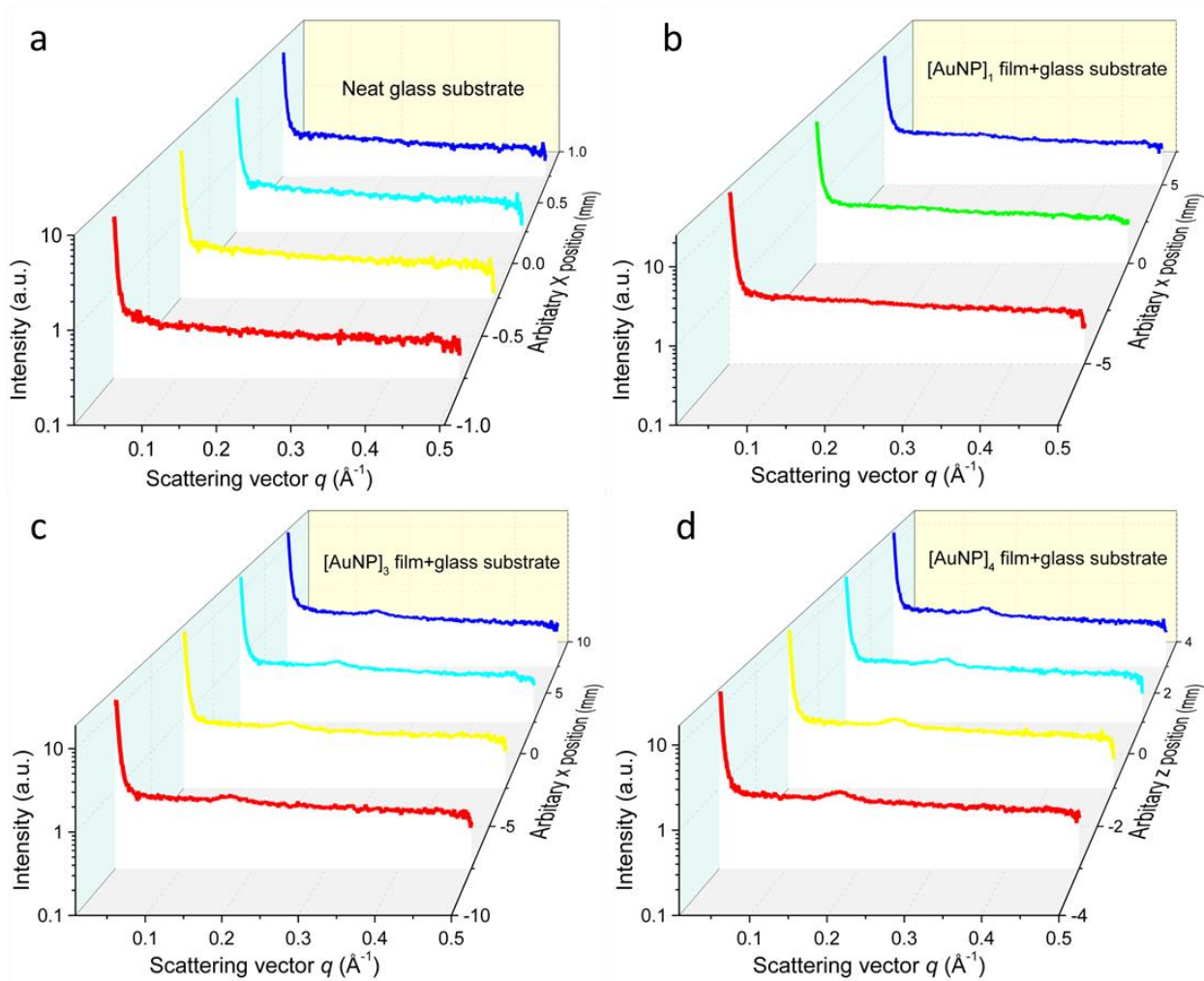


**Figure S10.** Waterfall diagrams of the small angle X-scattering patterns of  $[\text{AuNP}]_n$  films on cover glass: (a) neat glass substrate, (b)  $[\text{AuNP}]_1$  film, (c)  $[\text{AuNP}]_3$  film, and (d)  $[\text{AuNP}]_4$  film along  $x$ -axis.

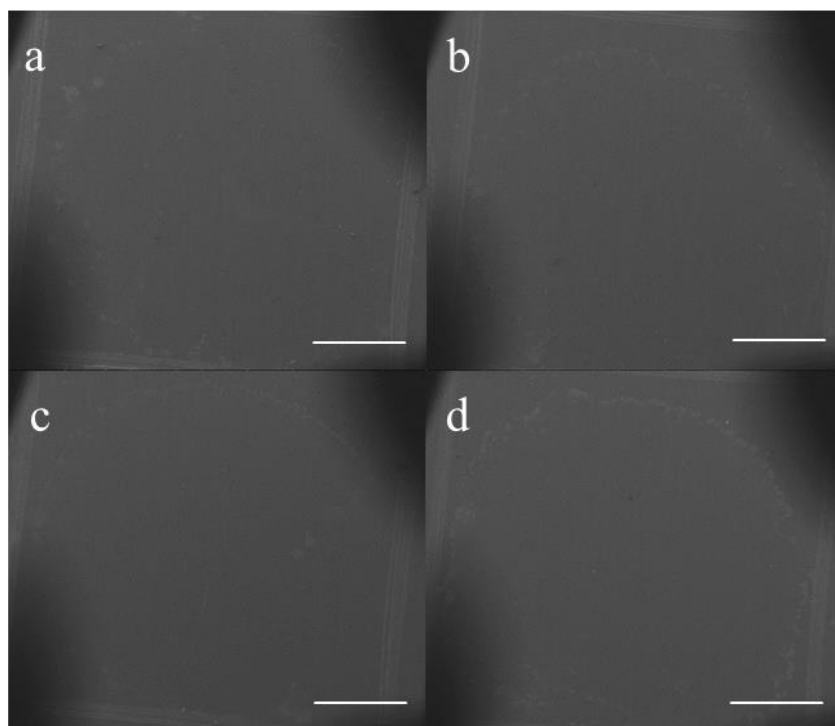


**Figure S11.** Panels (a), (b), (c) and (d) show SEM images of linoleic acid, erythromycin A, phenylalanine and fructose spotted onto an [AuNP]<sub>2</sub> substrate. The concentrations of linoleic acid, erythromycin A, phenylalanine and fructose were 100  $\mu\text{M}$  each. The scale bar is 1.0 mm long.

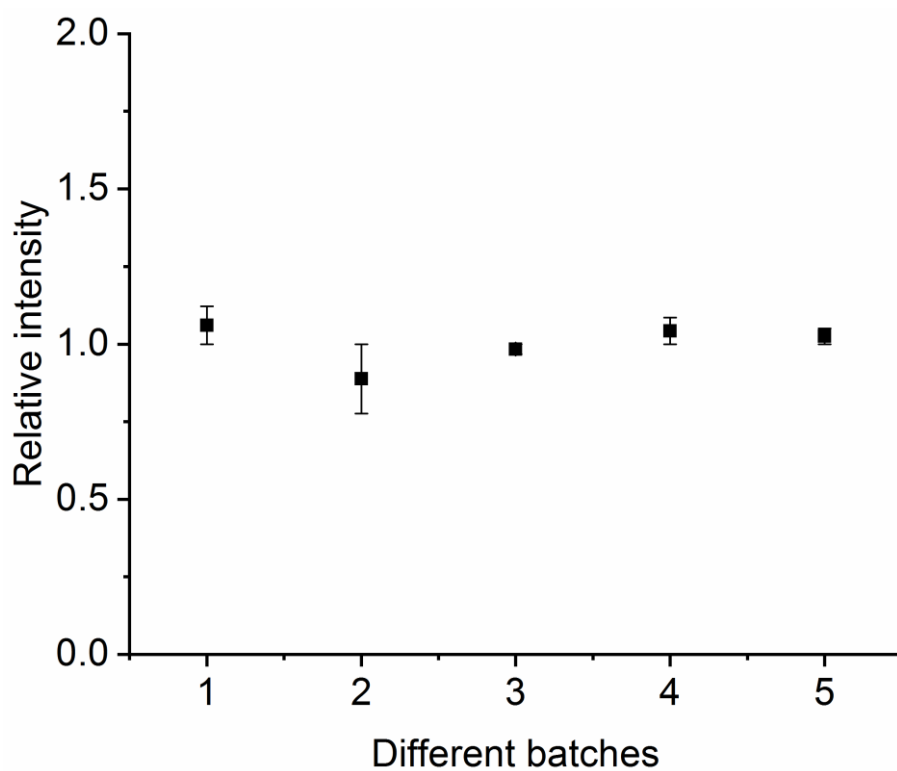


**Figure S12.** Stability of SALDI signal intensities of linoleic acid from different batches of [AuNP]<sub>2</sub> films (linoleic acid, 100  $\mu$ M).

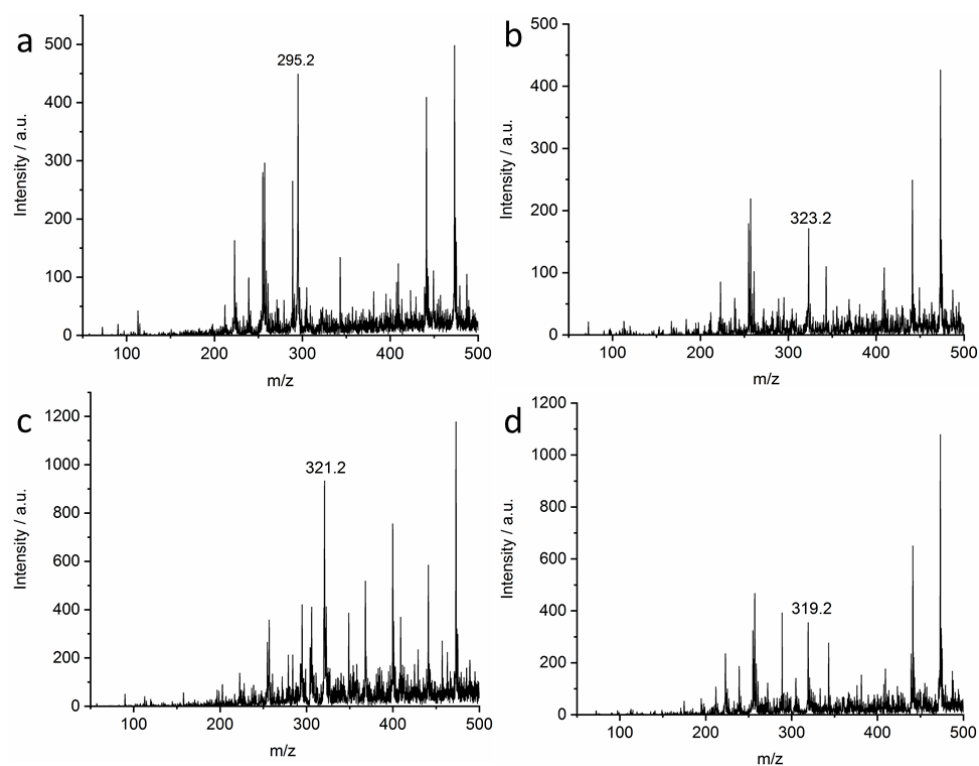


**Figure S13.** Signal-to-noise ratios near the the limit of detection for (a) palmitic acid, (b) stearic acid, (c) oleic acid and (d) linoleic acid on  $[\text{AuNP}]_2$  substrates. The concentration of palmitic acid, stearic acid, oleic acid and linoleic acid were 2.0, 2.0, 0.5  $\mu\text{M}$  and 0.5  $\mu\text{M}$ , respectively.

### **Publication 3**

## **Influence of core size and capping ligand of gold nanoparticles on the desorption/ionization efficiency of small biomolecules in AP-SALDI-MS**

Zhen Liu, Peng Zhang, Andrea Pyttlik, Tobias Kraus, Dietrich A. Volmer

Analytical Science Advance, 2020, in press. <https://doi.org/10.1002/ansa.202000002>

This article is open access and permits to use with proper citation.



## FULL ARTICLE

# Influence of core size and capping ligand of gold nanoparticles on the desorption/ionization efficiency of small biomolecules in AP-SALDI-MS

Zhen Liu<sup>1</sup> | Peng Zhang<sup>2</sup> | Andrea Pyttlik<sup>3</sup> | Tobias Kraus<sup>3,4</sup> | Dietrich A. Volmer<sup>5</sup>

<sup>1</sup>Institute of Bioanalytical Chemistry, Saarland University, Saarbrücken, Germany

<sup>2</sup>School of Materials Science and Engineering, Sun Yat-sen University, Guangzhou, China

<sup>3</sup>INM-Leibniz Institute for New Materials, Saarbrücken, Germany

<sup>4</sup>Institute of Colloid and Interface Chemistry, Saarland University, Saarbrücken, Germany

<sup>5</sup>Department of Chemistry, Humboldt-Universität zu Berlin, Berlin, Germany

**Correspondence**

Prof. Dr. Dietrich A. Volmer, Department of Chemistry, Humboldt-Universität zu Berlin, Brook-Taylor-Str. 2, 12489 Berlin, Germany  
Email: dietrich.volmer@hu-berlin.de

**Funding information**

China Scholarship Council

**Abstract**

Gold nanoparticles (AuNP) are frequently used in surface-assisted laser desorption/ionization mass spectrometry (SALDI-MS) for analysis of biomolecules because they exhibit suitable thermal and chemical properties as well as strong surface plasmonic effects. Moreover, the structures of AuNP can be controlled by well-established synthesis protocols. This was important in the present work, which studied the influence of the nanoparticles' structures on atmospheric pressure (AP)-SALDI-MS performance. A series of AuNP with different core sizes and capping ligands were investigated, to examine the desorption/ionization efficiency (DIE) under AP-SALDI conditions. The results showed that both the AuNP core size as well as the nature of the surface ligand had a strong influence on DIE. DIE increased with the size of the AuNP and the hydrophobicity of the ligands. Chemical interactions between ligand and analytes also influenced DIE. Moreover, we discovered that removing the organic ligands from the deposited AuNP substrate layer by simple laser irradiation prior to LDI further amplified DIE values. The optimized AuNP were successfully used to analyze a wide arrange of different low molecular weight biomolecules as well as a crude pig brain extract, which readily demonstrated the ability of the technique to detect a wide range of lipid species within highly complex samples.

## 1 | INTRODUCTION

Since cobalt nanoparticles were first used for surface-assisted laser desorption/ionization mass spectrometry (SALDI-MS) by Tanaka *et al.*,<sup>1</sup> nanomaterials made from carbon,<sup>2-4</sup> silicon,<sup>5-7</sup> metals (Au, Ag, Pa, etc.),<sup>8-10</sup> metal oxides,<sup>11-13</sup> and others materials<sup>14-17</sup> have been successfully applied to SALDI-MS. In general, nanoparticles are excellent substrate options for SALDI, because they require only simple and easy sample preparation techniques and the materials often exhibit minimal background signals – in particular in the low *m/z* range – as compared to matrix-assisted laser desorption/ionization (MALDI).<sup>18-20</sup> SALDI efficiencies can be enhanced by optimizing the nanoparticulate structures, for example, by modifying the core size and nature of the surface ligands,<sup>18</sup> which was shown to be vital for sensitive quantitative analysis of biomolecules.<sup>20</sup>

In previous studies, it was found that desorption/ionization efficiency of SALDI was highly dependent on physical (size, surface roughness, light absorption, electrical conductivity, melting point, etc.) and chemical (surface modification, binding energy to analytes, etc.) properties of the nanomaterials.<sup>18-23</sup> Gold nanoparticles (AuNP) exhibit excellent electrical conductivities, thermal and chemical stabilities and strong light

This is an open access article under the terms of the Creative Commons Attribution-NonCommercial License, which permits use, distribution and reproduction in any medium, provided the original work is properly cited and is not used for commercial purposes.

© 2020 The Authors. *Analytical Science Advances* published by WILEY-VCH Verlag GmbH & Co. KGaA, Weinheim.



absorption due to plasmonic effects. Furthermore, gold nanoparticles can be readily obtained using well-established synthesis protocols. Consequently, they have been frequently used for SALDI-MS analysis of biomolecules. Mclean *et al.*<sup>24</sup> applied AuNP of different sizes (2–10 nm) to detect peptides. The authors found a size effect on desorption/ionization efficiency of peptides, where larger AuNP provided better performance. Ligand-free AuNP were reported by Amendola *et al.*<sup>25</sup> that exhibited low background levels in the low mass range ( $m/z < 500$ ) as compared to AuNP with surface-protected agents, providing picomolar level detection levels for small molecules such as arginine, fructose, atrazine, anthracene, and paclitaxel. Flower-like gold nanoparticles were used by Havel *et al.* as mediators to enhance desorption/ionization of peptides.<sup>26</sup> The authors illustrated that the ion intensities for the peptides were up to 7.5-fold higher using gold nanoflowers as substrate as compared to  $\alpha$ -cyanohydroxycinnamic acid (CHCA) as MALDI matrix. Using gold nanorods (AuNR), Castellana *et al.* demonstrated that infrared laser desorption/ionization-MS was capable of analyzing peptides very efficiently.<sup>27</sup> Furthermore, fluorinated AuNP were prepared for comprehensive analysis of metabolites in biological tissues using nanostructure imaging mass spectrometry (NIMS) with minimal background noise levels and high sensitivity as illustrated by Palermo *et al.*<sup>28</sup> Only low laser energies were required during this process, which lead to very gentle desorption/ionization conditions with limited in-source fragmentation of the metabolites. Chiang *et al.*<sup>29</sup> used mixed gold nanoparticles with diameters of 3 and 14 nm as probes for SALDI-MS to detect amino-thiol groups. The authors illustrated that larger size gold nanoparticles selectively captured amino-thiol on the surface, while the smaller particles improved sensitivity. Glutathione, cysteine, and homocysteine were successfully detected at detection limits of 2, 20, and 44 nM, respectively. Son *et al.*<sup>30</sup> used citrate-capped AuNP with diameter of 12 nm to selectively detect triacylglycerols from crude lipid mixtures at very low levels, approximately 100-fold lower than by MALDI with dihydroxybenzoic acid (DHB) as matrix. Liu *et al.*<sup>31</sup> utilized ultra-thin, homogenous [AuNP]<sub>n</sub> monolayer substrates for SALDI, which provided excellent signal intensities and low background for a wide range of analytes such as fatty acids, peptides, amino acids, saccharides, and drugs. AuNP were also used to directly analyze endogenous and exogenous compounds from latent fingerprint and image their distribution, without disturbing the fingerprint patterns, as demonstrated by Tang *et al.*<sup>32</sup>

While AuNP were shown to be well-suited functional substrates for SALDI-MS, the factors governing their performance are not yet fully understood. In this paper, various parameters of AuNP influencing desorption/ionization efficiency of analytes were systematically studied. Several different ligands for functionalized AuNP of different sizes, including oleyamine, alkanethiol, 11-mercaptoundecanoic acid, and 11-mercapto-1-undecanol, were investigated as substrates for AP-SALDI-MS. The performance of AuNP was initially evaluated by using linoleic acid as analyte, followed by an application to a wider range of low molecular weight molecules, such as fatty acids, amino acids, small peptides, saccharides, drugs, and phospholipids. The optimized substrate was then used for analysis of fatty acids and phospholipids in an extract of pig brain.

## 2 | MATERIALS AND METHODS

### 2.1 | Chemicals and reagents

Palmitic acid, stearic acid, oleic acid, linoleic acid, erythromycin A, aspartic acid, and phenylalanine were purchased from Sigma-Aldrich (Steinheim, Germany); D-fructose and D-lactose from Merck (Darmstadt, Germany); 1,2-dioleoyl-sn-glycero-3-phosphatidylcholines (PC 36:2), 1,2-dioleoyl-sn-glycero-3-phosphatidylethanolamine (PE 36:2), docosahexaenoic acid (DHA), eicosatetraenoic acid (EPA), timolol maleate, leu-enkephalin, and bradykinin from Cayman Chemicals (Hamburg, Germany); and acetonitrile (ACN) and methanol from VWR chemicals (Darmstadt, Germany). All chemicals were used without further pretreatment. Deionized water was generated by a Millipore (Bedford, MA, USA) water purification system.

Pig brains were purchased from a local market. Liquid extraction of the brains was performed according to a published protocol<sup>33</sup> and the extract stored at  $-32^{\circ}\text{C}$  prior to SALDI-MS experiments.

AuNP with different core sizes, capping ligands, and dispersion solvents were prepared by using an adapted protocol by Zheng *et al.*<sup>34</sup> Briefly, oleyamine (OAm)-capped monodisperse AuNP were synthesized with an amine-borane complex as reducing agent. The nanoparticle sizes (radii, 1.2, 3.2, and 4.7 nm) were controlled by tuning the ratio of  $\text{HAuCl}_4 \cdot 3\text{H}_2\text{O}$  and reducing agent as well as the reaction time.<sup>35</sup> Ligand exchange was performed to cap the AuNP with butanethiol (B), decanethiol (D), hexadecanethiol (H), 11-mercaptoundecanoic acid (MA), and 11-mercaptoundecanol (MO). The prepared nanoparticles were separated from the precursor solution and re-dispersed in methanol, hexane, and toluene, to achieve good colloidal stability. For clarity, AuNP were named using the nomenclature AuNP[X-n-Y], with X, n, and Y corresponding to capping ligand, core size, and dispersion solvent, respectively. For example, AuNP[B-1-H] represents AuNP with capping ligand of butanethiol, core radius of 1.2 nm, dispersed in hexane (all nanoparticles are summarized in Table 1). The stock solutions of AuNP were prepared at 1 mg/mL and used directly for SALDI-MS if not otherwise specified.

### 2.2 | Spectroscopic characterization of AuNP

X-ray scattering experiments were performed using a Xeuss 2.0 (Xenocs, Sassenage, France) instrument, equipped with a GeniX Low Divergence Cu-K $\alpha$  source; the X-ray wavelength was 1.54 Å and the scattering signal was collected with a Dectris Pilatus 1 M detector; sample to detector

**TABLE 1** Investigated gold nanoparticles and naming scheme<sup>a</sup> for particles

Name	Composition		Solvent
	Ligand	Core size (radius, nm)	
AuNP[B-1-H]	Butanethiol	1.2	Hexane
AuNP[D-1-H]	Decanethiol	1.2	Hexane
AuNP[H-1-H]	Hexadecanethiol	1.2	Hexane
AuNP[OAm-1-H]	Oleyamine	1.2	Toluene
AuNP[MA-1-M]	11-Mercaptoundecanoic acid	1.2	Methanol
AuNP[MO-1-M]	11-Mercaptoundecanol	1.2	Methanol
AuNP[D-3-H]	Decanethiol	3.2	Hexane
AuNP[OAm-3-H]	Oleyamine	3.2	Toluene
AuNP[H-4-H]	Hexadecanethiol	4.7	Hexane
AuNP[OAm-4-H]	Oleyamine	4.7	Toluene

<sup>a</sup>AuNP were named using the nomenclature AuNP[X-*n*-Y], with X, *n*, and Y corresponding to capping ligand, core size, and dispersion solvent, respectively.

distance was calibrated with silver behenate. UV/Vis characterization of AuNP samples was performed with a Jasco V-650 spectrophotometer (Jasco, Easton, MD, USA). The concentration of the AuNP solutions for UV/Vis measurements was 6 µg/mL.

## 2.3 | Preparation of SALDI samples

Stock solutions of analytes were prepared as follows: fatty acids (palmitic acid, stearic acid, oleic acid, linoleic acid, EPA, DHA, EPA) and drugs (erythromycin A, timolol maleate) were dissolved in methanol at 1 mM; amino acids (aspartic acid, phenylalanine), small peptides (leu-enkephalin, bradykinin) and saccharides (D-fructose, D-lactose) were dissolved in water at 10 mM. All stock solutions were stored at –20°C and diluted to the required concentration prior to use. If not otherwise specified, analyte solutions were diluted to 100 µM in methanol prior to the SALDI experiments. Sodium and potassium ions were added to analyte solutions if needed.

SALDI sample deposition was performed using the two-layer dried droplet method. Initially, 0.5 µL of AuNP solution was pipetted onto the steel target. After solvent evaporation, 0.5 µL of analyte solution was pipetted onto the AuNP and dried at ambient conditions.

## 2.4 | Mass spectrometry

MS experiments were performed with a Bruker (Bremen, Germany) Esquire HCT<sup>+</sup> 3D quadrupole ion trap mass spectrometer coupled with a MassTech (Burlington, MD, USA) atmospheric pressure-MALDI source. A Nd:YAG laser emitting at 355 nm was used as light source. If not otherwise mentioned, the laser energy was set to 50% and the repetition rate to 200 Hz. Full scan mass spectra were acquired in positive ion mode from *m/z* 50 to 1000 using a linear rastering motion of the target plate. Ion currents were accumulated as follows: rastering velocity, 40.0 mm/min; scan length, 2.0 mm; scan height, 2.0 mm; raster spacing, 0.5 mm; step size, 0.5 mm, raster direction, horizontal. A drying gas temperature of 50°C at a flow rate of 5.0 L/min was used.

## 3 | RESULTS AND DISCUSSION

The SALDI experiments shown in this work were performed utilizing an atmospheric pressure (AP) MALDI source, which enabled simple and rapid sample preparation as compared to vacuum-based ion sources, which was important for quick method optimization. The soft ionization conditions at atmospheric pressure and the resulting reduced or absent precursor ion fragmentation<sup>36,37</sup> generally provides ionization and transport efficiencies comparable to vacuum MALDI.<sup>38,39</sup>

It has been previously shown that certain properties of nanomaterials (size, ligands, concentration, etc.) play vital roles in the desorption/ionization efficiency (DIE) under vacuum SALDI conditions.<sup>18-20</sup> However, to our knowledge, no such investigation has been performed for AP-SALDI. In this study, we investigated AP-AuNP-assisted LDl of different sizes, carrying various organic ligands at different concentration levels, and their effect on DIE of selected analytes.

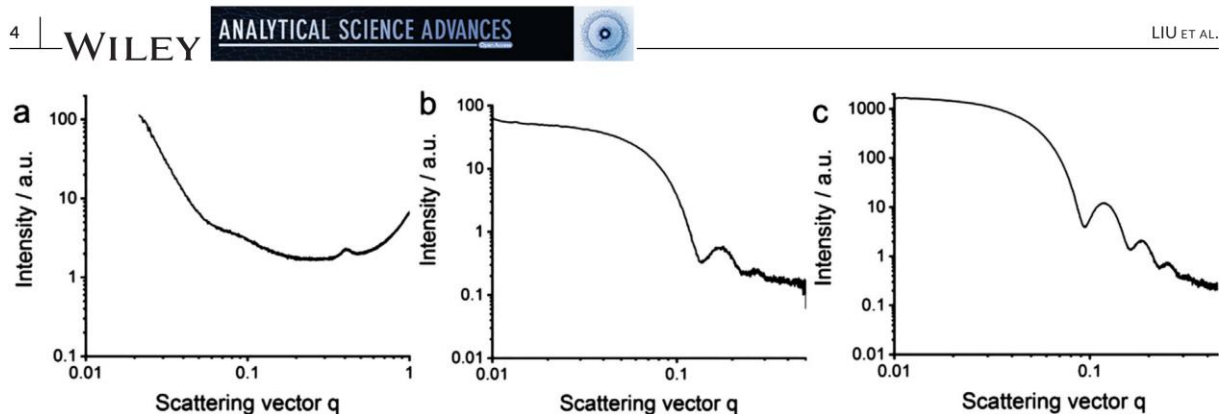


**FIGURE 1** SAXS characterization of AuNP: A, 1.2 nm; B, 3.2 nm; and C, 4.7 nm

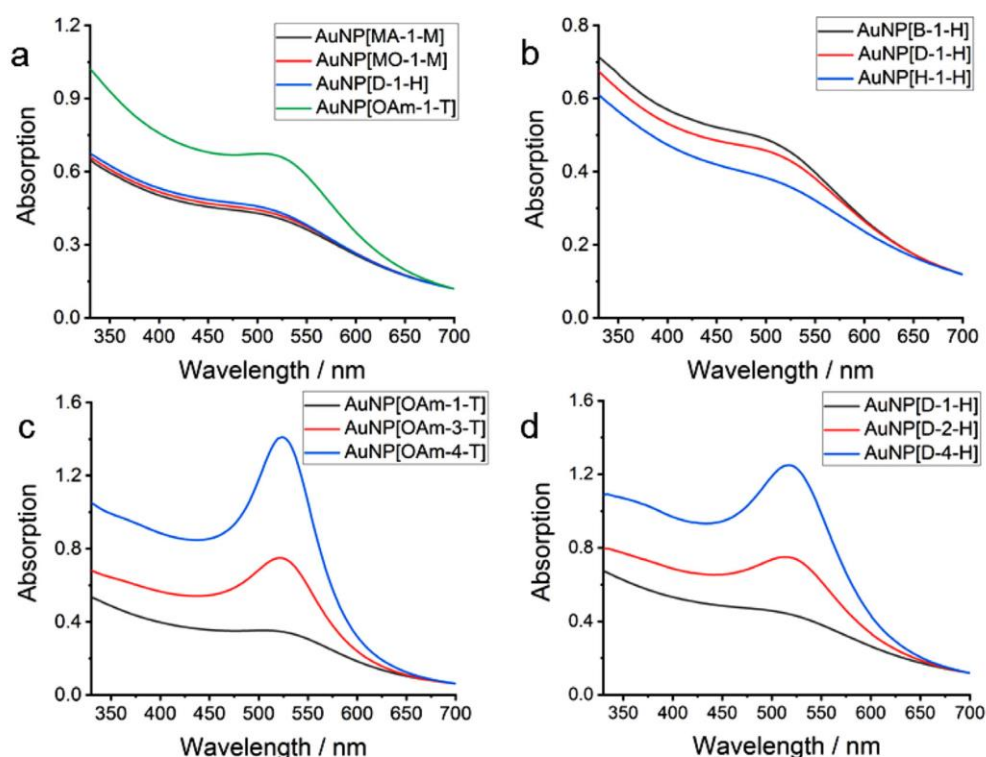


**FIGURE 2** UV/Vis spectra of (A) 1.2 nm radius AuNP with different types of ligands, (B) 1.2 nm AuNP with alkanethiol ligand of different size, (C) AuNP with oleyamine as ligand for different core sizes, and (D) AuNP with alkanethiol as ligand for different core sizes. The concentrations of AuNP solutions for UV/Vis measurement were  $6 \mu\text{g mL}^{-1}$

### 3.1 | Initial characterization of the AuNP

Sizes of AuNP[OAm-H] were characterized by small angle X-ray scattering (SAXS) (Figure 1). After fitting, the radii of AuNP[OAm-H] were determined as 1.4, 3.2, and 4.7 nm, respectively. Other AuNP including AuNP[B-H], AuNP[D-H], AuNP[H-H], AuNP[MA-M], AuNP[MO-M], and AuNP[AT-H] were subsequently obtained via ligand exchange from the AuNP[OAm-H] nanoparticles (see Section 2).

The light absorption properties of these gold nanoparticles were measured by UV/Vis spectroscopy (Figure 2). AuNP[MA-1-M], AuNP[MO-1-M], and AuNP[D-1-H] did not exhibit distinct absorption maxima, but rather absorption plateaus at  $\sim 490$  nm, while AuNP[OAm-1-H] absorbed with slightly higher intensity at 505 nm (Figure 2A). Similarly, AuNP[B-1-H], AuNP[D-1-H], and AuNP[H-1-H] exhibited plateau regions at  $\sim 490$  nm (Figure 2B), which shifted to red and absorption decreased as the ligand length was increased. For AuNP[OAm-1-H], AuNP[OAm-3-H], and

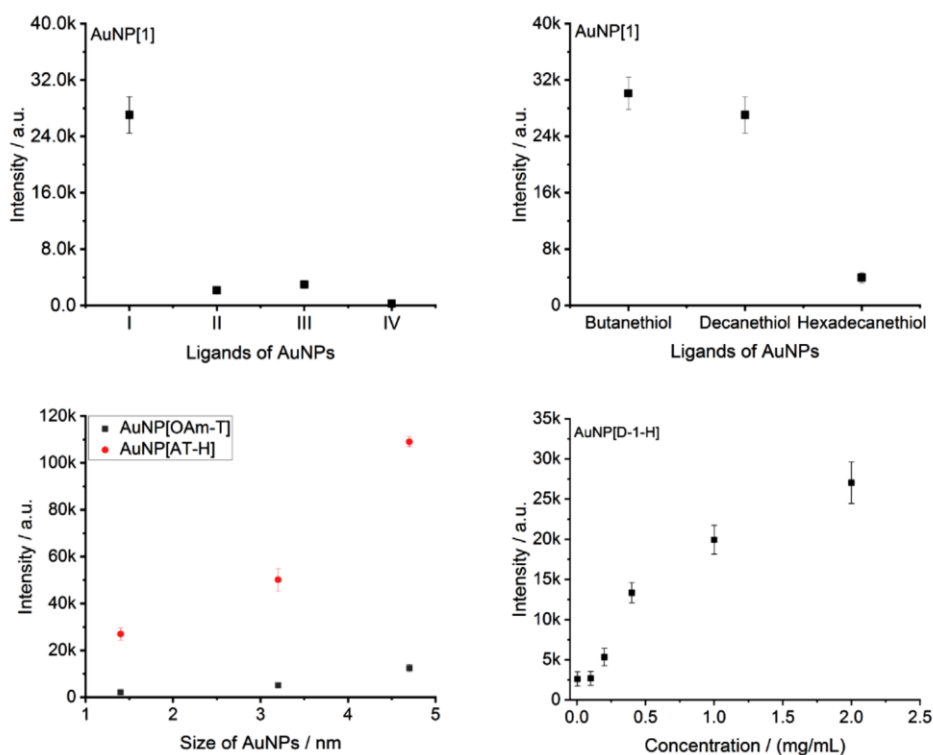


**FIGURE 3** Different effects for AuNP on signal intensity of linoleic acid in SALDI-MS: (A) type of ligand, (B) ligand size, (C) core size and (D) AuNP concentration. I, II, III, and IV denote 1-decanethiol, oleyamine, 11-mercaptoundecanoic acid, and 11-mercapto-1-undecanol ligands, respectively

AuNP[OAm-4-H], absorption showed maxima at 505, 521, and 524 nm, respectively (Figure 2C). There was some red-shifting as the size of AuNP increased. Finally, AuNP[AT-1-H], AuNP[AT-3-H], and AuNP[AT-4-H] exhibited maxima at 490, 513, and 517 nm, respectively, with red-shifting and strong absorption increase as the size of AuNP increased (Figure 2D).

### 3.2 | Effects of ligand and nanoparticle properties on DIE

#### 3.2.1 | Nature of the ligand

In this study, we compared different types of organic ligands for the AuNP to assess potential ligand effects on DIE in SALDI-MS, namely oleyamine, 11-mercaptoundecanoic acid, 11-mercapto-1-undecanol, and 1-decanethiol, all with identical radius of 1.2 nm. We chose linoleic acid as representative analyte in these experiments. As previously observed, salt adducts were common in the mass spectra and formed the base peaks in all experiments (for linoleic acid, these signals were at  $m/z$  303 and 319, corresponding to  $[M+Na]^+$  and  $[M+K]^+$ , respectively). We summed the ion currents of these two species and compared the four types of AuNP ligands. As shown in Figure 3A, the signal intensity for linoleic acid from AuNP[D-1-H] (= 1-decanethiol) was significantly higher than those obtained for the other three ligands, which is consistent with previous findings, showing that signal intensities from hydrophobic nanomaterials are higher than from hydrophilic nanomaterials.<sup>28</sup> This is related to higher local temperatures obtained with the hydrophobic nanomaterials and thus slower energy dispersion. However, surprisingly, analyte signals were much lower for the similarly hydrophobic oleyamine ligand, which is a weakly bound ligand in comparison to the covalently-bound thiol ligands. We hypothesize that this deviating behavior was due to excess amounts of oleyamine on the substrate surface. Stable AuNP-oleamine dispersions required large amounts of oleyamine to keep the nanoparticles in solution (the concentration was approximately one order of magnitude higher than for the thiol-containing ligands as described in the Section 2; further details are given in the Supporting Information). This excess ligand material can interfere with the desorption/ionization by potentially forming a dense layer or bilayer on the surface of the AuNP, thus separating the analyte from the nanoparticles. A similar behavior was seen during SALDI-MS analysis of peptides using cetyltrimethylammonium bromide (CTAB)-capped gold nanorods (AuNR).<sup>27</sup> The authors of that study suggested that the presence of CTAB on the surface of the nanorods inhibited desorption/ionization

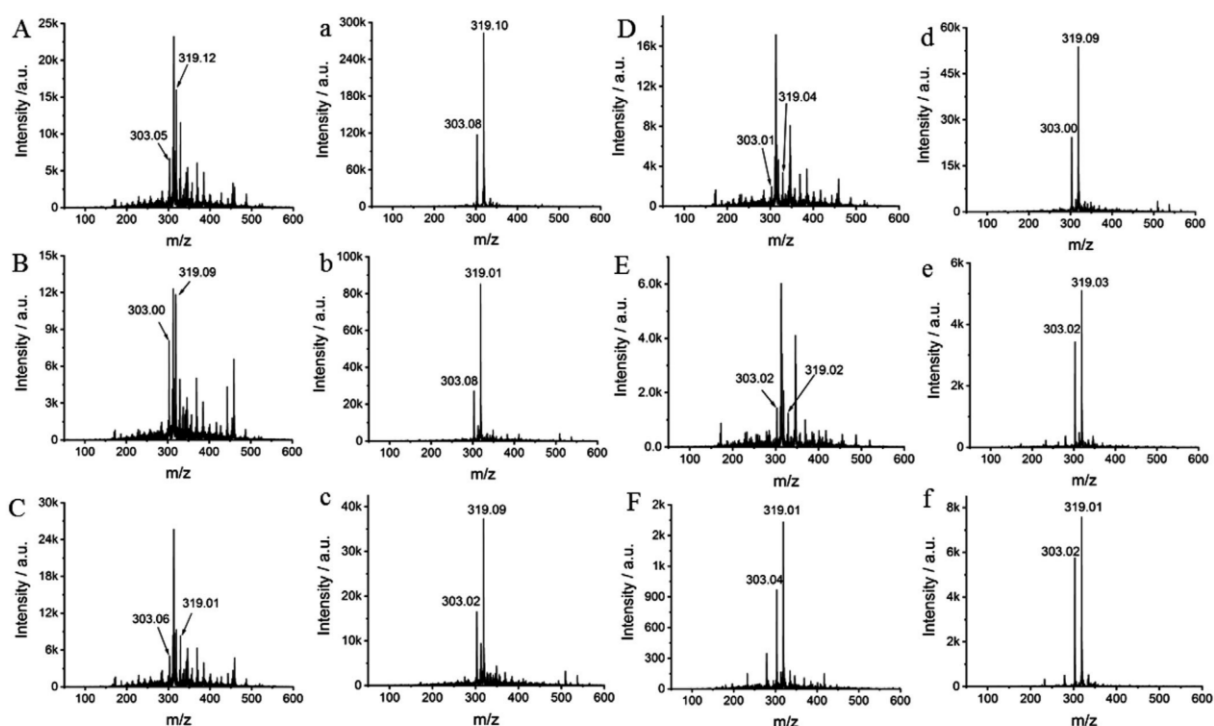


**FIGURE 4** AuNP[D-1-H]-assisted LDI mass spectra of linoleic acid at different concentrations: (A, a) 2.0, (B, b) 1.0, (C, c) 0.4, (D, d) 0.2, (E, e) 0.1, (F, f) 0.04 mg/mL. Panels A-F show mass spectra of linoleic acid from ligand-capped AuNP; panels a-f, mass spectra of linoleic acid after initial laser irradiation of the AuNP surface. (Signals at  $m/z$  303 and 319 correspond to  $[M+Na]^+$  and  $[M+K]^+$ , respectively)

of analyte because CTAB did not provide a sufficient source for ionizing protons and because the positively-charged CTAB bilayer inhibited the analyte from adsorbing to the nanorod surface. We believe that the AuNP-oleylamine system is similarly restricted in comparison to the hydrophobic AuNP-decanethiol nanoparticles.

For AuNP[MA-1-M], the obtained signal intensities for linoleic acid were higher than for AuNP[MO-1-M], which can be explained by the ligand's chemical properties in comparison to linoleic acid, which were more similar for 11-mercaptoundecanoic acid than for 11-mercaptoundecanol, enabling closer interaction of analyte and AuNP for AuNP[MA-1-M] than for AuNP[MO-1-M], with resulting improved energy transfer.

From the above observations, we suggest that the chemical properties of the nanoparticle's ligands and the interaction of ligand with analyte are more important for efficient desorption/ionization than increased UV/Vis absorption (see previous section).

### 3.2.2 | Length of ligand

In the next set of experiments, the influence of the length of the carbon chain of the ligands on DIE was investigated using alkanethiol-capped AuNP of different lengths. In these experiments, butanethiol, decanethiol, and hexadecanethiol were compared as ligands. Figure 3B demonstrates that the signal intensity of linoleic acid decreased strongly with increasing size of the ligand, declining approximately 10-fold from AuNP[B-1-H] over AuNP[D-1-H] to AuNP[H-1-H]. This is likely related to thermal conductivity and UV/Vis absorption, which both decrease with increasing size of the ligand and thus give reduced energy transfer from the AuNP to linoleic acid.

### 3.2.3 | Ligand-capped versus ligand-free AuNP

Chemical-free AuNP have been shown to provide improved performance in SALDI as compared to ligand-capped AuNP because the ligands can impede energy transfer to the analyte,<sup>19,25</sup> as they isolate the analyte from the AuNP. When the ligands were removed, analytes are closer to the nanoparticle surface and energy transfer is more effective, thus enhancing DIE.

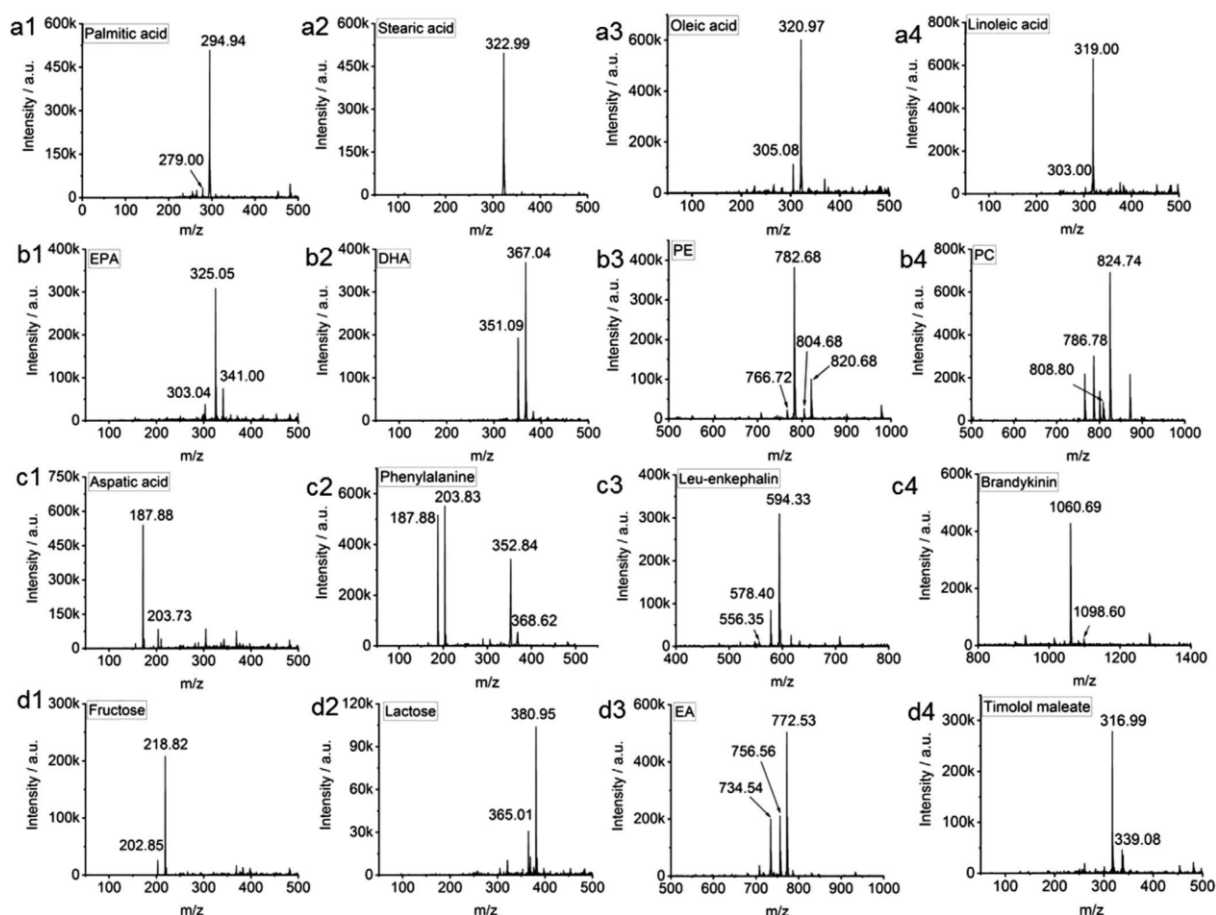


**FIGURE 5** AuNP[H-4-H]-assisted LDI mass spectra of (a1-b2) fatty acids, (b3, b4) lipids, (c1, c2) amino acids, (c3, c4) peptides, and (d1, d2) saccharides, (d3, d4) drugs (concentration, 100  $\mu$ M ea.)

An experiment was designed to investigate this effect for our AuNP, exemplified by AuNP[D-1-H]. In this experiment, the deposited AuNP were laser-irradiated prior to sample deposition, to remove the organic ligand as well as any impurities embedded in the AuNP or present on the metal target. Laser ablation is frequently used in analytical chemistry to remove small amounts of material from solids.<sup>40</sup> As previously reported for our experimental setup,<sup>31</sup> SALDI with laser powers  $\leq 50\%$  did not ablate gold from the substrate and consequently no gold-related ions were visible in the mass spectra under atmospheric pressure SALDI-MS conditions. For the cleaning step, different laser energies between 10% and 50% were investigated. For low energies ( $<30\%$ ), there was no noticeable ablation effect as no signals from ligands/impurities were visible in the mass spectra. For laser energies  $>30\%$ , strong signals of ligands and other impurities started to appear, mainly in the  $m/z$  range of 200 to 450 for AuNP[D-1-H] substrates. A setting of 50% was chosen for efficient removal, which was the same energy used in the subsequent LDI experiments of the analyte (see Section 2).

The comparison between the regular experiments and those utilizing the additional laser ablation is illustrated in Figure 4 for different concentration levels of the AuNP. It is immediate obvious that the background noise levels were significantly reduced across the investigated  $m/z$  range, in particular at high AuNP concentrations, which strongly increased signal-to-noise ratios for linoleic acid. Moreover, ion currents of the analyte also strongly increased as compared to the ligand-capped AuNP, further amplifying the sensitivity gain. In fact, for the highest AuNP concentration, ion currents for linoleic were amplified almost 20-fold in comparison to the capped AuNP (along with the reduced noise levels!). This amplification factor was lower for lower concentrations of AuNP. We hypothesize that this was due to ablation losses of nanoparticles during the initial laser irradiation phase, which are expected to have a higher relative impact for low concentrations of AuNP, which will then result in reduced DIE (the numerical differences between capped versus irradiated nanoparticles are summarized in Figure S1). As noise levels were also reduced at lower nanoparticle concentrations for the capped AuNP (Figure 4), the overall gain of this procedure was not as important for low

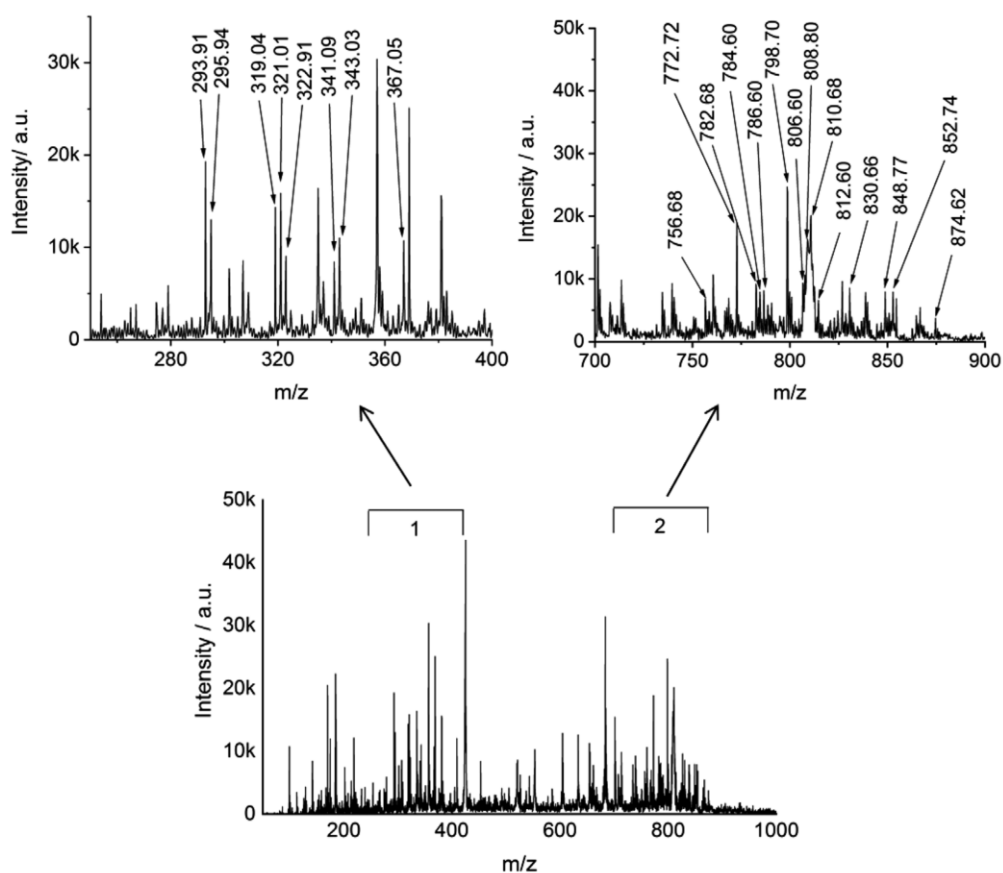


**FIGURE 6** AuNP[H-4-H]-assisted LDI mass spectra of a crude pig brain extract (the brain extract was diluted 10-fold prior to analysis; tentative lipid assignments are labelled with corresponding  $m/z$  value)

### 3.2.4 | Nanoparticle core size

AuNP with radii of 1.2, 3.2, and 4.7 nm were used to study core size effects on DIE of linoleic acid. As seen in Figure 3C, the signal intensity for linoleic acid always increased in the order  $4.7 > 3.2 > 1.2$  nm particle size, regardless of the nature of the organic ligand attached to the AuNP. As shown by McLean *et al.*,<sup>24</sup> the size of AuNP had a strong effect on signal intensity for angiotensin for gold nanoparticles in the range of 2–10 nm. Larger AuNP provided higher DIE in SALDI, although a strong noise background of gold ions was observed for the larger nanoparticles. In our experiments, no gold-related ions were seen in the mass spectra, even for larger nanoparticles. This is probably due to the softer nature of the AP-SALDI process in comparison to vacuum SALDI. As demonstrated in our previous work,<sup>31</sup> no gold-related ions were observed under atmospheric pressure for  $[\text{AuNP}]_n$  substrates, whereas gold-related ions were clearly seen under vacuum SALDI conditions. Under atmospheric pressure SALDI, there was insufficient energy for ablation and ionization of gold ions and the local temperature rise on the target plate upon laser irradiation was likely not as high. For AuNP containing alkanethiol ligands, the signal intensity of linoleic acid from AuNP with radius of 4.8 nm was approximately twofold higher than for AuNP of radius 3.2 nm and  $\sim 4.8$ -fold higher for particles of 1.2 nm. AuNP with oleyamine exhibited the same trend; that is, signal intensity for radius of 4.8 nm was  $\sim 2.3\times$  higher than for 3.2 nm, and  $6.5\times$  higher than for 1.2 nm. The size effect is probably related to the stronger UV/Vis absorption for larger nanoparticles than for smaller particles, allowing higher energy transfer from the larger nanoparticles to the analyte.

### 3.2.5 | Nanoparticle concentration

In order to investigate the influence of the concentration of the nanoparticle solution, the stock AuNP[D-1-H] solution (radius, 1.2 nm at 2 mg/mL) was diluted to give AuNP solutions of 1.0, 0.4, 0.2, 0.1, and 0.04 mg/mL, respectively, which were then deposited onto the SALDI targets (NB: AuNP solutions that were diluted more than 20 times were virtually without color). As shown in Figure 3D, the signal intensity of linoleic acid decreased



with decreasing AuNP concentration; for concentrations < 0.1 mg/mL, the signal intensity of linoleic acid stayed virtually the same. The signal intensity of linoleic acid from 2 mg/mL AuNP preparations was approximately 10-fold higher than for 0.2 mg/mL. As the number of ions formed during desorption/ionization is proportional to the amount of energy absorbed and transferred to the analytes,<sup>41</sup> the observed intensity decrease can be readily explained with decreased UV/Vis absorption of the AuNPs. For very small AuNP concentrations, with negligible UV/Vis absorption, we suggest that direct analyte LDI takes over as primary mechanism, which is not very efficient for the analyte linoleic acid, resulting in very low ion currents regardless of concentration.

### 3.3 | Application to wider range of biomolecules and brain extract

For application to other analytes, AuNP[H-4-H] was used as optimized material to analyze a wide range of biomolecules. Biomolecules including fatty acids (palmitic acid, stearic acid, oleic acid, linoleic acid), phospholipids (PE, PC), amino acids (aspartic acid, phenylalanine), small peptides (leu-enkephalin, bradykinin), saccharides (D-fructose, D-lactose) and drugs (erythromycin A, timolol maleate) were chosen for this application. Figure 5 illustrates that all investigated analytes were ionized intact without fragmentation. They were detected at limits of detection (LOD) of approximately 1  $\mu$ M (Figure S2 illustrates the SALDI spectra at different concentrations down to the LOD; LOD was defined as the lowest concentration, for which a signal-to-noise ratio of at least 3:1 was obtained). Please note that while these LOD numbers appear relatively high, they are mainly the result of the used instrument, which was an insensitive, older generation 3D ion trap utilized for the proof-of-concept work described in this study. Transferring this technique to a modern triple quadrupole instrument with a high duty cycle data acquisition mode (such as single reaction monitoring, SRM), would lower LOD by at least 100-1000-fold as previously shown for quantitative MALDI analysis of small molecules.<sup>42,43</sup>

Finally, as further proof-of-concept, we applied our AuNP-assisted LDI technique to a very complex biological mixture; that is, a crude extract of a pig brain. After sample preparation (see Section 2), these extracts contain a large number of lipid species such as fatty acids, PC, PE, cerebrosides etc.<sup>44,45</sup> AuNP[H-4-H] was used as substrate in the analysis and we were able to detect a wide range of lipids, as shown in Figure 6 (suggested, tentative structural assignments, and the implemented identification procedure for fatty acids as well as PC and PE species in the  $m/z$  ranges of 200-400 and 700-900 are summarized in Table S1). Obviously, the implemented mass analyzer, which operated at nominal mass resolution, did not provide sufficient mass accuracy for elemental formulae assignments, but this information could be readily obtained by using a high resolution mass spectrometer for the experiments.

## 4 | CONCLUSIONS

A series of AuNP of different core size and capping ligands were prepared for SALDI-MS. AuNP were first characterized by SAXS and UV/Vis spectra, followed by SALDI-MS to optimize the performance and the DIE of the test analyte linoleic acid. The results showed that core size, capping ligands, and concentration of AuNP played important roles in the performance of the substrate. For AuNP with larger core sizes, high concentrations of hydrophobic ligands provided higher DIE of analytes. It was found that the surface chemistry of the AuNP had a stronger influence on the DIE than the UV/Vis absorption of the material. For similar surface chemistries, stronger UV/Vis absorption will further improve the performance. In a separate experiment, we demonstrated that laser pretreatment of the AuNP, to remove the organic ligands and embedded impurities, increased DIE approximately 20-fold for high concentrations of AuNP. This amplification was less pronounced for lower concentrations of the nanoparticles.

Under optimized condition, the AuNP were successfully used to analyze a wide arrange of different low molecular weight biomolecules. In addition, the analysis of a crude pig brain extract readily demonstrated the ability of the technique to detect a wide range of lipid species within a highly complex sample. In the future, we are planning to expand this study and conduct a comprehensive method validation for quantitative SALDI-MS analysis of selected analytes for application to various biological samples.

We believe that the SALDI-MS technique described here would be particularly useful as a method for quantitative analysis of small biological molecules but would equally well serve as a molecular weight readout platform for metabolome analyses if combined with high resolution mass spectrometry.

### ACKNOWLEDGMENTS

The authors thank Dr. Ignacy Rzagalinski (Max-Planck Institute of Molecular Cell Biology and Genetics, Dresden) for providing the pig brain extracts and Caroline Hoffmann (Saarland University, Saarbrücken) for UV/Vis measurements. Z.L. acknowledges the China Scholarship Council for financial support.

### CONFLICT OF INTEREST

D.A.V. is Editor-in-Chief of *Analytical Science Advances*.



## DATA AVAILABILITY STATEMENT

The data that support the findings of this study are available from the corresponding author upon reasonable request.

## REFERENCES

1. Tanaka K, Waki H, Ido Y, et al. Protein and polymer analyses up to  $m/z$  100 000 by laser ionization time-of-flight mass spectrometry. *Rapid Commun Mass Spectrom.* 1988;2:151-153.
2. Cha S, Yeung ES. Colloidal graphite-assisted laser desorption/ionization mass spectrometry and MSn of small molecules. 1. Imaging of cerebrosides directly from rat brain tissue. *Anal Chem.* 2007;79:2373-2385.
3. Shi C, Deng C, Zhang X, Yang P. Synthesis of highly water-dispersible polydopamine-modified multiwalled carbon nanotubes for matrix-assisted laser desorption/ionization mass spectrometry analysis. *ACS Appl Mater Interfaces.* 2013;5:7770-7776.
4. Lin Z, Wu J, Dong Y, Xie P, Zhang Y, Cai Z. Nitrogen and sulfur co-doped carbon-dot-assisted laser desorption/ionization time-of-flight mass spectrometry imaging for profiling bisphenol S distribution in mouse tissues. *Anal Chem.* 2018;90:10872-10880.
5. Wei J, Buriak JM, Siuzdak G. Desorption-ionization mass spectrometry on porous silicon. *Nature.* 1999;399:243-246.
6. Yang H, Su R, Wishnok JS, et al. Magnetic silica nanoparticles for use in matrix-assisted laser desorption/ionization mass spectrometry of labile biomolecules such as oligosaccharides, amino acids, peptides and nucleosides. *Microchim Acta.* 2019;186:104.
7. Amin MO, Al-Hetlani E. Tailoring the surface chemistry of SiO<sub>2</sub>-based monoliths to enhance the selectivity of SALDI-MS analysis of small molecules. *Talanta.* 2019;200:458-467.
8. Silina YE, Koch M, Volmer DA. The Role of Physical and chemical properties of Pd nanostructured materials immobilized on inorganic carriers on ion formation in atmospheric pressure laser desorption/ionization mass spectrometry. *J Mass Spectrom.* 2014;49:468-480.
9. Ding F, Qian Y, Deng Z, et al. Size-selected silver nanoparticles for MALDI-TOF mass spectrometry of amyloid-beta peptides. *Nanoscale.* 2018;10:22044-22054.
10. Silina YE, Meier F, Nebolsin VA, Koch M, Volmer DA. Novel galvanic nanostructures of Ag and Pd for efficient laser desorption/ionization of low molecular weight compounds. *J Am Soc Mass Spectrom.* 2014;25:841-851.
11. Kim M, Park JM, Yun TG, Noh JY, Kang MJ, Pyun JC. TiO<sub>2</sub> nanowires from wet-corrosion synthesis for peptide sequencing using laser desorption/ionization time-of-flight mass spectrometry. *ACS Appl Mater Interfaces.* 2018;10:33790-33802.
12. Yan B, Jeong Y, Mercante LA, et al. Characterization of surface ligands on functionalized magnetic nanoparticles using laser desorption/ionization mass spectrometry (LDI-MS). *Nanoscale.* 2013;5:5063-5066.
13. Kim K, Um K, Yoon C, Ryoo WS, Lee K. Wafer-level detection of organic contamination by ZnO-rGO hybrid-assisted laser desorption/ionization time-of-flight mass spectrometry. *Talanta.* 2018;182:273-278.
14. Coffinier Y, Szunerits S, Drobecq H, Melnyk O, Boukherroub R. Diamond nanowires for highly sensitive matrix-free mass spectrometry analysis of small molecules. *Nanoscale.* 2012;4:231-238.
15. Lu T, Olesik SV. Electrospun nanofibers as substrates for surface-assisted laser desorption/ionization and matrix-enhanced surface-assisted laser desorption/ionization mass spectrometry. *Anal Chem.* 2013;85:4384-4391.
16. Kim YK, Wang LS, Landis R, Kim CS, Vachet RW, Rotello VM. A layer-by-layer assembled MoS<sub>2</sub> thin film as an efficient platform for laser desorption/ionization mass spectrometry analysis of small molecules. *Nanoscale.* 2017;9:10854-10860.
17. Wang H, Wu Y, Guo B, Sun W, Ding L, Chen B. Quantification of low-polar small molecules using room temperature ionic liquids matrix-assisted desorption corona beam ionization. *Analyst.* 2012;137:3982-3988.
18. Chiang CK, Chen WT, Chang HT. Nanoparticle-based mass spectrometry for the analysis of biomolecules. *Chem Soc Rev.* 2011;40:1269-1281.
19. Mandal A, Singha M, Addy PS, Basak A. Laser desorption ionization mass spectrometry: recent progress in matrix-free and label-assisted techniques. *Mass Spectrom Rev.* 2019;38:3-21.
20. Silina YE, Volmer DA. Nanostructured solid substrates for efficient laser desorption/ionization mass spectrometry (LDI-MS) of low molecular weight compounds. *Analyst.* 2013;138:7053-7065.
21. Unnikrishnan B, Chang CY, Chu HW, Anand A, Huang CC. Functional gold nanoparticles coupled with laser desorption ionization mass spectrometry for bioanalysis. *Anal Methods.* 2016;8:8123-8133.
22. Pilolli R, Palmisano F, Cioffi N. Gold nanomaterials as a new tool for bioanalytical applications of laser desorption ionization mass spectrometry. *Anal Bioanal Chem.* 2012;402:601-623.
23. Abdelhamid HN, Wu HF. Gold nanoparticles assisted laser desorption/ionization mass spectrometry and applications: from simple molecules to intact cells. *Anal Bioanal Chem.* 2016;408:4485-4502.
24. McLean JA, Stumpo KA, Russel DH. Size-selected (2-10 nm) gold nanoparticles for matrix assisted laser desorption ionization of peptides. *J Am Chem Soc.* 2005;127:5304-5305.
25. Amendola V, Littl L, Meneghetti M. LDI-MS assisted by chemical-free gold nanoparticles: enhanced sensitivity and reduced background in the low-mass region. *Anal Chem.* 2013;85:11747-11754.
26. Kolářová L, Kučera L, Vaňhara P, Hampel A, Havel J. Use of flower-like gold nanoparticles in time-of-flight mass spectrometry. *Rapid Commun Mass Spectrom.* 2015;29:1585-1595.
27. Castellana ET, Gamez RC, Gómez ME, Russell DH. Longitudinal surface plasmon resonance based gold nanorod biosensors for mass spectrometry. *Langmuir.* 2010;26:6066-6070.
28. Palermo A, Forsberg EM, Warth B, et al. Fluorinated gold nanoparticles for nanostructure imaging mass spectrometry. *ACS Nano.* 2018;12:6938-6948.
29. Chiang NC, Chiang CK, Lin ZH, Chlu TC, Chang HT. Detection of aminothiols through surface-assisted laser desorption/ionization mass spectrometry using mixed gold nanoparticles. *Rapid Commun. Mass Spectrom.* 2009;23:3063-3068.
30. Son J, Lee G, Cha S. Direct analysis of triacylglycerols from crude lipid mixtures by gold nanoparticle-assisted laser desorption/ionization mass spectrometry. *J Am Soc Mass Spectrom.* 2014;25:891-894.
31. Liu Z, Zhang P, Kister T, Kraus T, Volmer DA. Ultra-thin homogenous AuNP monolayers as tunable functional substrates for surface-assisted laser desorption/ionization of small biomolecules. *J Am Soc Mass Spectrom.* 2020;21:47-57.



32. Tang HW, Lu W, Che CM, Ng KM. Gold nanoparticles and imaging mass spectrometry: double imaging of latent fingerprints. *Anal Chem*. 2010;82:1589-1593.
33. Want EJ, Masson P, Michopoulos F, et al. Global metabolic profiling of animal and human tissues via UPLC-MS. *Nat Protoc*. 2013;8:17-32.
34. Wu BH, Yang HY, Huang HQ, Chen GX, Zheng NF. Solvent effect on the synthesis of monodisperse amine-capped Au nanoparticles. *Chinese Chem Lett*. 2013;24:457-462.
35. Kister T, Maurer JHM, González-García L, Kraus T. Ligand-dependent nanoparticle assembly and its impact on the printing of transparent electrodes. *ACS Appl Mater Interfaces*. 2018;10:6079-6083.
36. Laiko VV, Moyer SC, Cotter RJ. Atmospheric pressure MALDI/Ion trap mass spectrometry. *Anal Chem*. 2000;72:5239-5243.
37. Keller C, Maeda J, Jayaraman D, et al. Comparison of vacuum MALDI and AP-MALDI platforms for the mass spectrometry imaging of metabolites involved in salt stress in medicago truncatula. *Front Plant Sci*. 2018;9:1238.
38. Miller CA, Yi D, Perkins PD. An atmospheric pressure matrix-assisted laser desorption/ionization ion trap with enhanced sensitivity. *Rapid Commun Mass Spectrom*. 2003;17:860-868.
39. Tan PV, Laiko VV, Doroshenko VM. Atmospheric Pressure MALDI with pulsed dynamic focusing for high-efficiency transmission of ions into a mass spectrometer. *Anal Chem*. 2004;76:2462-2469.
40. Russo RE, Mao X, Liu H, Gonzalez J, Mao SS. Laser ablation in analytical chemistry—a review. *Talanta*. 2002;57:425-451.
41. Luo G, Marginean I, Vertes A. Internal energy of ions generated by matrix-assisted laser desorption/ionization. *Anal Chem*. 2002;74:6185-6190.
42. Volmer DA, Sleno L, Bateman K, et al. Comparison of MALDI to ESI on a triple quadrupole platform for pharmacokinetic analyses. *Anal Chem*. 2007;79:9000-9006.
43. Sleno L, Volmer DA. Toxin screening in phytoplankton: detection and quantitation using MALDI triple quadrupole mass spectrometry. *Anal Chem*. 2005;77:1509-1517.
44. Gode D, Volmer DA. Lipid imaging by mass spectrometry—a review. *Analyst*. 2013;138:1289-1315.
45. Cha S, Yeung ES. Colloidal graphite-assisted laser desorption/ionization mass spectrometry and MSn of small molecules. 1. Imaging of cerebroside directly from rat brain tissue. *Anal Chem*. 2007;79:2373-2385.

#### SUPPORTING INFORMATION

Additional supporting information may be found online in the Supporting Information section at the end of the article.

**How to cite this article:** Liu Z, Zhang P, Pyttlik A, Kraus T, Volmer DA. Influence of core size and capping ligand of gold nanoparticles on the desorption/ionization efficiency of small biomolecules in AP-SALDI-MS. *Anal Sci Adv*. 2020;1–11. <https://doi.org/10.1002/ansa.202000002>

*Supplementary Material*

**Influence of core size and capping ligand of gold nanoparticles on the desorption/ionization efficiency of small biomolecules in AP-SALDI-MS**

Zhen Liu, Peng Zhang, Andrea Pyttlik, Tobias Kraus, Dietrich A. Volmer

Analytical Science Advance, 2020, in press. <https://doi.org/10.1002/ansa.202000002>

**Calculation of the relative ratio of oleyamine to thiol-containing ligands**

To compare the ratio of oleyamine (OAm) to the thiol-containing ligands, we simply use the precursor materials in the nanoparticle synthesis. In the typical synthesis of OAm-stabilized AuNP, 0.25 mmol Au was mixed with 11 mL OAm [179]. The molar amount of OAm then was 0.033 mol ( $=11 \times 0.813 / 267.493$ ). We obtain the molar ratio of OAm/Au as 132 by dividing 33 with 0.25. For thiol-containing stabilized AuNP, a 10-fold higher molar amount of gold was used in the typical sample preparation [180]. Thus, the OAm used in AuNP synthesis was around one order of magnitude higher than for thiol-containing reagent.

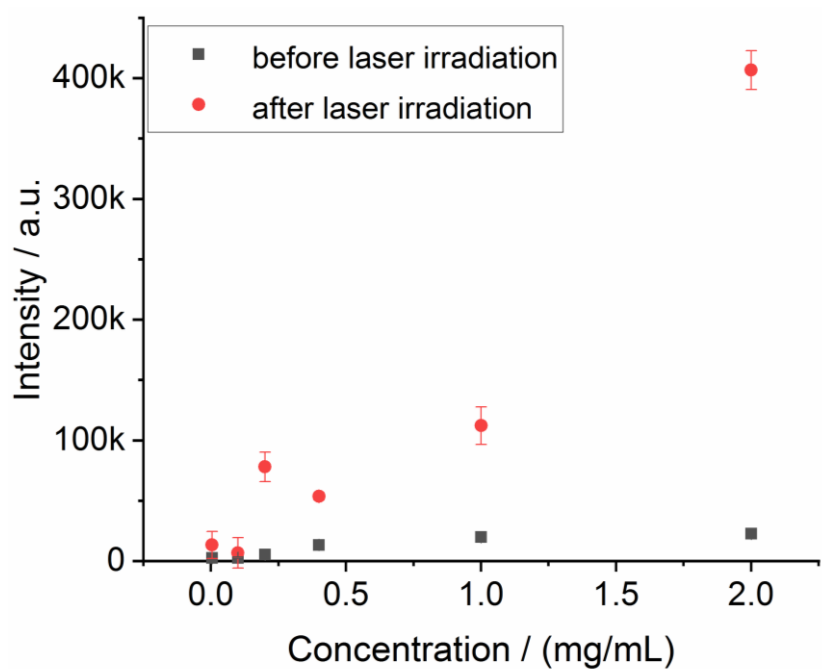


**Figure S1.** Concentration of AuNP (radius, 1.2 nm) and its effect on signal intensity of linoleic acid (concentration of nanoparticles increased from 0.04 to 2 mg/mL; concentration of linoleic acid, 100  $\mu$ M; AuNP ligand, decanethiol).

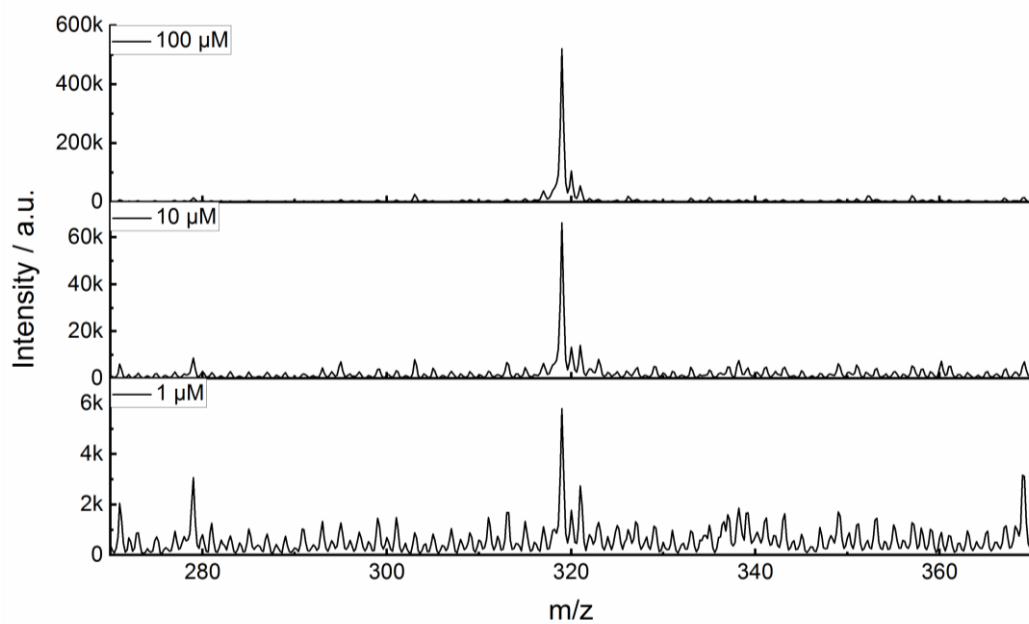


**Figure S2.** AuNP[H-4-H]-assisted LDI mass spectra of linoleic acid at different concentration levels of the analyte down to the limit of detection (LOD).

**Table S1.** Suggested assignments for lipids in crude brain extract.

$m/z$ <sup>1</sup>	Lipid species in SALDI-MS
293	[FFA 16:1 + K] <sup>+</sup>
295	[FFA 16:0 + K] <sup>+</sup>
319	[FFA 18:2 + K] <sup>+</sup>
321	[FFA 18:1 + K] <sup>+</sup>
322	[FFA 18:0 + K] <sup>+</sup>
341	[FFA 20:5 + K] <sup>+</sup>
343	[FFA 20:4 + K] <sup>+</sup>
367	[FFA 22:6 + K] <sup>+</sup>
756	[PE 34:1 + K] <sup>+</sup>
768	[PC 32:2 + K] <sup>+</sup>
772	[PC 32:0 + K] <sup>+</sup>
782	[PE 36:2 + K] <sup>+</sup>
784	[PE 36:1 + K] <sup>+</sup>
786	[PE 36:0 + K] <sup>+</sup>
798	[PC 34:1 + K] <sup>+</sup>
806	[PE 38:4 + K] <sup>+</sup>
808	[PE 38:3 + K] <sup>+</sup>
810	[PE 38:2 + K] <sup>+</sup>
812	[PE 38:1 + K] <sup>+</sup>
830	[PE 40:6 + K] <sup>+</sup>
848	[PC 38:4 + K] <sup>+</sup>
852	[PC 38:2 + K] <sup>+</sup>
874	[PC 40:5 + K] <sup>+</sup>

<sup>1</sup>These  $m/z$  values are nominal mass-to-charge ratios; As shown in our experiments, the background levels in the mass spectra from the AuNP materials were extremely low and peaks in the sample spectra were clearly generated from the brain extracts. Our tentative structure assignments focused on PC and PE compounds as these are major lipids in brain. We performed tentative peak assignment mainly based on previously reported identifications or MS/MS experiments [68]. Obviously, these are merely suggestions at this stage, as multiple species, isobars and isomers will likely be present at many  $m/z$  ratios. For examples, the peak at  $m/z$  782 could also be assigned to [PC 36:1 + Na]<sup>+</sup>; however we tentatively assigned the signal to [PE 36:2 + K]<sup>+</sup>, because virtually all signals in our SALDI experiments were potassiated species. Obviously, unambiguous identification would only be possible by combined use of high resolution mass spectrometry and collision-induced dissociation, ideally in combination with ion mobility separations.

## VI Conclusion and outlook

### Conclusion

Matrix assisted laser desorption/ionization (MALDI) and surface assisted laser desorption/ionization (SALDI) mass spectrometry (MS) are powerful tools for rapid analysis of biomolecules. However, the inhomogeneous distribution of the sample in the dried patch resulting from coffee-ring effect and sweet spot issue leads to poor signal reproducibility, which limits their applications in quantitative analysis. In the thesis, we designed several novel methods, with the analyte and matrix distributed homogeneously on the target plate, to achieve quantitative analysis of the biomolecules. The main findings of the thesis are summarized in the following.

Firstly, a simple method to distribute the matrix and analyte homogeneously in the target plate was developed by introducing regular channels into the plate for MALDI-MS. The dimensions of the channel was designed with 3.0 mm in length, 0.35 mm in width and 0.40 mm in depth, of which the width is a little smaller than the diameter of the implemented laser beam. These designed channels helped the mixture of matrix and analyte distribute homogeneously in the channels under the function of capillary interaction and ensured all the samples in the channel were irradiated efficiently by the laser. With these target plates, a quantitative study of the acetyl-L-carnitine (ALC) in human plasma was successfully achieved. The results showed that the reproducibility of ALC was greatly improved with RSD value of <5.9%, in comparison to a conventional MALDI value of 15.6%. Moreover, with these target plate, the LOQ of ALC was around 2 times lower compared with that obtained from a conventional MALDI. Furthermore, the matrix effects were assessed which showed that it was not negligible. At last, the developed method was applied to quantitative analysis of ALC in real sample of human plasma with reliable results. It is worth to mention that the new method does not need complex and expensive design of the target plate and is compatible with the standard sample deposition procedure, which can be scaled up easily. Therefore we expect that the new method has good potential for full automation and high throughput quantitative analysis of biomolecules.

Secondly,  $[\text{AuNP}]_n$  films, with n indicates the number of AuNP layer, were used as the SLADI-MS matrix. The design of the AuNP monolayer was inspired by the well-known Langmuir-Blodgett method in physical chemistry and layer thickness of the  $[\text{AuNP}]_n$  film was adjusted by layer-by-layer packing of the AuNP monolayers. The as-prepared  $[\text{AuNP}]_n$  films

showed good structural homogeneity that was confirmed by the transmission electron microscopy (TEM) and small angle X-ray scattering (SAXS) results. From the TEM image, it could be obviously seen that the as-prepared AuNPs had uniform distribution in terms of nanoparticle packing. By evaluating the peak intensity of Au in SAXS, it could be deduced that the structures of  $[\text{AuNP}]_n$  substrates were quite homogeneous, which was in accordance with the TEM results. To study the performance of the  $[\text{AuNP}]_n$  films as SALDI-MS matrix, we have studied several small molecules including fatty acids, drugs, amino acids, small peptides and saccharides. The ion current of analytes generated from the  $[\text{AuNP}]_1$  films was much higher than that from other AuNP morphologies, indicating that packing homogeneity of the  $[\text{AuNP}]_n$  substrates played a vital role in the desorption/ionization process in SALDI. Moreover, the intensity of the SALDI-MS signal could be optimized by varying layer number (n) of the  $[\text{AuNP}]_n$  films and reached a saturation point when n is 2 or 3. Using 4-amino-1-benzylpyridinium bromide (ABP) as thermometer, the desorption/ionization process of analytes from  $[\text{AuNP}]_n$  substrates was further investigated. The results showed that desorption/ionization of ABP increased as a function of the layer number and reached a plateau with  $[\text{AuNP}]_2$ , which has a close relation with the saturation of AuNP on the surface of the substrates. By analyzing the fragments of erythromycin A, we demonstrated that  $[\text{AuNP}]_n$  films provided soft ionization abilities during SALDI, which was much softer than MALDI with CHCA as matrix. The signal reproducibility of linoleic acid was assessed using linoleic acid with RSD < 8% and the LOD was 0.5  $\mu\text{M}$ . The  $[\text{AuNP}]_n$  substrates exhibited no distinct sweet spots and the generated signals under SALDI-MS conditions were very stable with clean background, readily allowing for quantitative analyses of fatty acids.

Thirdly, we did a systematic study of how the structural parameters of the AuNP influence the performance of AuNP in SALDI-MS. To achieve that, a series of AuNPs with different core size and capping ligands were prepared for SALDI-MS and the desorption/ionization efficiency (DIE) of analytes was used to evaluate the performance of the matrix. The results indicated that core size, capping ligands and concentration of AuNPs had strong influence on the DIE of the tested analytes. Higher DIE values were found in the matrix with bigger AuNP core size, high AuNP concentration and AuNPs capped with hydrophobic ligands. DIE was also influenced by UV/Vis absorption of AuNPs and chemical interactions between ligands and analytes. Compared with UV/Vis absorption, surface chemistry of the AuNPs had a stronger influence on the DIE. However, for the AuNPs with similar surface chemistry, a higher UV/Vis absorption would affect more on DIE. Moreover, it was found that laser ablation of the organic ligands could further increase the DIE, for example, 20 times higher

DIE was found after ligand removal for high concentration AuNPs. With the optimized structure of AuNP matrix, we have successfully analyzed a wide arrange of biomolecules as well as complex sample like pig brain extractions.

We believe that the MALDI-MS and SALDI-MS technique combined with the novel methods described in this thesis would be particularly useful for quantitative analysis of small biological molecules. Moreover, if the novel methods can be combined with high resolution mass spectrometer, a molecular weight readout platform suitable for metabolome analyses is expected.

## **Outlook**

It is quite important and useful to get reliable data from quantitative analysis of biomolecules with MALDI-MS and SALDI-MS. From our experience, there are many factors affecting signal reproducibility in MALDI-MS and SALDI-MS, among which, homogenous distribution of matrix and analyte and reproducible sample preparation process are two of the most important ones which should be addressed in the following studies. It is necessary to further develop novel easy-to-operate methods to prepare homogenous sample with simple and reliable protocol. The work in the dissertation and the referred reports have made significant progress and we believe these new methods would promote the quantitative analysis in a broad field of bioanalysis and bioanalytical chemistry. Meanwhile, the further development of mass spectroscopy has intertwined with the closely-related research fields like nano chemistry and nano characterization. For example, exploring the fundamentals of desorption/ionization process in SALDI-MS needs *in situ* study of the structural evolution with nanoparticles of well-designed and clearly-defined structure. The group of prof. Francesco Stellacci at EPFL, Switzerland and their collaborators with broad scientific backgrounds recently have done some nice work by unifying the knowledge of MS, nanochemistry and theoretical simulation for solving complex issues in bioanalysis.

In addition, high-resolution mass analyzer (e.g., FTICR) also plays important roles in the development of MALDI-MS and SALDI-MS, and they are especially important for the practical analysis of the complex bioanalysis, such as disease detection and proteomics.

## VII Reference

1. Cole, R.B.: *Electrospray and MALDI mass spectrometry: fundamentals, instrumentation, practicalities, and biological applications: Second Edition.* (2012).
2. Karas, M., Hillenkamp, F.: Laser Desorption ionization of proteins with molecular masses exceeding 10 000 Daltons. *Anal. Chem.* **60**, 2299–2301 (1988).
3. Hillenkamp, F., Karas, M., Beavis, R.C., Chait, B.T.: Matrix-assisted laser desorption/ionization mass spectrometry of biopolymers. *Anal. Chem.* **63**, 1193-1202 (1991).
4. Karas, M., Bachmann, D., Bahr, U., Hillenkamp, F.: Matrix-assisted ultraviolet laser desorption of non-volatile compounds. *Int. J. Mass Spectrom. Ion Process.* **78**, 53–68 (1987).
5. Jungblut, P., Thiede, B.: Protein identification from 2-DE gels by MALDI mass spectrometry. *Mass Spectrom. Rev.* **16**, 145–162 (1997).
6. Bahr, U., Deppe, A., Karas, M., Hillenkamp, F., Giessmann, U.: Mass spectrometry of synthetic polymers by UV-matrix-assisted laser desorption/ionization. *Anal. Chem.* **64**, 2866–2869 (1992).
7. Cohen, L.H., Gusev, A.I.: Small molecule analysis by MALDI mass spectrometry. *Anal. Bioanal. Chem.* **373**, 571–586 (2002).
8. Cohen, S.L., Chait, B.T.: Influence of matrix solution conditions on the MALDI-MS analysis of peptides and proteins. *Anal. Chem.* **68**, 31–37 (1996).
9. Chiu, W.C., Huang, C.C.: Combining fibrinogen-conjugated gold nanoparticles with a cellulose membrane for the mass spectrometry-based detection of fibrinolytic-related proteins. *Anal. Chem.* **85**, 6922–6929 (2013).
10. Karas, M., Krüger, R.: Ion formation in MALDI: The cluster ionization mechanism. *Chemical Reviews.* **103**, 427–440 (2003).
11. Karas, M., Glückmann, M., Schäfer, J.: Ionization in matrix-assisted laser desorption/ionization: Singly charged molecular ions are the lucky survivors. *J. Mass Spectrom.* **35**, 1–12 (2000).
12. Leopold, J., Popkova, Y., Engel, K.M., Schiller, J.: Recent developments of useful MALDI matrices for the mass spectrometric characterization of lipids. *Biomolecules.* **8**, 173-198, (2018).
13. Gross, J.H.: *Mass spectrometry: A textbook: Second edition.* Springer Berlin Heidelberg (2011).
14. Dreisewerd, K.: Recent methodological advances in MALDI mass spectrometry. *Anal. Bioanal. Chem.* **406**, 2261–2278 (2014).
15. Zenobi, R., Knochenmuss, R.: Ion formation in MALDI mass spectrometry. *Mass Spectrometry Reviews.* **17**, 337–366 (1998).
16. Dreisewerd, K.: The desorption process in MALDI. *Chem. Rev.* **102**, 395-425 (2003).

17. Mirza, S.P., Raju, N.P., Vairamani, M.: Estimation of the proton affinity values of fifteen matrix-assisted laser desorption/ionization matrices under electrospray ionization conditions using the kinetic method. *J. Am. Soc. Mass Spectrom.* **15**, 431–435 (2004).
18. Burton, R.D., Watson, C.H., Eyler, J.R., Lang, G.L., Powell, D.H., Avery, M.Y.: Proton affinities of eight matrices used for matrix-assisted laser desorption/ionization. *Rapid Commun. Mass Spectrom.* **11**, 443–446 (1997).
19. Shanta, S.R., Zhou, L.H., Park, Y.S., Kim, Y.H., Kim, Y., Kim, K.P.: Binary matrix for MALDI imaging mass spectrometry of phospholipids in both ion modes. *Anal. Chem.* **83**, 1252–1259 (2011).
20. Laugesen, S., Roepstorff, P.: Combination of two matrices results in improved performance of MALDI MS for peptide mass mapping and protein analysis. *J. Am. Soc. Mass Spectrom.* **14**, 992–1002 (2003).
21. Vorm, O., Roepstorff, P., Mann, M.: Improved Resolution and Very High sensitivity in MALDI TOF of matrix surfaces made by fast evaporation. *Anal. Chem.* **66**, 3281–3287 (1994).
22. Li, S., Zhang, Y., Liu, J., Han, J., Guan, M., Yang, H., Lin, Y., Xiong, S., Zhao, Z.: Electrospray deposition device used to precisely control the matrix crystal to improve the performance of MALDI MSI. *Sci. Rep.* **6**, 37903–37913 (2016).
23. Owen, S.J., Meier, F.S., Brombacher, S., Volmer, D.A.: Increasing sensitivity and decreasing spot size using an inexpensive, removable hydrophobic coating for matrix-assisted laser desorption/ionisation plates. *Rapid Commun. Mass Spectrom.* **17**, 2439–2449 (2003).
24. Chen, C.J., Lai, C.C., Tseng, M.C., Liu, Y.C., Lin, S.Y., Tsai, F.J.: Simple fabrication of hydrophobic surface target for increased sensitivity and homogeneity in matrix-assisted laser desorption/ionization time-of-flight mass spectrometry analysis of peptides, phosphopeptides, carbohydrates and proteins. *Anal. Chim. Acta.* **783**, 31–38 (2013).
25. Fukuyama, Y., Nakaya, S., Yamazaki, Y., Tanaka, K.: Ionic liquid matrixes optimized for MALDI-MS of sulfated/sialylated/neutral oligosaccharides and glycopeptides. *Anal. Chem.* **80**, 2171–2179 (2008).
26. Li, Y.L., Gross, M.L.: Ionic-liquid matrices for quantitative analysis by MALDI-TOF mass spectrometry. *J. Am. Soc. Mass Spectrom.* **15**, 1833–1837 (2004).
27. O'Connor, P.B., Hillenkamp, F.: MALDI mass spectrometry instrumentation, In *MALDI MS: a practical guide to instrumentation, methods and applications*. Second Edition. (2007).
28. Qiao, H., Spicer, V., Ens, W.: The effect of laser profile, fluence, and spot size on sensitivity in orthogonal-injection matrix-assisted laser desorption/ionization time-of-flight mass spectrometry. *Rapid Commun. Mass Spectrom.* **22**, 2779–2790 (2008).
29. Niehaus, M., Schnapp, A., Koch, A., Soltwisch, J., Dreisewerd, K.: New insights into the wavelength dependence of MALDI mass spectrometry. *Anal. Chem.* **89**, 7734–7741 (2017).
30. Knochenmuss, R.: Ion formation mechanisms in UV-MALDI. *Analyst.* **131**, 966–986 (2006).

31. Lu, I. C., Lee, C., Lee, Y. T., Ni, C. K.: Ionization mechanism of matrix-assisted laser desorption/ionization. *Annu. Rev. Anal. Chem.* **8**, 21–39 (2015).
32. Schiller, J.: MALDI-MS of Lipids, In MALDI MS: a practical guide to instrumentation, methods and applications. Second Edition. (2007).
33. van den Boom, D., Berkenkamp, S.: MALDI-MS of nucleic acids and practical implementations in genomics and genetics, In MALDI MS: a practical guide to instrumentation, methods and applications. Second Edition. (2007).
34. Li, L.: Overview of MS and MALDI MS for Polymer Analysis, In MALDI Mass Spectrometry for Synthetic Polymer Analysis. (2009).
35. Hou, T.Y., Chiang-Ni, C., Teng, S.H.: Current status of MALDI-TOF mass spectrometry in clinical microbiology. *Journal of food and drug analysis.* **27**, 404-414 (2019).
36. Aubry, S., Aussedat, B., Delaroche, D., Jiao, C. Y., Bolbach, G., Lavielle, S., Chassaing, G., Sagan, S., Burlina, F.: MALDI-TOF mass spectrometry: A powerful tool to study the internalization of cell-penetrating peptides. *Biochim. Biophys. Acta Biomembr.* **1798**, 2182–2189 (2010).
37. Ferroni, A., Suarez, S., Beretti, J. L., Dauphin, B., Bille, E., Meyer, J., Bougnoux, M. E., Alanio, A., Berche, P., Nassif, X.: Real-time identification of bacteria and species in positive blood culture broths by matrix-assisted laser desorption ionization-time of flight mass spectrometry. *J. Clin. Microbiol.* **48**, 1542-1548 (2010).
38. Ferreira, L., Sánchez-Juanes, F., González Ávila, M., Cembrero Fuciños, D., Herrero Hernández, A., González Buitrago, J.M., Muñoz Bellido, J.L.: Direct identification of urinary tract pathogens from urine samples by matrix-assisted laser desorption ionization-time of flight mass spectrometry. *J. Clin. Microbiol.* **48**, 2110–2115 (2010).
39. Ferreira, L., Sánchez-Juanes, F., Porras Guerra, I., García García, M.I., García Sánchez, J.E., González Buitrago, J.M., Muñoz Bellido, J.L.: Microorganisms direct identification from blood culture by matrix-assisted laser desorption/ionization time-of-flight mass spectrometry. *Clin. Microbiol. Infect.* **17**, 546–551 (2011).
40. Barreau, M., Pagnier, I., Scola, B. La: Improving the identification of anaerobes in the clinical microbiology laboratory through MALDI-TOF mass spectrometry. *Anaerobe.* **22**, 123–125 (2013).
41. Schriemer, D.C., Li, L.: Detection of high molecular weight narrow polydisperse polymers up to 1.5 million daltons by MALDI mass spectrometry. *Anal. Chem.* **68**, 2721–2725 (1996).
42. Sunner, J., Dratz, E., Chen, Y.C.: Graphite surface-assisted laser desorption/ionization time-of-flight mass spectrometry of peptides and proteins from liquid solutions. *Anal. Chem.* **67**, 4335–4342 (1995).
43. Tanaka, K., Waki, H., Ido, Y., Akita, S., Yoshida, Y., Yoshida, T., Matsuo, T.: Protein and polymer analyses up to m/z 100 000 by laser ionization time - of - flight mass spectrometry. *Rapid Commun. Mass Spectrom.* **2**, 151–153 (1988).
44. Kolářová, L., Kučera, L., Vaňhara, P., Hampl, A., Havel, J.: Use of flower-like gold nanoparticles in time-of-flight mass spectrometry. *Rapid Commun. Mass Spectrom.* **29**, 1585–1595 (2015).

45. Wu, H.F., Gopal, J., Abdelhamid, H.N., Hasan, N.: Quantum dot applications endowing novelty to analytical proteomics. *Proteomics*. **12**, 2949-5961 (2012).
46. Zhu, Z.J., Rotello, V.M., Vachet, R.W.: Engineered nanoparticle surfaces for improved mass spectrometric analyses. *Analyst*. **134**, 2183-2188 (2009).
47. Lim, A.Y., Ma, J., Boey, Y.C.F.: Development of nanomaterials for SALDI-MS analysis in forensics. *Adv. Mater.* **24**, 4211–4216 (2012).
48. Guinan, T., Kirkbride, P., Pigou, P.E., Ronci, M., Kobus, H., Voelcker, N.H.: Surface-assisted laser desorption ionization mass spectrometry techniques for application in forensics. *Mass Spec Rev.* **34**, 627-640. (2015).
49. Abdelhamid, H.N.: Nanoparticle assisted laser desorption/ionization mass spectrometry for small molecule analytes. *Mikrochim Acta.* **185**, 200-216 (2018).
50. Abdelhamid, H.N.: Nanoparticle-based surface assisted laser desorption ionization mass spectrometry: a review. *Mikrochim. Acta.* **186**, 682 (2019).
51. Pilolli, R., Palmisano, F., Cioffi, N.: Gold nanomaterials as a new tool for bioanalytical applications of laser desorption ionization mass spectrometry. *Anal Bioanal Chem.* **402**, 601-623 (2012).
52. Abdelhamid, H.N., Wu, H.F.: Gold nanoparticles assisted laser desorption/ionization mass spectrometry and applications: from simple molecules to intact cells. *Anal Bioanal Chem.* **408**, 4485-4502 (2016).
53. Chau, S.L., Tang, H.W., Ng, K.M.: Gold nanoparticles bridging infra-red spectroscopy and laser desorption/ionization mass spectrometry for direct analysis of over-the-counter drug and botanical medicines. *Anal. Chim. Acta.* **919**, 62–69 (2016).
54. Son, J., Lee, G., Cha, S.: Direct analysis of triacylglycerols from crude lipid mixtures by gold nanoparticle-assisted laser desorption/ionization mass spectrometry. *J. Am. Soc. Mass Spectrom.* **25**, 891–894 (2014).
55. Kailasa, S.K., Wu, H.F.: One-pot synthesis of dopamine dithiocarbamate functionalized gold nanoparticles for quantitative analysis of small molecules and phosphopeptides in SALDI- and MALDI-MS. *Analyst*. **137**, 1629–1638 (2012).
56. Nayak, R., Knapp, D.R.: Matrix-free LDI mass spectrometry platform using patterned nanostructured gold thin film. *Anal. Chem.* **82**, 7772–7778 (2010).
57. Huang, Y.F., Chang, H.T.: Nile red-adsorbed gold nanoparticle matrixes for determining aminothiols through surface-assisted laser desorption/ionization mass spectrometry. *Anal. Chem.* **78**, 1485–1493 (2006).
58. Su, C.L., Tseng, W.L.: Gold nanoparticles as assisted matrix for determining neutral small carbohydrates through laser desorption/ionization time-of-flight mass spectrometry. *Anal. Chem.* **79**, 1626–1633 (2007).
59. Cang, J., Chen, L.Y., Lin, Y.S., Chang, H.T.: Detection of metabolites in cells through surface-assisted laser desorption/ionization mass spectrometry. *ACS Omega.* **3**, 17386–17391 (2018).
60. Chiang, N.C., Chiang, C.K., Lin, Z.H., Chlu, T.C., Chang, H.T.: Detection of aminothiols through surface-assisted laser desorption/ionization mass spectrometry using mixed gold nanoparticles. *Rapid Commun. Mass Spectrom.* **23**, 3063–3068 (2009).

61. Amendola, V., Litti, L., Meneghetti, M.: LDI-MS assisted by chemical-free gold nanoparticles: Enhanced sensitivity and reduced background in the low-mass region. *Anal. Chem.* **85**, 11747–11754 (2013).
62. Zhu, Z.-J.J., Ghosh, P.S., Miranda, O.R., Vachet, R.W., Rotello, V.M.: Multiplexed screening of cellular uptake of gold nanoparticles using laser desorption/ionization mass spectrometry. *J. Am. Chem. Soc.* **130**, 14139–14143 (2008).
63. Castellana, E.T., Gamez, R.C., Gómez, M.E., Russell, D.H.: Longitudinal surface plasmon resonance based gold nanorod biosensors for mass spectrometry. *Langmuir*. **26**, 6066–6070 (2010).
64. Yao, G., Zhang, H., Deng, C., Lu, H., Zhang, X., Yang, P.: Facile synthesis of 4-mercaptophenylboronic acid functionalized gold nanoparticles for selective enrichment of glycopeptides. *Rapid Commun. Mass Spectrom.* **23**, 3493–3500 (2009).
65. Duan, J., Linman, M.J., Chen, C. Y., Cheng, Q.J.: CHCA-modified Au nanoparticles for laser desorption ionization mass spectrometric analysis of peptides. *J. Am. Soc. Mass Spectrom.* **20**, 1530–1539
66. Chen, T. H., Yu, C. J., Tseng, W. L.: Sinapinic acid-directed synthesis of gold nanoclusters and their application to quantitative matrix-assisted laser desorption/ionization mass spectrometry. *Nanoscale*. **6**, 1347–1353 (2014).
67. Sekuła, J., Nizioł, J., Rode, W., Ruman, T.: Silver nanostructures in laser desorption/ionization mass spectrometry and mass spectrometry imaging. *Analyst*. **140**, 6195–6209 (2015).
68. Jackson, S.N., Baldwin, K., Muller, L., Womack, V.M., Schultz, J.A., Balaban, C., Woods, A.S.: Imaging of lipids in rat heart by MALDI-MS with silver nanoparticles. *Anal. Bioanal. Chem.* **406**, 1377–1386 (2014)
69. Hong, M., Xu, L., Wang, F., Geng, Z., Li, H., Wang, H., Li, C.Z.: A direct assay of carboxyl-containing small molecules by SALDI-MS on a AgNP/rGO-based nanoporous hybrid film. *Analyst*. **141**, 2712–2726 (2016).
70. Wang, M.T., Liu, M.H., Wang, C.R.C., Chang, S.Y.: Silver-coated gold nanoparticles as concentrating probes and matrices for surface-assisted laser desorption/ionization mass spectrometric analysis of aminoglycosides. *J. Am. Soc. Mass Spectrom.* **20**, 1925–1932 (2009).
71. Chiu, T.C., Chang, L.C., Chiang, C.K., Chang, H.T.: Determining estrogens using surface-assisted laser desorption/ionization mass spectrometry with silver nanoparticles as the matrix. *J. Am. Soc. Mass Spectrom.* **19**, 1343–1346 (2008).
72. Hua, L., Chen, J., Ge, L., Tan, S.N.: Silver nanoparticles as matrix for laser desorption/ionization mass spectrometry of peptides. *J. Nanoparticle Res.* **9**, 1133–1138 (2007).
73. Hong, S., Lee, J.S., Ryu, J., Lee, S.H., Lee, D.Y., Kim, D.P., Park, C.B., Lee, H.: Bio-inspired strategy for on-surface synthesis of silver nanoparticles for metal/organic hybrid nanomaterials and LDI-MS substrates. *Nanotechnology*. **22**, 494020–494027 (2011).
74. Muller, L., Baldwin, K., Barbacci, D.C., Jackson, S.N., Roux, A., Balaban, C.D., Brinson, B.E., McCully, M.I., Lewis, E.K., Schultz, J.A., Woods, A.S.: Laser desorption/ionization mass spectrometric imaging of endogenous lipids from rat brain

- tissue implanted with silver nanoparticles. *J. Am. Soc. Mass Spectrom.* **28**, 1716–1728 (2017).
75. Sherrod, S.D., Diaz, A.J., Russell, W.K., Cremer, P.S., Russell, D.H.: Silver nanoparticles as selective ionization probes for analysis of olefins by mass spectrometry. *Anal. Chem.* **80**, 6796–6799 (2008).
76. Kuo, T.R., Chen, Y.C., Wang, C.I., Shen, T.H., Wang, H.Y., Pan, X.Y., Wang, D.Y., Liou, C.C., Chang, Y.H., Chen, Y.C., Wu, Y.H., Liu, Y.R., Lin, Y.H., Hu, C.C., Chen, C.C.: Highly oriented Langmuir-Blodgett film of silver cuboctahedra as an effective matrix-free sample plate for surface-assisted laser desorption/ionization mass spectrometry. *Nanoscale.* **9**, 11119–11125 (2017).
77. Silina, Y.E., Meier, F., Nebolsin, V.A., Koch, M., Volmer, D.A.: Novel galvanic nanostructures of Ag and Pd for efficient laser desorption/ionization of low molecular weight compounds. *J. Am. Soc. Mass Spectrom.* **25**, 841–851 (2014).
78. Yang, M., Fujino, T.: Silver nanoparticles on zeolite surface for laser desorption/ionization mass spectrometry of low molecular weight compounds. *Chem. Phys. Lett.* **576**, 61–64 (2013).
79. Cheng, Y.H., Zhang, Y., Chau, S.L., Lai, S.K.M., Tang, H.W., Ng, K.M.: Enhancement of image contrast, stability, and SALDI-MS detection sensitivity for latent fingerprint analysis by tuning the composition of silver-gold nanoalloys. *ACS Appl. Mater. Interfaces.* **8**, 29668–29675 (2016).
80. Shrivastava, K., Wu, H.F.: Modified silver nanoparticle as a hydrophobic affinity probe for analysis of peptides and proteins in biological samples by using liquid-liquid microextraction coupled to AP-MALDI-ion trap and MALDI-TOF mass spectrometry. *Anal. Chem.* **80**, 2583–2589 (2008).
81. Kailasa, S.K., Wu, H.F.: Surface modified silver selenide nanoparticles as extracting probes to improve peptide/protein detection via nanoparticles-based liquid phase microextraction coupled with MALDI mass spectrometry. *Talanta.* **83**, 527–534 (2010).
82. Shastri, L., Abdelhamid, H.N., Nawaz, M., Wu, H.F.: Synthesis, characterization and bifunctional applications of bidentate silver nanoparticle assisted single drop microextraction as a highly sensitive preconcentrating probe for protein analysis. *RSC Adv.* **5**, 41595–41603 (2015).
83. Lee K. H., Chiang C. K., Lin Z. H., Chang H. T.: Determining enediol compounds in tea using surface-assisted laser desorption/ionization mass spectrometry with titanium dioxide nanoparticle matrices. *Rapid Commun. Mass Spectrom.* **21**, 2023–2030 (2007).
84. Chiang, C.K., Chiang, N.C., Lin, Z.H., Lan, G.Y., Lin, Y.W., Chang, H.T.: Nanomaterial-based surface-assisted laser desorption/ionization mass spectrometry of peptides and Proteins. *J. Am. Soc. Mass Spectrom.* **21**, 1204–1207 (2010).
85. Shrivastava, K., Agrawal, K., Wu, H.F.: Application of platinum nanoparticles as affinity probe and matrix for direct analysis of small biomolecules and microwave digested proteins using matrix-assisted laser desorption/ionization mass spectrometry. *Analyst.* **136**, 2852–2857 (2011).
86. Silina, Y.E., Fink-Straube, C., Hayen, H., Volmer, D.A.: Analysis of fatty acids and triacylglycerides by Pd nanoparticle-assisted laser desorption/ionization mass spectrometry. *Anal. Methods.* **7**, 3701–3707 (2015).

87. Popović, I., Nešić, M., Vranješ, M., Šaponjić, Z., Petković, M.: TiO<sub>2</sub> nanocrystals - Assisted laser desorption and ionization time-of-flight mass spectrometric analysis of steroid hormones, amino acids and saccharides. Validation and comparison of methods. *RSC Adv.* **6**, 1027–1036 (2016).
88. Popović, I., Milovanović, D., Miletić, J., Nešić, M., Vranješ, M., Šaponjić, Z., Petković, M.: Dependence of the quality of SALDI TOF MS analysis on the TiO<sub>2</sub> nanocrystals' size and shape. *Opt. Quantum Electron.* **48**, 1–6 (2016).
89. Sonderegger, H., Rameshan, C., Lorenz, H., Klauser, F., Klerks, M., Rainer, M., Bakry, R., Huck, C.W., Bonn, G.K.: Surface-assisted laser desorption/ionization-mass spectrometry using TiO<sub>2</sub>-coated steel targets for the analysis of small molecules. *Anal. Bioanal. Chem.* **401**, 1963–1974 (2011).
90. Chen, C.T., Chen, Y.C.: Fe<sub>3</sub>O<sub>4</sub>/TiO<sub>2</sub> core/shell nanoparticles as affinity probes for the analysis of phosphopeptides using TiO<sub>2</sub> surface-assisted laser desorption/ionization mass spectrometry. *Anal. Chem.* **77**, 5912–5919 (2005).
91. Yuan, M., Shan, Z., Tian, B., Tu, B., Yang, P., Zhao, D.: Preparation of highly ordered mesoporous WO<sub>3</sub>-TiO<sub>2</sub> as matrix in matrix-assisted laser desorption/ionization mass spectrometry. *Microporous Mesoporous Mater.* **78**, 37–41 (2005).
92. Watanabe, T., Kawasaki, H., Yonezawa, T., Arakawa, R.: Surface-assisted laser desorption/ionization mass spectrometry (SALDI-MS) of low molecular weight organic compounds and synthetic polymers using zinc oxide (ZnO) nanoparticles. *J. Mass Spectrom.* **43**, 1063–1071 (2008).
93. Pan, C., Xu, S., Hu, L., Su, X., Ou, J., Zou, H., Guo, Z., Zhang, Y., Guo, B.: Using oxidized carbon nanotubes as matrix for analysis of small molecules by MALDI-TOF MS. *J. Am. Soc. Mass Spectrom.* **16**, 883–892 (2005).
94. Tang, H.W., Ng, K.M., Lu, W., Che, C.M.: Ion desorption efficiency and internal energy transfer in carbon-based surface-assisted laser desorption/ionization mass spectrometry: Desorption mechanism(s) and the design of SALDI substrates. *Anal. Chem.* **81**, 4720–4729 (2009).
95. Amini, N., Shariatgorji, M., Thorsén, G.: SALDI-MS signal enhancement using oxidized graphitized carbon black nanoparticles. *J. Am. Soc. Mass Spectrom.* **20**, 1207–1213 (2009).
96. Wang, J., Liu, Q., Liang, Y., Jiang, G.: Recent progress in application of carbon nanomaterials in laser desorption/ionization mass spectrometry Young Investigators in Analytical and Bioanalytical Science. *Anal. Bioanal. Chem.* **408**, 2861–2873 (2016).
97. Lu, W., Li, Y., Li, R., Shuang, S., Dong, C., Cai, Z.: Facile Synthesis of N-doped carbon dots as a new matrix for detection of hydroxy-polycyclic aromatic hydrocarbons by negative-ion matrix-assisted laser desorption/ionization time-of-flight mass spectrometry. *ACS Appl. Mater. Interfaces.* **8**, 12976–12984 (2016).
98. Ma, R., Lu, M., Ding, L., Ju, H., Cai, Z.: Surface-assisted laser desorption/ionization mass spectrometric detection of biomolecules by using functional single-walled carbon nanohorns as the matrix. *Chem. - A Eur. J.* **19**, 102–108 (2013).
99. Hopwood, F.G., Michalak, L., Alderdice, D.S., Fisher, K.J., Willett, G.D.: C<sub>60</sub> - assisted laser desorption/ionization mass spectrometry in the analysis of phosphotungstic acid. *Rapid Commun. Mass Spectrom.* **8**, 881–885 (1994).

100. Xu, S., Li, Y., Zou, H., Qiu, J., Guo, Z., Guo, B.: Carbon Nanotubes as assisted matrix for laser desorption/ionization time-of-flight mass spectrometry. *Anal. Chem.* **75**, 6191–6195 (2003).
101. Shi, C., Deng, C., Zhang, X., Yang, P.: Synthesis of highly water-dispersible polydopamine-modified multiwalled carbon nanotubes for matrix-assisted laser desorption/ionization mass spectrometry analysis. *ACS Appl. Mater. Interfaces.* **5**, 7770–7776 (2013).
102. Kim, Y.K., Min, D.H.: The structural influence of graphene oxide on its fragmentation during laser desorption/ionization mass spectrometry for efficient small-molecule analysis. *Chem. - A Eur. J.* **21**, 7217–7223 (2015).
103. Huang, R.C., Chiu, W.J., Li, Y.J., Huang, C.C.: Detection of microRNA in tumor cells using exonuclease III and graphene oxide-regulated signal amplification. *ACS Appl. Mater. Interfaces.* **6**, 21780–21787 (2014).
104. Liu, Y., Liu, J., Deng, C., Zhang, X.: Graphene and graphene oxide: Two ideal choices for the enrichment and ionization of long-chain fatty acids free from matrix-assisted laser desorption/ionization matrix interference. *Rapid Commun. Mass Spectrom.* **25**, 3223–3234 (2011).
105. Hua, P.Y., Manikandan, M., Abdelhamid, H.N., Wu, H.F.: Graphene nanoflakes as an efficient ionizing matrix for MALDI-MS based lipidomics of cancer cells and cancer stem cells. *J. Mater. Chem. B.* **2**, 7334–7343 (2014).
106. Liu, Y., Li, Y., Liu, J., Deng, C., Zhang, X.: High throughput enzyme inhibitor screening by functionalized magnetic carbonaceous microspheres and graphene oxide-based MALDI-TOF-MS. *J. Am. Soc. Mass Spectrom.* **22**, 2188–2198 (2011).
107. Tang, L.A.L., Wang, J., Loh, K.P.: Graphene-based SELDI probe with ultrahigh extraction and sensitivity for DNA oligomer. *J. Am. Chem. Soc.* **132**, 10976–10977 (2010).
108. Liu, J., Liu, Y., Gao, M., Zhang, X.: High throughput detection of tetracycline residues in milk using graphene or graphene oxide as MALDI-TOF MS matrix. *J. Am. Soc. Mass Spectrom.* **23**, 1424–1427 (2012).
109. Chen, S., Zheng, H., Wang, J., Hou, J., He, Q., Liu, H., Xiong, C., Kong, X., Nie, Z.: Carbon nanodots as a matrix for the analysis of low-molecular-weight molecules in both positive- and negative-ion matrix-assisted laser desorption/ionization time-of-flight mass spectrometry and quantification of glucose and uric acid in real samples. *Anal. Chem.* **85**, 6646–6652 (2013).
110. Wei, J., Buriak, J.M., Siuzdak, G.: Desorption–ionization mass spectrometry on porous silicon. *Nature.* **399**, 243–246 (1999).
111. Shmigol, I. V., Alekseev, S.A., Lavrynenko, O.Y., Vasylieva, N.S., Zaitsev, V.N., Barbier, D., Pokrovskaya, V.A.: Chemically modified porous silicon for laser desorption/ionization mass spectrometry of ionic dyes. *J. Mass Spectrom.* **44**, 1234–1240 (2009).
112. Chen, Y., Li, D., Bie, Z., He, X., Liu, Z.: Coupling of phosphate-imprinted mesoporous silica nanoparticles-based selective enrichment with matrix-assisted laser desorption ionization-time-of-flight mass spectrometry for highly efficient analysis of protein phosphorylation. *Anal. Chem.* **88**, 1447–1454 (2016).

113. Dupré, M., Cantel, S., Durand, J.O., Martinez, J., Enjalbal, C.: Silica nanoparticles pre-spotted onto target plate for laser desorption/ionization mass spectrometry analyses of peptides. *Anal. Chim. Acta.* **741**, 47–57 (2012).
114. Bhisare, M.L., Abdelhamid, H.N., Wu, B.S., Wu, H.F.: Rapid and direct MALDI-MS identification of pathogenic bacteria from blood using ionic liquid-modified magnetic nanoparticles ( $\text{Fe}_3\text{O}_4@\text{SiO}_2$ ). *J. Mater. Chem. B.* **2**, 4671–4683 (2014).
115. Wang, Y., Zeng, Z., Li, J., Chi, L., Guo, X., Lu, N.: Biomimetic antireflective silicon nanocones array for small molecules analysis. *J. Am. Soc. Mass Spectrom.* **24**, 66–73 (2013).
116. Cuiffi, J.D., Hayes, D.J., Fonash, S.J., Brown, K.N., Jones, A.D.: Desorption - ionization mass spectrometry using deposited nanostructured silicon films. *Anal. Chem.* **73**, 1292–1295 (2001).
117. Zhu, Q., Teng, F., Wang, Z., Wang, Y., Lu, N.: Confining analyte droplets on visible Si pillars for improving reproducibility and sensitivity of SALDI-TOF MS. *Anal. Bioanal. Chem.* **411**, 1135–1142 (2019).
118. Korte, A.R., Morris, N.J., Vertes, A.: High throughput complementary analysis and quantitation of metabolites by maldi- A nd silicon nanopost array-laser desorption/ionization-mass spectrometry. *Anal. Chem.* **91**, 3951–3958 (2019).
119. Wang, C., Reed, J.M., Ma, L., Qiao, Y., Luo, Y., Zou, S., Hickman, J.J., Su, M.: Biomimic light trapping silicon nanowire arrays for laser desorption/ionization of peptides. *J. Phys. Chem. C.* **116**, 15415–15420 (2012).
120. Go, E.P., Apon, J. V., Luo, G., Saghatelian, A., Daniels, R.H., Sahi, V., Dubrow, R., Cravatt, B.F., Vertes, A., Siuzdak, G.: Desorption/ionization on silicon nanowires. *Anal. Chem.* **77**, 1641–1646 (2005).
121. Shen, Q., Toyoda, T.: Dependence of thermal conductivity of porous silicon on porosity characterized by photoacoustic technique. *Rev. Sci. Instrum.* **74**, 601–603 (2003).
122. Alimpiev, S., Nikiforov, S., Karavanskii, V., Minton, T., Sunner, J.: On the mechanism of laser-induced desorption-ionization of organic compounds from etched silicon and carbon surfaces. *J. Chem. Phys.* **115**, 1891–1901 (2001).
123. Guinan, T., Ronci, M., Vasani, R., Kobus, H., Voelcker, N.H.: Comparison of the performance of different silicon-based SALDI substrates for illicit drug detection. *Talanta.* **132**, 494–502 (2015).
124. Gao, J., Louie, K.B., Steinke, P., Bowen, B.P., Raad, M. De, Zuckermann, R.N., Siuzdak, G., Northen, T.R.: Morphology-driven control of metabolite selectivity using nanostructure-initiator mass spectrometry. *Anal. Chem.* **89**, 6521–6526 (2017).
125. Woo, H.K., Northen, T.R., Yanes, O., Siuzdak, G.: Nanostructure-initiator mass spectrometry: A protocol for preparing and applying NIMS surfaces for high-sensitivity mass analysis. *Nat. Protoc.* **3**, 1341–1349 (2008).
126. Rejeeth, C., Pang, X., Zhang, R., Xu, W., Sun, X., Liu, B., Lou, J., Wan, J., Gu, H., Yan, W., Qian, K.: Extraction, detection, and profiling of serum biomarkers using designed  $\text{Fe}_3\text{O}_4@\text{SiO}_2@\text{HA}$  core-shell particles. *Nano Res.* **11**, 68–79 (2018).
127. Guinan, T.M., Kirkbride, P., Della Vedova, C.B., Kershaw, S.G., Kobus, H., Voelcker, N.H.: Direct detection of illicit drugs from biological fluids by desorption/ionization

- mass spectrometry with nanoporous silicon microparticles. *Analyst*. **140**, 7926–7933 (2015).
128. Stopka, S.A., Holmes, X.A., Korte, A.R., Compton, L.R., Retterer, S.T., Vertes, A.: Trace analysis and reaction monitoring by nanophotonic ionization mass spectrometry from elevated bowtie and silicon nanopost arrays. *Adv. Funct. Mater.* **28**, 1–9 (2018).
  129. Korte, A.R., Stopka, S.A., Morris, N., Razunguzwa, T., Vertes, A.: Large-scale metabolite analysis of standards and human serum by laser desorption ionization mass spectrometry from silicon nanopost arrays. *Anal. Chem.* **88**, 8989–8996 (2016).
  130. Stopka, S.A., Rong, C., Korte, A.R., Yadavilli, S., Nazarian, J., Razunguzwa, T.T., Morris, N.J., Vertes, A.: Molecular imaging of biological samples on nanophotonic laser desorption ionization platforms. *Angew. Chemie - Int. Ed.* **55**, 4482–4486 (2016).
  131. Walker, B.N., Stolee, J.A., Vertes, A.: Nanophotonic ionization for ultratrace and single-cell analysis by mass spectrometry. *Anal. Chem.* **84**, 7756–7762 (2012).
  132. Morris, N.J., Anderson, H., Thibeault, B., Vertes, A., Powell, M.J., Razunguzwa, T.T.: Laser desorption ionization (LDI) silicon nanopost array chips fabricated using deep UV projection lithography and deep reactive ion etching. *RSC Adv.* **5**, 72051–72057 (2015).
  133. Walker, B.N., Stolee, J.A., Pickel, D.L., Retterer, S.T., Vertes, A.: Tailored silicon nanopost arrays for resonant nanophotonic ion production. *J. Phys. Chem. C*. **114**, 4835–4840 (2010).
  134. Trauger, S.A., Go, E.P., Shen, Z., Apon, J. V., Compton, B.J., Bouvier, E.S.P., Finn, M.G., Siuzdak, G.: High sensitivity and analyte capture with desorption/ionization mass spectrometry on silylated porous silicon. *Anal. Chem.* **76**, 4484–4489 (2004).
  135. Daniels, R.H., Dikler, S., Li, E., Stacey, C.: Break free of the matrix: sensitive and rapid analysis of small molecules using nanostructured surfaces and LDI-TOF mass spectrometry. *J. Lab. Autom.* **13**, 314–321 (2008).
  136. Hu, J.B., Chen, Y.C., Urban, P.L.: Coffee-ring effects in laser desorption/ionization mass spectrometry. *Anal. Chim. Acta.* **766**, 77–82 (2013).
  137. Wagner, M., Varesio, E., Hopfgartner, G.: Ultra-fast quantitation of saquinavir in human plasma by matrix-assisted laser desorption/ionization and selected reaction monitoring mode detection. *J. Chromatogr. B*. **872**, 68–76 (2008).
  138. Solouki, T., White, F.M., Marto, J.A., Guan, S., Marshall, A.G.: Attomole biomolecule mass analysis by matrix-assisted laser desorption/ionization fourier transform ion cyclotron resonance. *Anal. Chem.* **67**, 4139–4144 (1995).
  139. Szájli, E., Fehér, T., Medzihradzky, K.F.: Investigating the quantitative nature of MALDI-TOF MS. *Mol. Cell. Proteomics*. **7**, 2410–2418 (2008).
  140. Sleno, L., Volmer, D.A.: Assessing the properties of internal standards for quantitative matrix-assisted laser desorption/ionization mass spectrometry of small molecules. *Rapid Commun. Mass Spectrom.* **20**, 1517–1524 (2006).
  141. Hatsis, P., Brombacher, S., Corr, J., Kovarik, P., Volmer, D.A.: Quantitative analysis of small pharmaceutical drugs using a high repetition rate laser matrix-assisted laser/desorption ionization source. *Rapid Commun. Mass Spectrom.* **17**, 2303–2309 (2003).

142. Sleno, L., Volmer, D.A.: Toxin screening in phytoplankton: Detection and quantitation using MALDI triple quadrupole mass spectrometry. *Anal. Chem.* **77**, 1509–1517 (2005).
143. Elsilá, J.E., De Leon, N.P., Zare, R.N.: Factors Affecting quantitative analysis in laser desorption/ionization mass spectrometry. *Anal. Chem.* **76**, 2430–2437 (2004).
144. Horak, J., Werther, W., Schmid, E.R.: Optimisation of the quantitative determination of chlormequat by matrix-assisted laser desorption/ionisation mass spectrometry. *Rapid Commun. Mass Spectrom.* **15**, 241–248 (2001).
145. Koulman, A., Petras, D., Narayana, V.K., Wang, L., Volmer, D.A.: Comparative high-speed profiling of carboxylic acid metabolite levels by differential isotope-coded MALDI mass spectrometry. *Anal. Chem.* **81**, 7544–7551 (2009).
146. Thomas, H., Havliš, J., Peychl, J., Shevchenko, A.: Dried-droplet probe preparation on AnchorChip<sup>TM</sup> targets for navigating the acquisition of matrix-assisted laser desorption/ionization time-of-flight spectra by fluorescence of matrix/analyte crystals. *Rapid Commun. Mass Spectrom.* **18**, 923–930 (2004).
147. Porta, T., Grivet, C., Knochenmuss, R., Varesio, E., Hopfgartner, G.: Alternative CHCA-based matrices for the analysis of low molecular weight compounds by UV-MALDI-tandem mass spectrometry. *J. Mass Spectrom.* **46**, 144–152 (2011).
148. Hensel, R.R., King, R.C., Owens, K.G.: Electrospray sample preparation for improved quantitation in matrix-assisted laser desorption/ionization time-of-flight mass spectrometry. *Rapid Commun. Mass Spectrom.* **11**, 1785–1793 (1997).
149. Önnérfford, P., Ekström, S., Bergquist, J., Nilsson, J., Laurell, T., Marko-Varga, G.: Homogeneous sample preparation for automated high throughput analysis with matrix-assisted laser desorption/ionisation time-of-flight mass spectrometry. *Rapid Commun. Mass Spectrom.* **13**, 315–322 (1999).
150. Ho, Y.C., Tseng, M.C., Lu, Y.W., Lin, C.C., Chen, Y.J., Fuh, M.R.: Nanoparticle-assisted MALDI-TOF MS combined with seed-layer surface preparation for quantification of small molecules. *Anal. Chim. Acta.* **697**, 1–7 (2011).
151. Zhang, B.T., Zheng, X., Li, H.F., Lin, J.M.: Application of carbon-based nanomaterials in sample preparation: A review. *Anal. Chim. Acta.* **784**, 1–17 (2013).
152. Keller, B.O., Li, L.: Three-layer matrix/sample preparation method for MALDI MS analysis of low nanomolar protein samples. *J. Am. Soc. Mass Spectrom.* **17**, 780–785 (2006).
153. Patil, A.A., Chiang, C.K., Wen, C.H., Peng, W.P.: Forced dried droplet method for MALDI sample preparation. *Anal. Chim. Acta.* **1031**, 128–133 (2018).
154. Pabst, M., Fagerer, S.R., Köhling, R., Küster, S.K., Steinhoff, R., Badertscher, M., Wahl, F., Dittrich, P.S., Jefimovs, K., Zenobi, R.: Self-aliquoting microarray plates for accurate quantitative matrix-assisted laser desorption/ionization mass spectrometry. *Anal. Chem.* **85**, 9771–9776 (2013).
155. Kim, Y., Hurst, G.B., Doktycz, M.J., Buchanan, M. V.: Improving spot homogeneity by using polymer substrates in matrix-assisted laser desorption/ionization mass spectrometry of oligonucleotides. *Anal. Chem.* **73**, 2617–2624 (2001).
156. Distler, A.M., Allison, J.: Improved MALDI-MS analysis of oligonucleotides through the use of fucose as a matrix additive. *Anal. Chem.* **73**, 5000–5003 (2001).

157. Palmblad, M., Cramer, R.: Liquid matrix deposition on conductive hydrophobic Surfaces for tuning and quantitation in UV-MALDI mass spectrometry. *J. Am. Soc. Mass Spectrom.* **18**, 693–697 (2007).
158. Moon, J.H., Park, K.M., Ahn, S.H., Lee, S.H., Kim, M.S.: Investigations of some liquid matrixes for analyte quantification by MALDI. *J. Am. Soc. Mass Spectrom.* **26**, 1657–1664 (2015).
159. Okuno, S., Wada, Y., Arakawa, R.: Quantitative analysis of polypropyleneglycol mixtures by desorption/ionization on porous silicon mass spectrometry. *Int. J. Mass Spectrom.* **241**, 43–48 (2005).
160. Kuo, T.R., Chen, J.S., Chiu, Y.C., Tsai, C.Y., Hu, C.C., Chen, C.C.: Quantitative analysis of multiple urinary biomarkers of carcinoid tumors through gold-nanoparticle-assisted laser desorption/ionization time-of-flight mass spectrometry. *Anal. Chim. Acta.* **699**, 81–86 (2011).
161. Chiu, T.C.: Steroid hormones analysis with surface-assisted laser desorption/ionization mass spectrometry using catechin-modified titanium dioxide nanoparticles. *Talanta.* **86**, 415–420 (2011).
162. Huang, M.F., Chang, H.T.: Detection of carbohydrates using surface-assisted laser desorption/ionization mass spectrometry with HgTe nanostructures. *Chem. Sci.* **3**, 2147–2152 (2012).
163. Lin, Z., Zheng, J., Lin, G., Tang, Z., Yang, X., Cai, Z.: Negative ion laser desorption/ionization time-of-flight mass spectrometric analysis of small molecules using graphitic carbon nitride nanosheet matrix. *Anal. Chem.* **87**, 8005–8012 (2015).
164. Bibi, A., Ju, H.: Quantum dots assisted laser desorption/ionization mass spectrometric detection of carbohydrates: Qualitative and quantitative analysis. *J. Mass Spectrom.* **51**, 291–297 (2016).
165. Huang, Y.F., Chang, H.T.: Analysis of adenosine triphosphate and glutathione through gold nanoparticles assisted laser desorption/ionization mass spectrometry. *Anal. Chem.* **79**, 4852–4859 (2007).
166. Chen, W.T., Chiang, C.K., Lin, Y.W., Chang, H.T.: Quantification of captopril in urine through surface-assisted laser desorption/ionization mass spectrometry using 4-mercaptobenzoic acid-capped gold nanoparticles as an internal standard. *J. Am. Soc. Mass Spectrom.* **21**, 864–867 (2010).
167. Chiang, C.K., Lin, Y.W., Chen, W.T., Chang, H.T.: Accurate quantitation of glutathione in cell lysates through surface-assisted laser desorption/ionization mass spectrometry using gold nanoparticles. *Nanomedicine Nanotechnology, Biol. Med.* **6**, 530–537 (2010).
168. Alhmoud, H.Z., Guinan, T.M., Elnathan, R., Kobus, H., Voelcker, N.H.: Surface-assisted laser desorption/ionization mass spectrometry using ordered silicon nanopillar arrays. *Analyst.* **139**, 5999–6009 (2014).
169. Teng, F., Zhu, Q., Wang, Y., Du, J., Lu, N., Teng, F., Wang, Z., Wang, Y., Lu, N.: Enhancing reproducibility of SALDI MS detection by concentrating analytes within laser spot. *Talanta.* **179**, 583–587 (2018).

170. Pan, X.Y., Chen, C.H., Chang, Y.H., Wang, D.Y., Lee, Y.C., Liou, C.C., Wang, Y.X., Hu, C.C., Kuo, T.R.: Osteoporosis risk assessment using multilayered gold-nanoparticle thin film via SALDI-MS measurement. *Anal. Bioanal. Chem.* **411**, 2793–2802 (2019).
171. Li, W., Khan, M., Li, H., Lin, L., Mao, S., Lin, J.M.: Homogenous deposition of matrix-analyte cocrystals on gold-nanobowl arrays for improving MALDI-MS signal reproducibility. *Chem. Commun.* **55**, 2166–2169 (2019).
172. Choi, Y.K., Oh, J.Y., Han, S.Y.: Large-area graphene films as target surfaces for highly reproducible matrix-assisted laser desorption/ionization suitable for quantitative mass spectrometry. *J. Am. Soc. Mass Spectrom.* **29**, 2003–2011 (2018).
173. Wu, Z., Khan, M., Mao, S., Lin, L., Lin, J.M.: Combination of nano-material enrichment and dead-end filtration for uniform and rapid sample preparation in matrix-assisted laser desorption/ionization mass spectrometry. *Talanta*. **181**, 217–223 (2018).
174. Kuo, T.R., Wang, D.Y., Chiu, Y.C., Yeh, Y.C., Chen, W.T., Chen, C.H., Chen, C.W., Chang, H.C., Hu, C.C., Chen, C.C.: Layer-by-layer thin film of reduced graphene oxide and gold nanoparticles as an effective sample plate in laser-induced desorption/ionization mass spectrometry. *Anal. Chim. Acta.* **809**, 97–103 (2014).
175. Kawasaki, H., Sugitani, T., Watanabe, T., Yonezawa, T., Moriwaki, H., Arakawa, R.: Layer-by-layer self-assembled multilayer films of gold nanoparticles for surface-assisted laser desorption/ionization mass spectrometry. *Anal. Chem.* **80**, 7524–7533 (2008).
176. Liu, R., Liu, J.F., Zhou, X.X., Jiang, G. Bin: Cysteine modified small ligament au nanoporous film: An easy fabricating and highly efficient surface-assisted laser desorption/ionization substrate. *Anal. Chem.* **83**, 3668–3674 (2011).
177. Go, E.P., Shen, Z., Harris, K., Siuzdak, G.: Quantitative analysis with desorption/ionization on silicon mass spectrometry using electrospray deposition. *Anal. Chem.* **75**, 5475–5479 (2003).
178. Liu, Z., Zhang, P., Kister, T., Kraus, T., Volmer, D.A.: Ultrathin homogenous AuNP monolayers as tunable functional substrates for surface-assisted laser desorption/ionization of small biomolecules. *J. Am. Soc. Mass Spectrom.* **31**, 47–57 (2020).
179. Wu, B.H., Yang, H.Y., Huang, H.Q., Chen, G.X., Zheng, N.F.: Solvent effect on the synthesis of monodisperse amine-capped Au nanoparticles. *Chinese Chem. Lett.* **24**, 457–462 (2013).
180. Kister, T., Maurer, J.H.M., González García, L., Kraus, T.: Ligand-dependent nanoparticle assembly and its impact on the printing of transparent electrodes. *ACS Appl. Mater. Interfaces.* **10**, 6079–6083 (2018).

## VIII Curriculum vitae

### Education

- 09.2016 – 10.2019    Ph.D. in Analytical Chemistry  
Saarland University, Institute of Bioanalytical Chemistry, Germany  
Thesis: Novel approaches for quantitative analysis of small biomolecules in MALDI-MS and SALDI-MS
- 09.2008 – 06.2011    Master in Analytical Chemistry  
Sichuan University, Department of Chemistry  
Thesis: Preparation of Ru(bpy)<sub>3</sub><sup>2+</sup>/Nafion and AuNPs/PAN composite nanofibers and its application in the electrochemiluminescence sensor
- 09.2004 – 06.2008    Bachelor in Chemistry  
Henan University, College of Chemistry and Chemical Engineering

### Professional positions

- 07.2011 – 01.2013    Laboratory assistant  
Chinese Academy of Science, Changchun Institute of Applied Chemistry, Engineering Laboratory of Polymer Composites, China
- Work topic: Morphology evolution of the light-responsive Azo-labeled-PS/PMMA blend thin film

### Awards

- 2016                    Chinese Scholarship Council (CSC)
- 2009                    Scholarship of “Longsheng”,
- 2008                    Scholarship of Bank of China,
- 2006                    Second Prize Scholarship of Henan University
- 2006                    “Three Good” Student of Henan University

## IX Scientific contribution

### Publications:

1. **Zhen Liu**, Peng Zhang, Andrea Pyttlik, Tobias Kraus, Dietrich A. Volmer, Influence of core size and capping ligand of gold nanoparticles on the desorption/ionization efficiency of small biomolecules in AP-SALDI-MS, *Analytical Science Advance*, 2020, in press.
2. **Zhen Liu**, Peng Zhang, Thomas Kister, Tobias Kraus, Dietrich A. Volmer, Ultra-thin homogenous AuNP monolayers as tunable functional substrates for surface-assisted laser desorption/ionization of small biomolecules, *Journal of American society for mass spectrometry*. 2020, 31, 1, 47-57.
3. **Zhen Liu**, Peng Zhang, Lars Kaestner, Dietrich A Volmer, A simple MALDI target plate with channel design to improve detection sensitivity and reproducibility for quantitative analysis of biomolecules. *Journal of mass spectrometry*, 2019, 54, 878–884.
4. **Zhen Liu**, Baozhan Zheng, Cuisong Zhou, Lei Qian and Dan Xiao\*, In-situ Synthesis of Gold Nanoparticles on Porous Polyacrylonitrile Nanofibers for Sensing Application, *Analyst*, 2011, 136, 4545-4551.
5. Cuisong Zhou, **Zhen Liu**, Jianyuan Dai and Dan Xiao\*, Electrospun Ru(bpy)<sub>3</sub><sup>2+</sup> -doped nafion nanofibers for electrochemiluminescence sensing, *Analyst*, 2010, 135, 1004–1009.
6. Lei Qian, **Zhen Liu**, Yan Mo, Hongyan Yuan, Dan Xiao, Large scale preparation of urchin like Li doped ZnO using simple radio frequency chemical vapor synthesis, *Materials Letters*, 2013, 100, 124-126.

### Projects

1. National Natural Science Foundation of China (No. 20775050, No.20927007);
2. Youth Foundation of Sichuan University (No.2010SCU11048);
3. Specialized Research Fund for the Doctoral Program of Education Ministry of China (No.20070610030);
4. Research on on-line quality control system and key technologies of food physical and chemical analysis (2010-2011).

### Conferences

- 2018      **Zhen Liu**, Thomas Kister, Dietrich A. Volmer. Homogenous Langmuir-Blodgett films of gold nanoparticles for quantification in surface-assisted laser desorption/ionization mass spectrometry, poster presentation  
PhD Students Day of UdS 2018, Saarbrücken, Germany

- 2018      **Zhen Liu**, Thomas Kister, Dietrich A. Volmer. Homogenous Langmuir-Blodgett films of gold nanoparticles for quantification in surface-assisted laser desorption/ionization mass spectrometry, poster presentation European Mass Spectrometry Conference (EMSC 2018), Saarbrücken, Germany
- 2011      Bilateral exchanges with cigarette factory (ChuanYu Zhongyan), Chengdu, China
- 2010      Instrumental seminar (HITACHI) in southwest of China, Chengdu, China